CONSIDERATION OF FRICTIONAL BOUNDARY MODELLING IN METAL FORMING

By

AHMAD ASSEMPOOR

Bachelor of Science
Tehran Polytechnic
Tehran, Iran
1979

Master of Science
Tehran Polytechnic
Tehran, Iran
1985

Submitted to the Faculty of the
Graduate College of the
Oklahoma State University
in partial fulfillment of
the requirements for
the Degree of
DOCTOR OF PHILOSOPHY
December, 1989

CONSIDERATION OF FRICTIONAL BOUNDARY

MODELLING IN METAL FORMING

Thesis Approved:

Delcie R. Durham
Thesis Advisor

Dean of the Graduate College

ACKNOWLEDGMENTS

I wish to express my sincere appreciation to my major adviser, Dr. Delcie R. Durham, for her invaluable assistance and guidance at all stages of this research. Appreciation is also extended to other committee members, Dr. C. Eric Price, Dr. Richard Lowery, Dr. J. Keith Good, Dr. G. S. Gipson, Dr. F. Zwerneman, and Dr. I. T. Hong.

Profound gratitude is expressed to Mr. Ron Markum and Mr. Fred Dodds for their technical assistance in the lab experiments.

Thanks are expressed to Mrs. Daleene Caldwell for her typing skills and to Ms. Linda Gray for typing assistance.

Sincere gratitude is expressed to my mother, brothers and sisters for their moral support, encouragement and financial support.

TABLE OF CONTENTS

Chapter Page

LIST OF TABLES

LIST OF FIGURES

NOMENCLATURE

A	junction area
E	Young's modulus
F	tangential force
f	friction factor
g	body force
H'	slope of the equivalent stress-equivalent strain curve at the current value of the plastic curve
k	yield shear stress
p	pressure
p'	pressure at the limit of proportionality
p_o	normal yield pressure
S_{ij}	nominal stress tensor (non-symmetric) in Hill's equilibrium equations
t	time
T^{Δ}_{ij}	Jaumann or corotational rate of Kirchoff stress (symmetric)
v	volume
w	normal force
α	a constant used by Bowden and Tabor to simplify the yield criterion in three-dimension
β	contact area ratio in friction model proposed by Bay, also $\beta = f/(1-f)$ in modelling of friction by Hartley [16]
γ_o	asperity angle before deformation
γ_L	left asperity angle
γ_R	right asperity angle
δ_{ik}	Kronecker delta

μ	coefficient of friction
ν	Poisson ratio
ε_{ij}	Euler strain
σ	the generalized (equivalent) stress
σ_{ij}	Cauchy or Euler stress
σ'_{ij}	the deviatoric Cauchy stress
σ_o	yield stress
τ	friction, shear stress
τ'	friction stress at the limit of proportionality

CHAPTER I

INTRODUCTION

In the practical analysis of metal forming processes, particular attention must be paid to the die boundary conditions. Controlling the free surfaces and modelling the frictional forces significantly influence the results of the analysis.

The effect of the friction in metal forming is very complex. I. V. Krageli'ski and V. S. Shchedrov (1956) in their introduction to the "Development of the Science of Friction" wrote:

> The physical aspects of dry friction are not yet sufficiently clear. The engineer who encounters friction everywhere is not yet only incapable of controlling it, but is even unable to allow for it correctly, whereas the physicist lacks the data to provide comprehensive explanation for the phenomena.

Muurice Godet (1988) in his discussion and conclusion of "Modeling of Friction and Wear Phenomena" wrote: Neither friction nor wear are sufficiently understood to offer a solid basis for modeling.

Besides the complexity of the analysis another problem is faced when friction as a tangential force is modelled and introduced to an approximate numerical or analytical method in bulk deformation analysis. This difficulty arises from the existence of a point (neutral point or region) at the boundary where the friction force changes its orientation. In complex geometries (non-symmetric die or workpiece), finding the location of this point is difficult and proposed methods have, to date, proven unsuccessful. Also, an abrupt jump in the

friction value (positive to negative) at the neutral point in the friction modelling makes the analysis of the deformation ill conditioned.

Another problem encountered is the change of the geometry during the deformation, parts of the free boundary come to touch the dies. Sometimes, by changing the free surfaces, the position (positions) and the number of the neutral points change. This results in a change in the flow direction which makes the modelling of friction even more complicated.

1.1 Objective and Scope

This work concerns the development of a general methodology for finite-element modelling of friction in non-symmetric geometries. The basic approach involves first fixing the boundary nodes to the die, and then appropriately applying a friction model as the limit of the interface shear strength and the boundary between sliding and sticking conditions.

Some basic friction laws and theories suitable for numerical modelling are discussed in Chapter II. Previous works concerning finite element modelling of friction are also addressed. Some aspects of process modelling are outlined in Chapter III. To examine any friction model, having access to a source code is necessary. The source codes of softwares, typically commercial, were not available. Therefore, an elastic-plastic finite element code was developed and is discussed in Chapter IV. The method of incorporating the frictional boundary conditions into finite-element simulation of plastic deformation in the present work is also addressed in Chapter IV. Chapters V and VI are

devoted to verifications of the elastic-plastic program and the method(s) of friction modelling developed in Chapter IV. Chapter VII provides a summary and outlines the main conclusions of this work. This chapter also outlines some recommendations for future research.

CHAPTER II

FRICTION AND MODELLING OF FRICTION IN METAL FORMING

2.1 Friction

Friction is most commonly characterized by using the constant coefficient of friction in the Amontons/Coulomb Law or by using the constant friction factor in the Law of Constant Friction. In some metal forming processes such as forging, when the hydrostatic pressure is high, application of the constant coefficient of friction is questionable. Also, there is some evidence [1] that the application of the Constant Friction Law along the entire interface is incorrect. In their most recent friction model, Bay [2] pointed out that Amontons Law is valid only at low pressures while the Constant Friction Law is permissible at high pressures. Neither of them is valid at the intermediate pressures. It is the objective of this section to investigate the sources of these models and to provide some basis for modelling of friction in Chapter IV.

2.1.1 Causes of Friction

Friction is the resistance to the relative movement (sliding) between two surfaces in contact. Due to the mechanism of surface interaction, friction has a dual molecular-mechanical nature.

In microscopic scale, surfaces are rough no matter how finely finished they are (Figure 2.1). One source of friction is the asperity

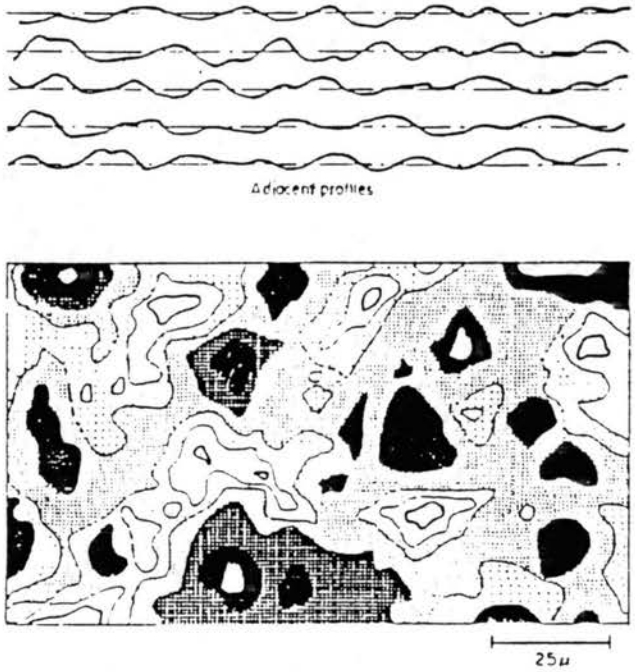

Figure 2.1 Typical surface map [7]. Lighter areas correspond to higher surface.

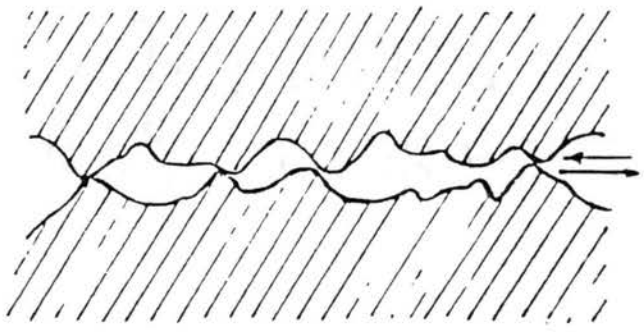

Figure 2.2 Asperity interlocking.

interlocking which is illustrated in Figure 2.2. According to this figure sliding cannot take place without cutting or deforming the softer asperities. Also it is possible the asperities of the harder material (die) plow through the softer one (workpiece) and contribute to the frictional force (Figure 2.3). At high pressure, atoms approach each other and interatomic forces come into play. It is said that adhesion takes place (Figure 2.4) When the surfaces are clean or the surface contaminant films are broken through, the metallic adhesion that takes place is very strong. Adhesion can be the weaker joints between the contaminant films of the contacting surfaces. In bulk deformation, metallic adhesion has been known as the major source of friction.

2.1.2 Laws of Friction

There are two basic friction laws which are empirical in nature. The first law states that friction is independent of the apparent contact area. The second law indicates that friction is proportional to the normal load between the surfaces. These laws are due to the French engineer G. Amontons (1699) and are usually referred to as 'Amontons Laws'. Laws of friction enable us to define a coefficient of friction:

$$\mu = \frac{F}{W} = \frac{\tau}{P} \tag{2.1}$$

where: μ = coefficient of friction

F = tangential force required for sliding

τ = interface shear stress

W = normal force

P = pressure

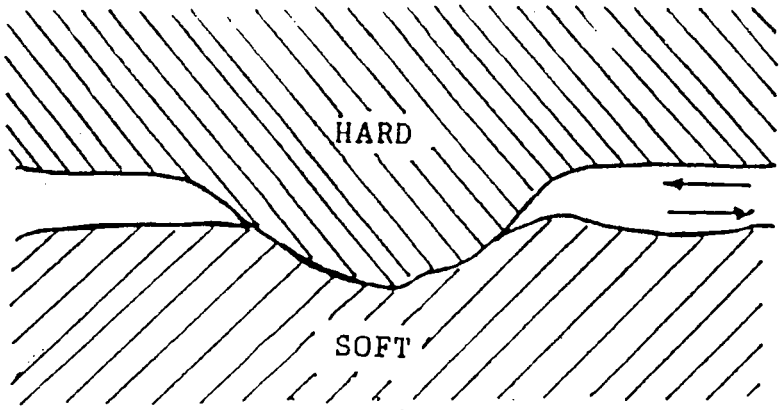

Figure 2.3 Plowing

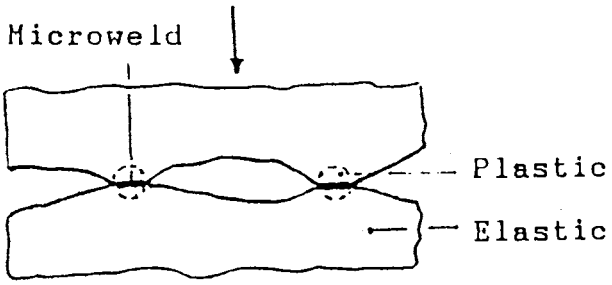

Figure 2.4 Adhesion

According to this equation, F is proportional to W when μ is constant. In metalworking, this is not necessarily realistic. For example in forging, due to the hydrostatic pressure, P reaches a multiple of the equivalent yield stress (σ_o). Since the maximum limit of τ is the bulk shear strength ($K = 1/\sqrt{3}\ \sigma_o$), μ drops to a very unrealistic value otherwise $\mu P > K$ which means the interface shear strength is higher than K (Figure 2.5). Therefore, the coefficient of friction is meaningless when P is very high.

To avoid this difficulty, the interface shear strength (friction stress) is sometimes described by:

$$\tau = fk \tag{2.2}$$

where f (frictional shear factor) is a constant less than one. f = 0 means the frictionless interface and f = 1 means condition of full sticking. Equation 2.2 is known as the Law of Constant Friction.

The Law of Constant Friction is mathematically more convenient than Amontons Law because the value of k is known from the beginning while in contrast, the value of P must be found. Sometimes it is suitable to use the combination of these laws in metal forming (Figure 2.6).

Values of μ and f are functions of several factors. Temperature, pressure, hardness, velocity, atmosphere, solubility of the mating pairs and surface crystal structure have shown to have some influence on friction. The effects of these factors have been well summarized in detail [3, 4]. Due to the variation of some of these factors, within the die/workpiece contact zone, μ and f must also vary. Therefore, an average μ or f is most often assumed in calculations. This is permissible for force calculation but can lead to errors in the

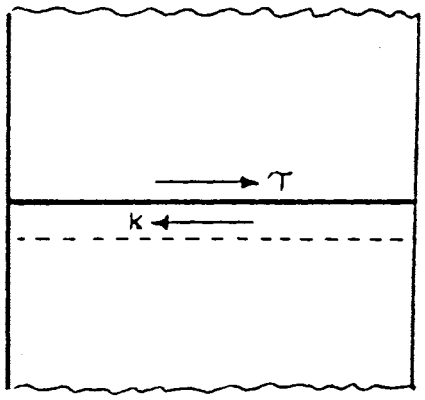

Figure 2.5 Interface shear strength. When this strength is greater than the shear strength of the bulk it is easier for the material to shear inside.

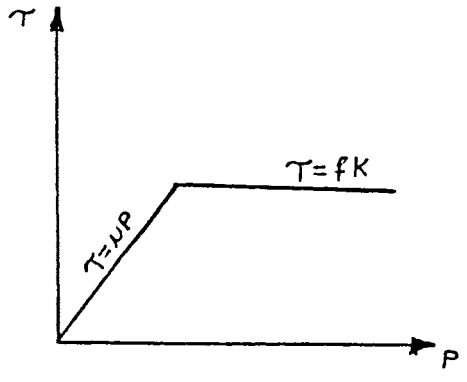

Figure 2.6 Combination of Amontons and Constant friction Laws

calculation of strain distribution [5, pp. 16].

2.1.3 Theory of Adhesion

2.1.3.1 Initial Theory of Adhesion. The theory of adhesion, due to Bowden and Tabor [6], is based on the analysis of real contact between rough surfaces in plastic deformation of the individual surface asperities. According to this theory, when two clean metallic surfaces are pressed together, they make contact only at the tips of the asperities. The true contact area increases by plastic deformation of the asperities until it is sufficient to carry the load (Figure 2.7). If the load is W and the yield pressure of the metal is P_o then the contact area A between the two asperities is:

$$A = \frac{W}{P_o} \tag{2.3}$$

Bowden and Tabor stated that strong adhesion occurs at the regions of real contact and before sliding takes place the adhered junctions must be sheared. If τ is the required shear stress for shearing of the junctions then the friction force F is:

$$F = A\tau + F_p \tag{2.4}$$

where F_p is an extra force due to the mechanical source of friction (plowing). Bowden and Tabor stated that for most situations with metallic surfaces F_p is small compared with $A\tau$ and can be neglected. Therefore, the friction force can be written as:

$$F = A\tau = \frac{W\tau}{P_o} \tag{2.5}$$

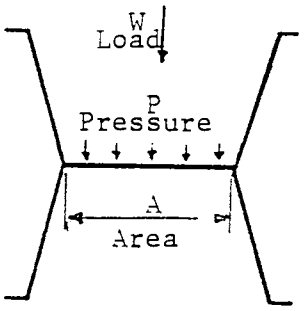

Figure 2.7 Contact between two isolated asperities

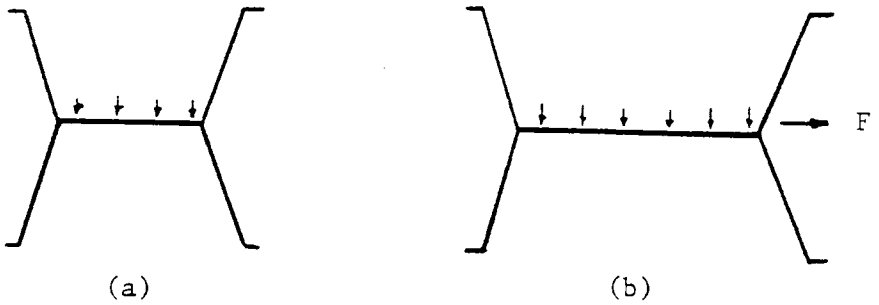

Figure 2.8 Junction area between the asperities.
a) Contact under normal load alone
b) Contact with application of tangential force F.

This equation indicates that F is proportional to the normal load W and independent of the area A (Amontons Law). According to Equation 2.5 the coefficient of friction μ is:

$$\mu = \frac{F}{W} = \frac{\tau}{P_o} \tag{2.6}$$

For an ideal plastic material the local yield pressure P_o is three times the yield stress σ_o [6, pp. 323] or:

$$P_o = 3\sigma_o \tag{2.7}$$

In clean metals, under vacuum, τ is equal to the yield shear stress K of material. Also, according to the Von Mises yield criterion:

$$\tau = k = \frac{1}{\sqrt{3}} \sigma_o \tag{2.8}$$

Inserting Equations 2.7 and 2.8 into Equation 2.6:

$$\mu = \frac{1}{3\sqrt{3}} \simeq 0.2 \tag{2.9}$$

However, the coefficient of friction in most clean metals is much higher than 0.2. One may explain this due to the work-hardening characteristic of the real material where τ increases during the deformation process. Bowden and Tabor indicated that this was an unlikely explanation since P_o increases parallel in τ and it is for this reason that the hardness of metals has little effect on the coefficient of friction. This problem led Bowden and Tabor to review the simple theory and to present a more realistic description of friction in terms of adhesion.

2.1.3.2 Modified Theory of Adhesion. The simple theory of adhesion

was developed in the absence of the tangential force F from the beginning. In other words, the normal pressure P was independent of the shear stress τ. This led to equation:

$$A = \frac{W}{P_o} \tag{2.10}$$

In the real condition when the tangential force F is applied, due to the theory of plasticity, yielding in the junction must occur as a result of the combined normal and shear stresses. To illustrate this consider the simplified two-dimensional model in Figure 2.8. In the absence of the tangential force (Figure 2.8a) the material starts to flow when the pressure reaches the yield pressure P_o and area A can be found according to Equation 2.10. Now if a tangential force F (friction) is gradually applied (Figure 2.8b), the material continues to flow under the condition:

$$P^2 + 3\tau^2 = K^2 \tag{2.11}$$

where K is a constant comparable to the yield stress of the metal. At the beginning when τ is zero $P = P_o$. Therefore, Equation 2.11 becomes:

$$P^2 + 3\tau^2 = P_o^2 \tag{2.12}$$

According to this equation when shear stress increases, further plastic flow occurs and the contact area A increases. When A increases, pressure (W/A) and shear stress (τ) drops. Again shear stress must increase to a value such that the combined stresses satisfy Equation

2.12 and further junction growth occurs. According to this model, there is a steady junction growth in the area of contact as τ increases. Based on Equation 2.12, when shear stress reaches the yield shear stress of the material k, pressure becomes zero. Under this condition to carry the load (W = PA) surface area should approach infinity. This is true only for absolutely clean surfaces in vacuum (sliding never occurs). However, due to the weak contaminant films at the interface, τ never reaches k. For the three dimensional case the criterion of plastic flow over the contact region is:

$$P^2 + \alpha\tau^2 = K^2 \tag{2.13}$$

where α is a suitable constant and its value does not greatly affect the amount of junction growth in many practical cases (α = 9 in [6], α = 27 in [2]). Again, when shear stress is zero K is equal to the yield pressure P_o. Therefore,

$$P^2 + \alpha\tau^2 = P_o^2 \tag{2.14}$$

Equation 2.14 is similar to Equation 2.12 and the same mechanism of junction growth can be explained for the three dimensional case.

According to the above discussion, for clean metals large-scale junction area is possible. This results in a higher coefficient of friction which can be confirmed experimentally [7, pp. 83].

2.1.3.3 Condition of Macroscopic Sliding. In the preceding section it was shown that due to the contaminant films such as oxides, the shear strength of the interface is less than k. In other words if

"f" is a positive constant less than one then:

$$\text{interface shear strength} = fk \tag{2.15}$$

In Equation 2.15 when $\tau = fk$ the interface cannot resist and sliding occurs (Figure 2.9). Therefore, the condition of sliding is:

$$P^2 + \alpha f^2 k^2 = P_o^2 \tag{2.16}$$

In Equation 2.14 when pressure is zero ($\tau = k$):

$$\alpha k^2 = P_o^2 \tag{2.17}$$

Inserting Equation 2.17 into Equation 2.16:

$$P^2 + \alpha f^2 k^2 = \alpha k^2 \tag{2.18}$$

or

$$P^2 = \alpha k^2 (1 - f^2) \tag{2.19}$$

The coefficient of friction μ becomes:

$$\mu = \frac{F}{W} = \frac{fKA}{PA} = \frac{f}{[\alpha(1 - f^2)]^{1/2}} \tag{2.20}$$

When $f = 1$ (uncontaminate metals in vacuum), μ is infinity. In this condition the interface shear strength is equal to K and junction growth never ceases ($A \to \infty$). However, even a small amount of contaminant (e.g. moisture in the atmosphere) causes a sudden fall in coefficient of

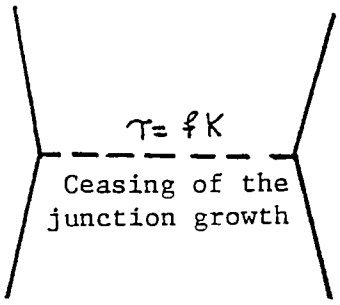

Figure 2.9 Commencement of sliding

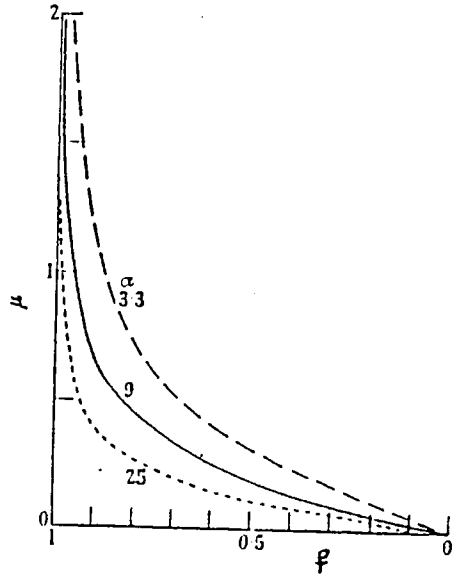

Figure 2.10 Coefficient of friction as function of f and α . The exact value of α is important only at large f.

friction (Figure 2.10). This is due to the weakening of the interface which in turn causes the ceasing of junction growth and sliding of one surface on the other.

Equation 2.20 indicates the condition for the start of gross sliding. Sliding commences when a maximum static frictional resistance is developed and the junction separates. At this point frictional resistance is zero but new junctions form elsewhere and the process is continued this way (stick-slip). The static frictional resistance persists for a distance of the order of 10^{-4} cm as sliding commences then its magnitude falls up to a distance of 10^{-3} cm [8, pp. 35], when the kinetic component of frictional resistance is reached (Figure 2.11). The magnitude of kinetic friction depends on the life of the stationary contact. It is small when the contact time is measurable in milliseconds and large when it is a few seconds but always smaller than the static friction.

2.1.4 Theory of Friction By Halling and Edwards

After Bowden and Tabor, a number of researchers were inspired by the analysis of plastic deformation of isolated asperities to develop a more advanced frictional model. Most important amongst these are Edwards and Halling [7, 9]. Considering two wedge-shaped asperities (Figure 2.12) and using slip-line and upper-bound analyses, a solution was proposed which enables the value of coefficient of friction to be obtained at each time interval during the life history of a junction interaction. In this theory, the shear and normal forces are calculated from the first contact until the asperities separate (Figure 2.13). The coefficient of friction, μ, is the ratio of the instantaneous shear force

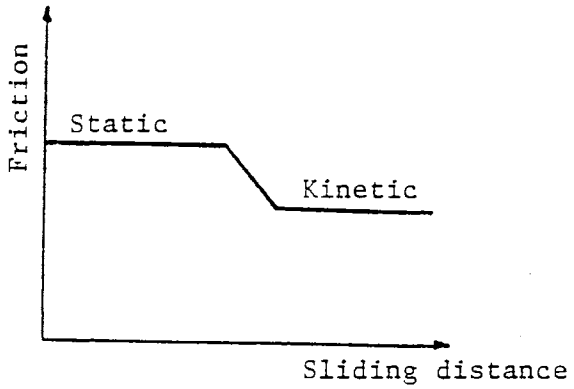

Figure 2.11 Schematic representation of static and kinetic friction

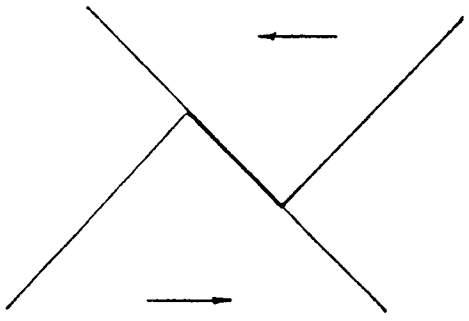

Figure 2.12 The idealized wedge-shaped asperities in Edward and Halling theory

and the instantaneous normal force. Therefore, the coefficient of friction can be calculated from Figure 2.13 and plotted against f for various junction angles (Figure 2.14). The general relationship proposed by Edwards and Halling is:

$$\mu = \left[\frac{f}{\alpha(1 - f^2)^{1/2}} + \phi\right] / \left[1 - \frac{f}{\alpha(1 - f^2)^{1/2}}\phi\right] \qquad (2.21)$$

where ϕ is a function of the geometry and f. ϕ is zero when the asperity angle is zero. This indicates that the Bowden and Tabor theory (Equation 2.20) is a special case of the Edwards and Halling theory.

2.1.5 Plastic Interaction of Neighboring Asperities

In Edwards-Halling and Bowden-Tabor theories, the deformation of each individual asperity was considered isolated. However, at high pressure, asperities make contact and their deformation cannot be viewed in isolation. By different slip line models, several aspects of this problem have been studied by Wanheim, Bay and co-workers and their results are well summarized in [2].

By a slip-line analysis under the statical loading condition, Wanheim estimated the relationship between the nominal pressure P and the ratio between real and apparent contact area β (Figure 2.15). According to this analysis, proportionality between β and P exists only at low pressure. At higher pressure, when the neighboring asperities make contact, the β-P curve bends away. At very high pressure, when the real contact area becomes equal to the apparent contact area, β becomes independent of P.

2.1.5.1 Asperity Deformation With Tangential Force. Analysis of

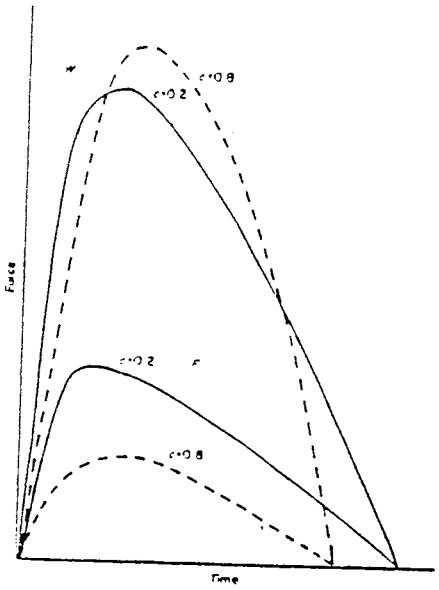

Figure 2.13 The variation of the normal force W and the friction force F through the junction life [7]

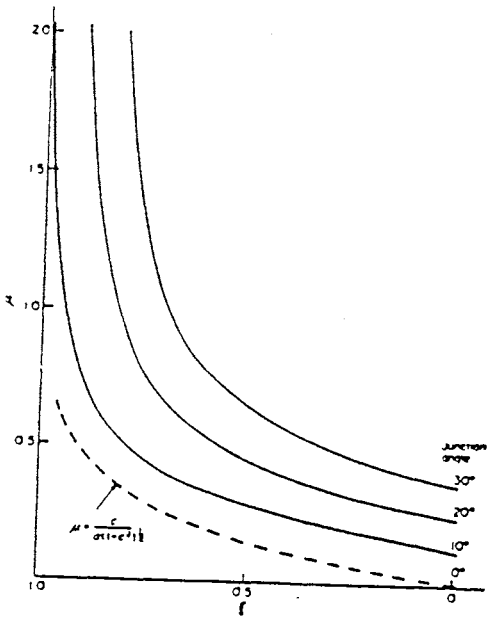

Figure 2.14 The variation of coefficient of friction with f for various junction angle [7]

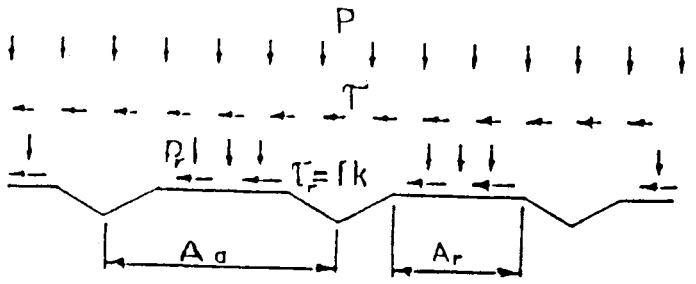

P =Nominal pressure
P_r =Real pressure
A_a =Apparent area
τ =Nominal sear stress
τ_r = Real shear stress
A_r = Real area

(a)

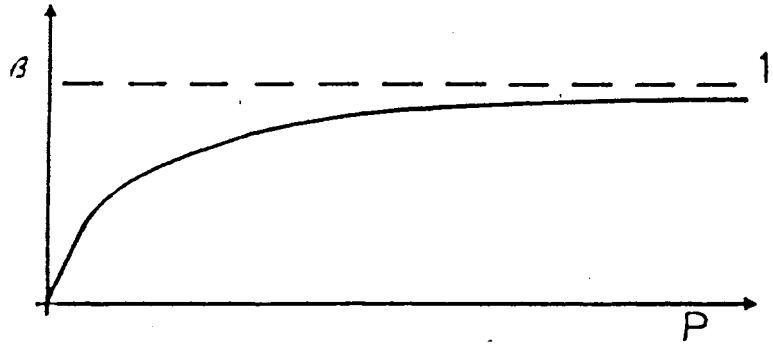

(b)

Figure 2.15 The neighbouring asperities deformation
a) Pressure and contact geometry between two rough surfaces.
b) Contact area ratio as function of normal pressure[2].

asperity deformation by Wanheim was performed under static contact where no tangential force (friction) existed. Wanheim, Bay and Peterson [2] proposed a new slip-line field taking relative sliding and friction stress in the asperity contact into consideration (Figure 2.16). Since the angle between the free surface and bordering slip-line must be 45°, it was assumed that the asperity angle γ is small and it remains small during the deformation (initial value of γ is usually less than 15°). Based on this slip-line field, the real contact area and the friction stress were computed. Figures 2.17 and 2.18 show the results of this analysis. In these figures the contact area ratio β (Figure 2.17) and the normalized friction stress τ/K (Figure 2.18) are plotted as functions of the normalized pressure P/σ_0 (σ_0 = equivalent yield stress) and friction factor f. At low normal pressure ($P/\sigma_0 < 1.5$) the contact area ratio and friction increase proportionally to the pressure. At higher pressure the neighboring asperities interaction start and the curves are no longer linear. At very high pressure ($P > 3.5\sigma_0$) the contact area ratio and friction become constant and independent of friction factor.

This friction model (Figure 2.18) includes both the Amontons Law $\tau = \mu P$ (Equation 2.1) and the Law of Constant Friction $\tau = fK$ (Equation 2.2) According to this model the Amontons Law is valid only at low pressure ($P/\sigma_0 < 1.5$). The Constant Friction Law is valid at high friction ($P/\sigma_0 > 3.5$). At the intermediate pressure ($1.5 < P/\sigma_0 < 3.5$) neither of these laws are valid. Figure 2.18 can be presented by equation:

$$\tau = f\beta K \qquad (2.22)$$

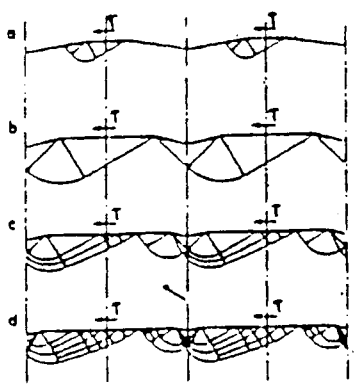

Figure 2.16 The slip line field proposed by Bay et al cosidering friction stress [2]

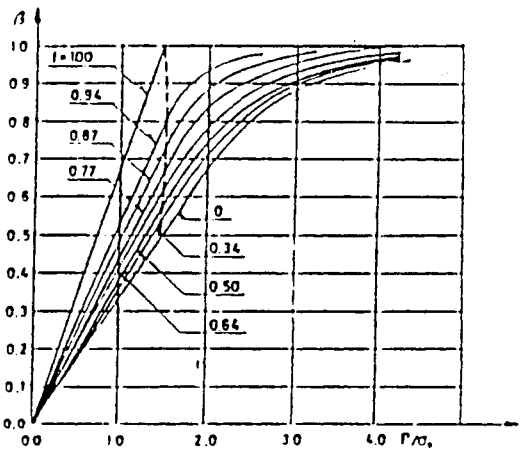

Figure 2.17 Variation of the contact area ratio [2]

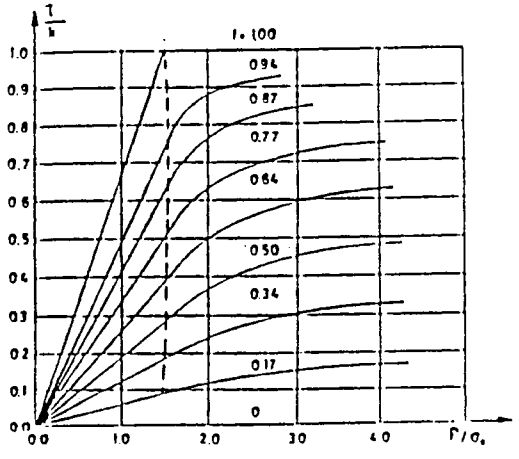

Figure 2.18 The initial friction model proposed by Bay et al [2]

2.1.5.2 Effect of Asperity Angle on Friction. In the preceding analysis it was assumed that the asperity angle remains small during the deformation. However, this assumption is valid only when friction is not too large. At high friction, asperities tilt and their angles can change. In a new slip-line field (Figure 2.19), Bay took the variation of the asperity angle into consideration. When there is no friction (Figure 2.19a), the slip-line field remains symmetric. When friction increases and acts from right to left, the slip-line field becomes asymmetric (Figure 2.19b, c) and the right asperity angle γ_R (Figure 2.20) becomes bigger than the left asperity angle γ_L. In Figure 2.20, the original asperity ACD is deformed into the quadrangle BCDE and the right-hand angle of valley increases from γ_0 to γ_R whereas the left-hand angle remains constant $\gamma_L = \gamma_0$. Bay explained that at larger pressure further change of the asperity slope is small. This development ended to a comprehensive friction model which is illustrated in Figure 2.21. In Figure 2.21 (the general friction model) friction has been plotted as functions of the initial asperity angle γ_0, friction factor f and pressure P. The influence of asperity angle is limited when f is small. For pressure below the two marked lines ($P/\sigma_0 < 1.5$ for $\gamma_0 = 0$ and $P/\sigma_0 < 0.8$ for $\gamma_0 = 15°$), friction varies proportionally to pressure and the Amontons Law can be applied. Above this limit the curves become non-linear and approach a limiting value. The analytical development of the friction curves in Figure 2.21 are beyond the scope of this work but the final expressions are:

$$\frac{\tau}{K} = \frac{P/\sigma_0}{P'/\sigma_0} \cdot \frac{\tau'}{K} \qquad (\text{for } P \leq P') \qquad (2.23)$$

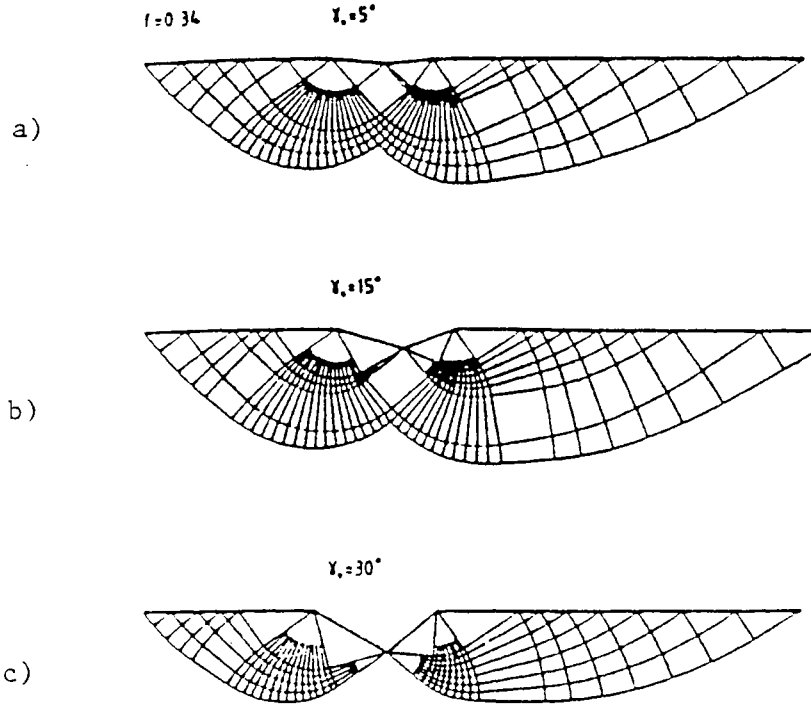

Figure 2.19 The modified slip line field proposed by Bay [2]

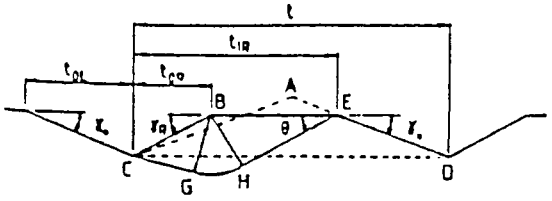

Figure 2.20 The asperity geometry before and after deformation

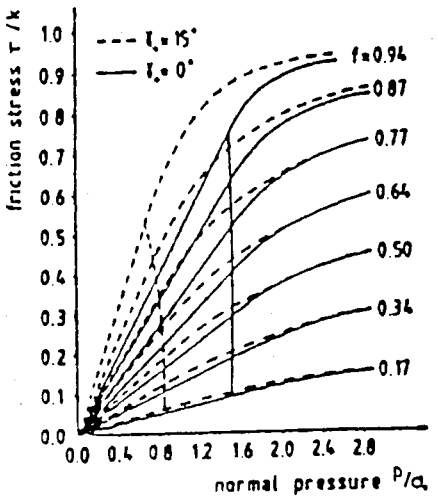

Figure 2.21 The developed friction model by Bay [2]

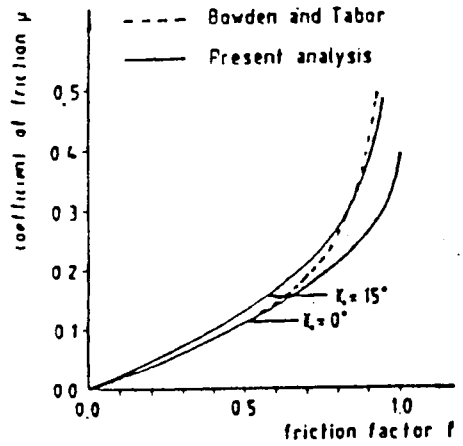

Figure 2.22 The coefficient of friction as function of asperity angle and f [2]

and

$$\frac{\tau}{K} = \frac{\tau'}{K} + (f - \frac{\tau'}{K})(1 - \exp[\frac{(P'/\sigma_o - P/\sigma_o)\tau'/K}{(f - \tau'/K)P'/\sigma_o}]) \qquad (\text{for } P > P') \quad (2.24)$$

where τ' and P' are friction stress and pressure at the limit of proportionality. Up to the limit of proportionality the coefficient of friction μ is:

$$\mu = \frac{f}{1 + \frac{\pi}{2} + \arccos f - 2\gamma_R\sqrt{1 - f^2}} \qquad (2.25)$$

Figure 2.22 compares the coefficient of friction according to Equation 2.25 and that by Bowden and Tabor in Equation 2.20 when $\alpha = 27$. A very good agreement is noticed between the Bowden and Tabor's curve and the curve for $\gamma_o = 0°$ when $f \sim 0.6$. Based on Figure 2.22 Bay proposed a simple way for the estimation of the friction factor in metal-forming. A ring compression test [38] is performed, the coefficient of friction can be estimated and then Figure 2.22 can be used to find the friction factor f.

2.2 Review of the Literature in the Inclusion of Surface Friction in the Finite Element Solutions

Due to the great influence of friction on material flow, several attempts have been made for the proper inclusion of the surface friction in metal-forming analyses. Friction distribution and orientation are the two major problems in any metal forming analysis. Depending on the methods of handling these two difficulties, three major approaches can

be found in the literature and this section is concerned with the discussion of these approaches. Also a brief description of these methods can be found in Table I.

2.2.1 Direct Method

One approach in finite element modelling of friction is the introduction of friction as the surface nodal force or surface shear stress against the motion. The conventional models in this approach adopt either the Amontons Law $\tau = \mu p$ (τ - friction stress, μ = coefficient of friction, P = pressure) or the Constant Friction Law $\tau = fk$ (f = friction factor, k = shear yield stress of the workpiece). The direction of the friction is determined to be opposite to the direction of the material flow.

Application of the Constant Friction Law or the Amontons law all along the interface causes a sudden jump in friction distribution at the neutral point, where the flow changes its direction (Figure 2.23). Experimental observations by some investigators [10, 11] in upsetting of a circular disk show a linear decrease of the friction towards zero in the center and such a jump is not likely to occur. Bay [2, pp. 26] explains that this is due to a central sticking zone (dead zone) where the shear stress is not large enough to overcome the frictional stress and sliding cannot occur. The radius of the central sticking zone was approximated [12] by the upper bound method as a function of the Diameter/Height ratio (Figures 2.24 a and b). Sometimes, because of the existence of the sticking zone, the term "neutral region" is used instead of the "neutral point".

In most cases the location of the neutral point is unknown and

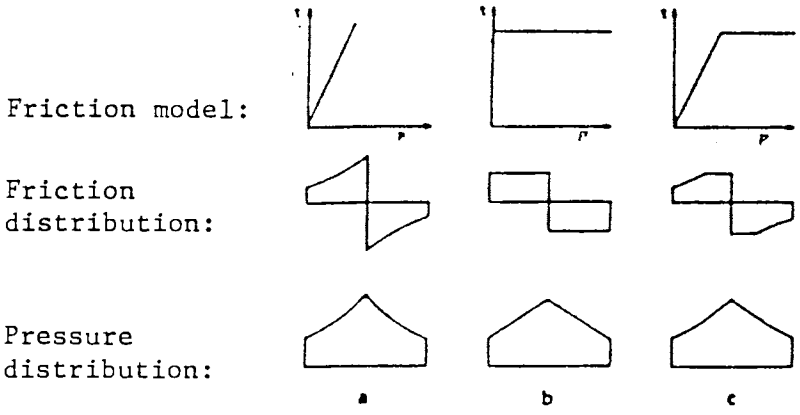

Figure 2.23 The conventionally assumed friction models and the correspondig pressure distributions in upsetting of cylinder.
a) Amontons Law
b) Constant Friction Law
c) Combination Of the Laws

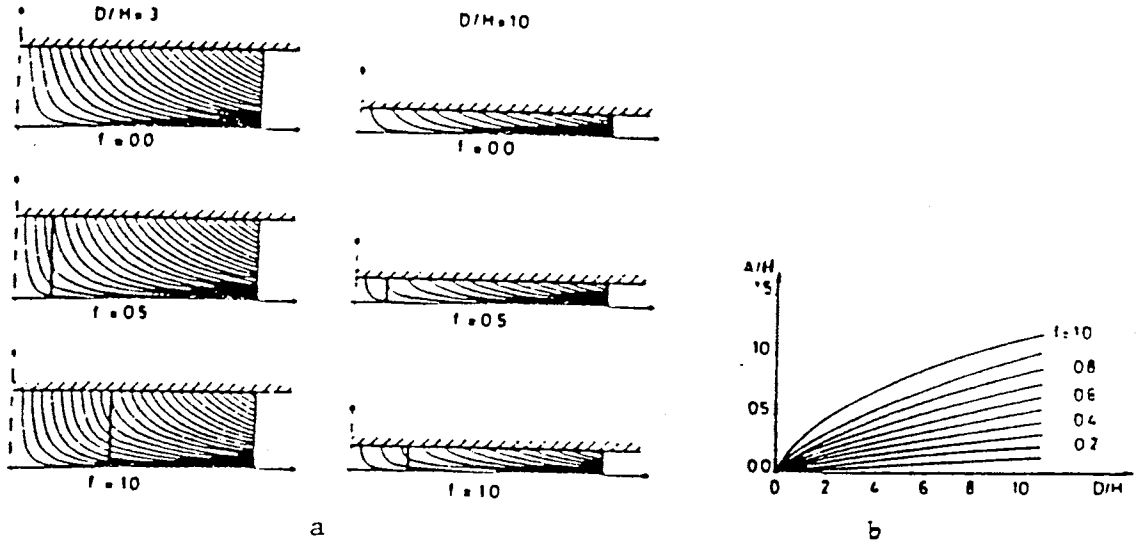

Figure 2.24 Upsetting of a circular disk [12]
a) Velocity pattern.
b) Radius of sticking region as a function of diameter/height ratio and friction factor.

therefore the flow and friction direction is unpredictable. Such a case can be observed in compression of a ring. In well lubricated conditions, the ring deforms in the same way as a solid disk and material flows radially outward at a rate proportional to the distance from the center (Figure 2.25a). At low friction, the internal diameter of the ring increases (Figure 2.25c) and at high friction, the internal diameter reduces (Figure 2.25b). Thus, due to the unpredictable flow direction, friction cannot be modelled in the compression of a ring.

In all the non-symmetric geometries, the location of the neutral point (region) is unknown and very few examples can be found in the literature which examine the effect of friction in the analysis of deformation in complex geometries by this approach. Park and Kobayashi [13] in the compression of wedge shaped blocks, modelled the surface friction as an arc tangent function of the relative velocity between the die and the workpiece:

$$\tau_s = -2/\pi \; fk\tan^{-1}(v_s/a) \qquad (2.26)$$

where: τ_s = friction stress

f = friction factor

k = shear yield stress

v_s = relative velocity between the die and the workpiece.

a = a constant several order of magnitude less than the die velocity

By using Equation 2.26, an abrupt jump in the value of friction at the neutral point is prevented (Figure 2.26).

According to Equation 2.26 the direction of the surface friction is specified in the opposite direction to the relative movement of the

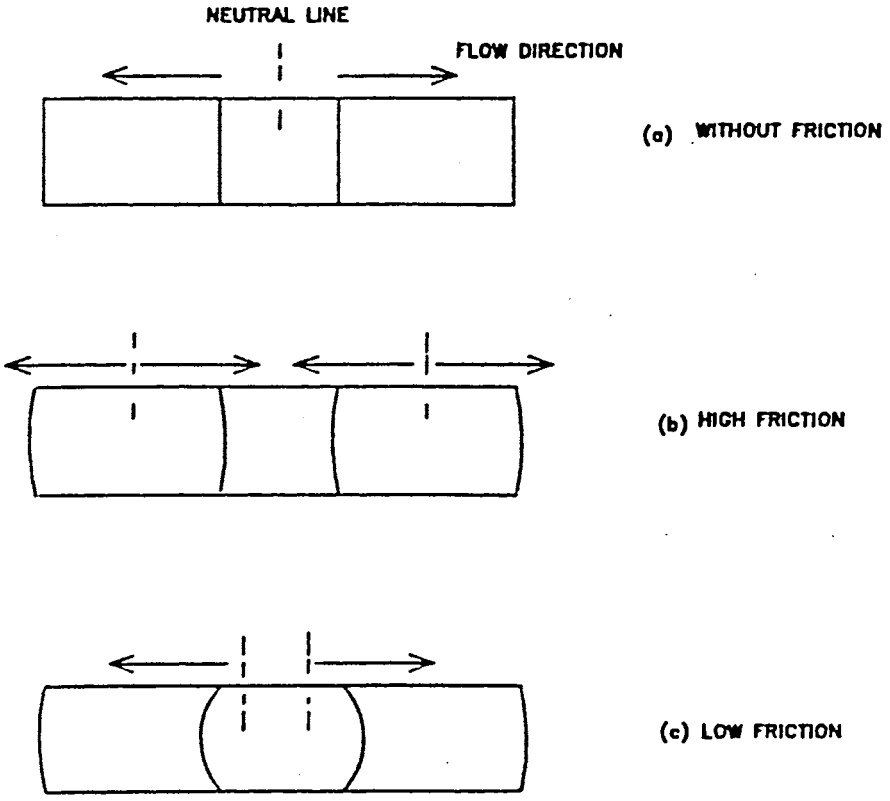

Figure 2.25 Possible mode of flow in ring compression

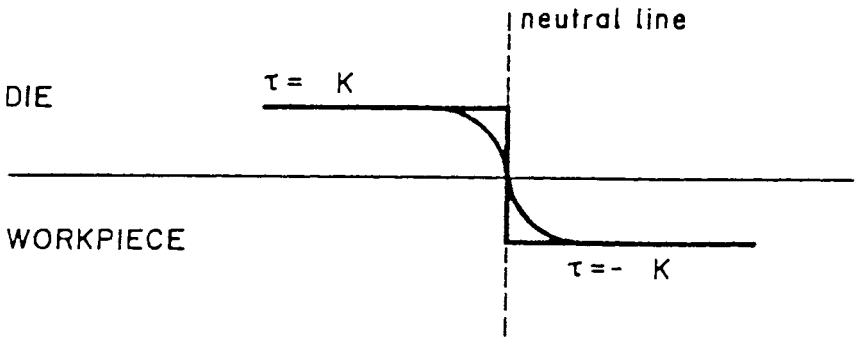

Figure 2.26 Distribution of friction according to equation 2.26 around the neutral point

workpiece with respect to the die. In finite element method, to avoid the singularity condition, at least one node should be constrained in each direction. The position of the constrained nodes have a strong influence on the velocity field and therefore, the friction direction. In the complex geometries, it is very difficult to decide the correct location of the constrained nodes (the best choice is the neutral point which is unknown) and it is not clear how Kobayashi et al considered the constraints in their analysis.

Another example of friction treatment in complex geometries is the compression analysis of wedge shaped blocks by Guo, Huang and Chen [14] (Figure 2.27). In this work friction, f, was prescribed in the following expression:

$$\tau = \begin{cases} -fk\ vs/|v_s|, & \text{when } |v_s| > u_c \\ -fk\ v_s/u_c, & \text{when } |v_s| < u_c \end{cases} \qquad (2.27)$$

where: f = friction factor

k = shear yield stress

v_s = slip at the generic point

u_c = a positive constant smaller than the average slip over the whole die/workpiece interface.

Equation 2.27, the same as Equation 2.26, is capable of explicitly giving the decreasing friction stress towards the center of the upset specimen. "f" is the function of the slip which in turn is related to the velocity or displacement field. Figure 2.28 shows some of the results of this analysis. For the theoretical results the transverse flow at the corners is too much and the longitudinal spread around the tip of the wedge which has become a thin "tongue" seems not enough.

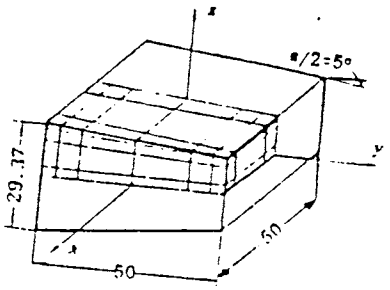

Figure 2.27 Wedge for compression and finite element discretization [14]

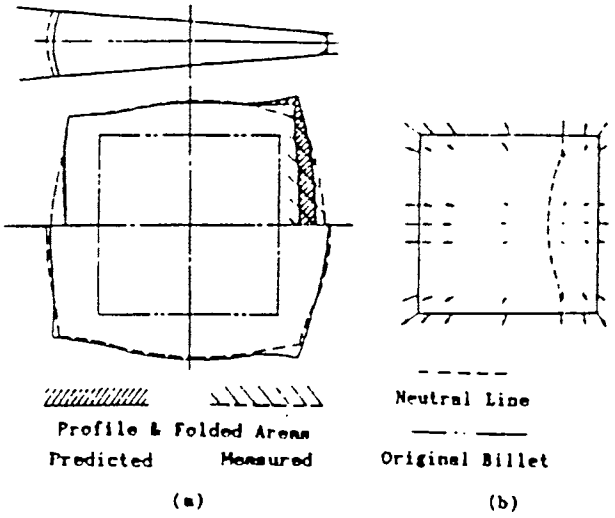

Figure 2.28 Contact surface of wedge and horizontal section through its center at 50% reduction [14]

Chen et al explained these differences due to the coarse meshes in their finite element analysis.

Rebelo et al [15] used the slab method to find the location of the neutral point in closed die forging of a turbine blade under plane strain conditions (Figure 2.29). In this method the section between the upper and the lower dies is considered subdivided into small deformation zones. Starting from the right and the left, stress distributions are obtained element by element until two distribution curves cross each other (Figure 2.30). The point of intersection of two curves is the neutral point.

Although the slab method looks successful in prediction of the location of the neutral point, it fails when the flow changes its direction at more than one point at the die/workpiece boundary (Figure 2.31).

At this point it is very clear that due to the effect of the surface flow direction, which is usually unpredictable, modelling of friction by the introduction of nodal forces or surface shear stress is not always satisfactory.

2.2.2 Surface Element Method

The second approach for the inclusion of the friction in finite element analysis of metal forming is the surface element method. This method, which is independent of the material flow direction, requires the addition of a narrow surface element between the die and the workpiece where friction is present. The surface nodes of this element are fixed to the die and the workpiece. The elemental properties are such as $\tau = fk$ (τ = shear strength of the element, k = yield shear

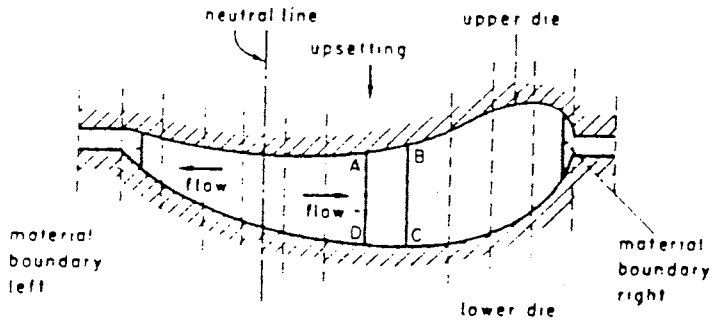

Figure 2.29 Slab method principle for plane strain closed die forging
[15]

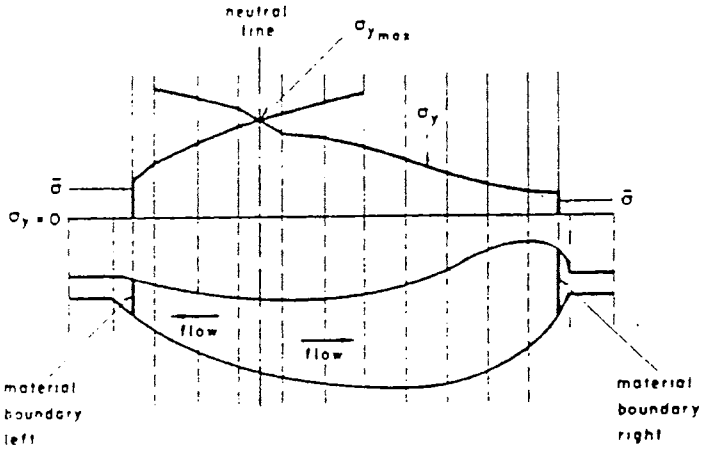

Figure 2.30 Neutral line determination with the slab method [15]

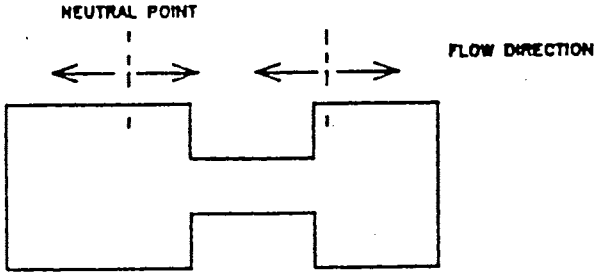

Figure 2.31 One example when flow changes its direction at more than one point

stress of the workpiece) or $\sigma_y = \mu\sigma_m$ (σ_y = yield stress of the element, σ_m = mean stress of the adjacent workpiece element).

The extra element is simply a mathematical description of the lubricant (for convenience) and is not a physical representation of the interface. Due to its practicability, several examples can be found in the literature for the simulation of the surface friction using this method.

The interface element with the specifications stated above is not appropriate for the large deformation and collapses. To remove this instability, Hartley, Sturges and Rowe [16] defined a modified factor $\beta = f/(1 - f)$ instead of f in equation $\tau = fk$. By this modification the surface element becomes stiffer and it can undergo more elongation. Also, in β technique, the forces are applied to the surface of the workpiece instead of the elemental surface nodes (Figure 2.32). The β technique was applied to the two dimensional analysis of ring compression and good agreement between the theoretical results and experimental observations was achieved. Later, the same technique was applied to the three dimensional analysis of upsetting of a rectangular block [17] and it was determined that the frictional restraint becomes too high, compared to the experimental results (Figure 2.33).

The surface element method is not influenced by the flow direction. But, even if the answers with small errors are obtained, always there is some doubt about its appropriateness because boundary conditions do not simulate the actual phenomena.

2.2.3 Slip Method

The third approach in the finite element modelling of friction is

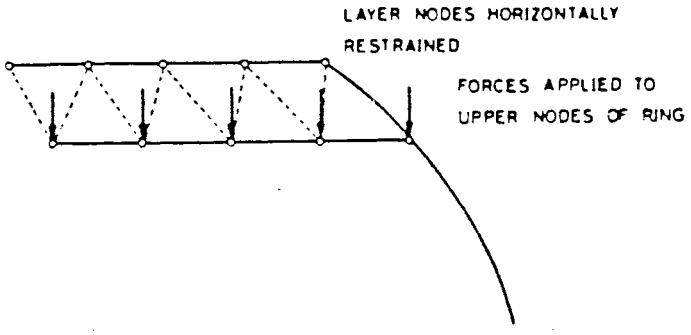

Figure 2.32 Surface element modification
[16]

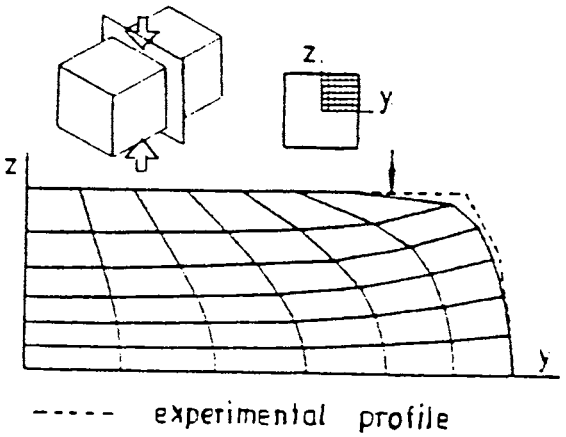

Figure 2.33 Comparison of finite element and experimental deformation at 40% reduction in height [17]

to solve a boundary problem of constrained displacements for the nodes between the die and the workpiece. Two examples of such approach are the works done by Nagamatsu et al [18] and Devoux et al [1].

Nagamatsu et al proposed a relative slip ratio for the surface nodes instead of the coefficient of friction. In case of plane strain compression of rectangular blocks, the relative slip ratio ν was defined as:

$$\nu = -(Hv_x)/(xv_y) \tag{2.28}$$

where v_s is the velocity of the relative slip between the tool and the surface of material at an instant in processing, v_y is normal velocity of the die, 2H is height of the block, and x is the distance between the center and a generic point on the surface.

Distribution of ν on the interface in Equation 2.3 was measured experimentally for different height to width ratio h_o (Figure 2.34) and the results were introduced to an elastic-plastic computation.

Devaux et al, [1] in upsetting of solid cylinders, expressed the radial displacements (u_r) on the faces in contact with the dies as

$$n + 1_{(Ur)_i} = \phi(n_{r_i}, n_{\delta_h} = h_o - n_h) \tag{2.29}$$

where n is the step of computation, i is the surface node number and h is the instantaneous height of the cylinder. This relation was experimentally evaluated by measuring the displacement of the indentation marks on the faces in contact with the die at different upsetting steps and further used as the boundary condition in an elastic-plastic finite element computation. Among the results, it was

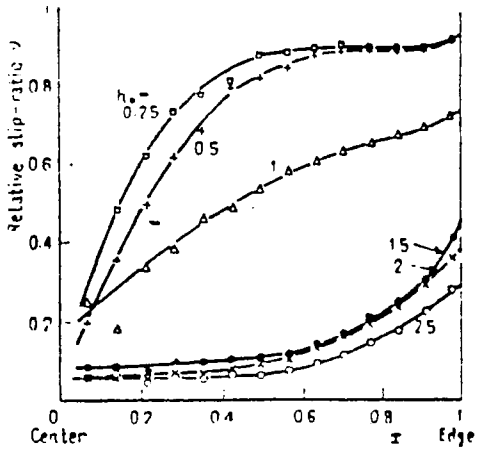

Figure 2.34 Distribution of relative slip ratio on the interface [18]

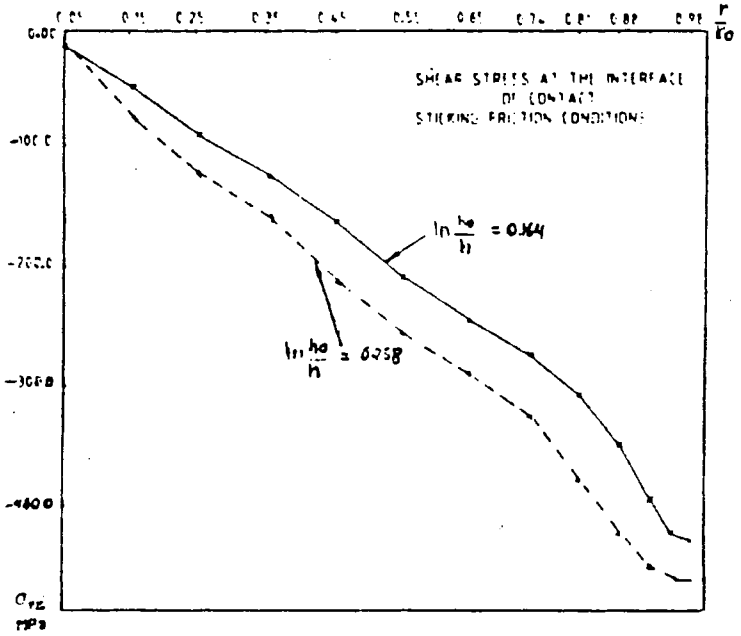

Figure 2.35 Distribution of shear stress under the die in sticking condition [1]

found that the hypothesis of a constant shear stress is not correct and its local value increases with the average strain $\varepsilon = \ln (h_o/h)$ (Figure 2.35). Also, it was found that the variation of shear strain under the die is almost linear from the center of the specimen to the half outer radius, after which the variation is parabolic up to the maximum value of r (Figure 2.36).

The main objection to this approach is the need to conduct experimental measurements prior to the computations.

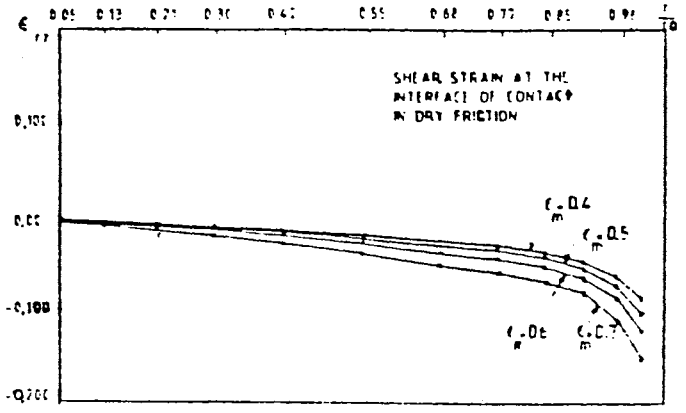

Figure 2.36 Distribution of shear strain under the die in dry friction condition [1]

TABLE I

MAJOR APPROACHES FOR INCORPORATING THE FRICTIONAL BOUNDARY CONDITIONS INTO METAL FORMING SIMULATION

Approaches	Method of modelling	Advantages	disadvantages
1	Introduction of friction as surface nodal force.	Effective if friction distribution is correct.	Fails when flow direction is unknown.
2	Surface element	Independent of the flow direction.	Unreliable.
3	Modifying the surface displacement.	simulates the actual phenomena.	Requires experimental data prior to the analysis.

CHAPTER III

AN OUTLINE OF THE PROCESS MODELLING OF FORGING

In their introduction to the "Process Modelling of Metal Forming and Thermomechanical Treatment." Rebelo et al [15] wrote the following:

> The expression process model refers to a mathematical model which has been developed to a level at which it can quantitatively describes the essential characteristics of a process and which, when implemented as a computer program, permits the stepwise simulation of the process.

Often in metal forming it is required to transform the initial geometry into a complex geometry without causing material failure or degrading material properties. The mathematical modelling provides some information to assist the forming engineer for the proper design and control of the process.

The process modelling comprises several variables which interact with each other during the plastic flow. The flow stress, the die and workpiece geometries, the friction at the tool/workpiece interface and temperature are among these variables. Due to the influence of these variables on each other it is very difficult to express the physical phenomena of a forming operation with quantitative relationships. Figure 3.1 shows the interactions of some important variables in forging process. Interactions start with the ram displacement which influences:

1. The flow stress in work hardening and strain rate sensitive material.

2. The geometry and contact area which themselves affect the heat

transfer, flow stress and friction condition.

Friction, geometry and flow stress are three major variables to be used in the analysis of deformation.

There are several approximate methods (numerical and analytical) for the analysis of deformation. Due to the assumptions made in developing the mathematical approach, none of these methods is perfect. Also, every method requires some data which must be determined by experiment. The inaccuracy of the experimental data, such as friction factor and flow stress, affect the accuracy of the analysis. With this view the exact analysis of a process is not feasible in most cases. Figure 3.2 shows the contribution of some experimental data in the forging system.

The most widely known methods among the analytical techniques are the slip line method, upper bound method and slab method.

The slip line method [19, pp. 381] is used for the analysis of deformation in rigid-perfectly isotropic solids. This method has the capability to determine the stress and the velocity fields but it fails to take into account the behavior of real material properties such as workhardening, strain rate and temperature effects.

The upper bound method was developed by Johnson [20] and Kudo [21] and it is widely applied in metal forming analysis to estimate the maximum load required to perform a certain operation. The load (power) computation in this method is based on the strain rate field considering the redundant work. The stress distribution cannot be analyzed by this method.

The slab method [15, pp. 29] can be used for the elementary analysis of stresses and loads in plane strain or axisymmetric

conditions. The velocity field cannot be determined by this method.

Several other analytical techniques in this area exist and have been well summarized in different books [19, 22, 23].

Besides the analytical techniques, several numerical methods have been developed for the analysis of deformation in metal forming. Outstanding among these are the methods using finite difference and finite element methods. Usually, finite difference technique is used for the calculation of temperature distribution and finite element method (FEM) has proved to be superior to the classical methods due to its flexibility and ability to obtain a detailed solution.

FEM was developed originally as a concept of structural analysis. The general applicability of FEM made it a powerful and versatile tool for a wide range of problems. Several computer program packages have been developed for the solution of a variety of solid mechanics problems. Some of the programs have been developed in such a manner that the same program can be used for the solution of problems belonging to different branches of engineering with little or no modification. Table II shows a summary of the more widely used packages.

In the field of plasticity, Rigid Plastic and Elastic Plastic are the two main approaches of finite element formulations. For an analysis of elastic plastic problems, the use of the plastic stress-strain matrix developed by Yamada et al [24] has been very useful. Using this matrix and the incremental variational formulations, developments have been made in the analysis of metal forming [25, 26, 27, 28]. Today, the finite element has proved to be a very effective tool in the elasto-plastic analysis of metal forming processes. However, due to the elasto-plastic property the use of large deformation is not permitted in

this approach. With this view Rigid-Plastic finite element method called "matrix method" was developed by Lee and Kobayashi [29, 30]. Rigid-plastic FEM is more effective in terms of the computation time but less accurate because of the neglection of the elastic strains at the beginning of the deformation. Some of the capabilities and characteristics of various methods are summarized in Table III. Figure 3.3 exemplifies some important information obtained by process modeling of forging:

1. Prediction of the microstructure and mechanical properties of the workpiece during and after deformation.

2. Effects of the position of the flash line on the microstructure, extraction of the workpiece from the dies after the process is finished and furthermore the material lost.

3. Flow of the material and its effects on the filling of the cavity between the dies.

4. Effect of the geometry of the preform on the material flow.

5. Initial position of the preform between the dies and its effect on the material flow and center of loading which has great influence on the press structure.

6. Prediction of the forces and the energy necessary to carry out the forging operation.

TABLE II

LIST OF MAJOR FINITE ELEMENT PACKAGES [32]

Area: / Program name:	ADINA	ANSYS	ANGUS	ASAS	ASEF	ASKA	ASOP	BERSAFE	BOSOR	CAOENSE	CHILES	DYNAL	ELAS	GIFTS	FLUSH	MAGIC	MARC	MARCS	NASTRAN	NEPSAP	NONLIN	NONSAP	PAFEC	PICES	PIPESD	PIPESTRESS	SAAS	SABOR/DRASTIC	SAQSYS	SAMIS	SAP	SHASOR/DYNAPLAS	STARDYNE	STRESS	SINUOL	VISCEL
Nonlinear continua	*	*				*		*		*							*		*	*		*		*			*	*							
Plastic analysis	*	*		*		*		*									*			*		*	*												
Fracture mechanics		*		*				*			*					*											*								
Thermal stress and creep		*		*		*		*									*		*	*			*												
Thick shells		*			*	*		*					*			*	*		*												*	*			
Piping systems		*										*					*		*						*	*					*				
Ship structures		*				*			*										*					*							*		*		*
Shock wave propagation																								*											
Weld problems																	*																		
Viscoelastic analysis		*		*		*							*				*			*			*												*
Structural optimization							*																											*		
Transient analysis	*	*				*						*					*		*		*	*	*	*				*		*	*		*		*	
Thin shells									*										*													*				
Bridge and girder systems																																			*	
Composite materials			*																*																	
Aeroelasticity																			*																	
Rotor-bearing systems										*																										
Structural stability		*			*	*			*								*	*	*	*	*								*						
Structural members and mechanical elements																			*																	
Graphics-oriented finite element program														*																						
Seismic analysis															*																					
Off-shore structures																		*																		
Frame analysis																												*						*		

TABLE III

SUMMARY OF VARIOUS ANALYSIS METHODS [31]

Method	Input: Flow stress	Input: Friction	Output: Velocity field	Output: Stress field	Output: Temperature field	Output: Stresses on tools	Comments
Slab	Average	(a)(b)	No	Yes	No	Yes	Ignores redundant work
Uniform energy	Average	(b)	No	No	No	Average	Redundant work can be included approximately
Slip line	Average	(a)(b)	Yes	Yes	No	Yes	Valid for plane-strain problems
Upper bound	Distribution	(b)	Yes	No	No	Average	Gives upper bound on loads, can determine free boundaries
Hill's	Distribution	(a)(b)	Yes	No	No	Average	Can treat 3-D problems
Finite difference	Distribution	(a)(b)	Yes	Yes	Yes	Yes	Requires considerable computer time
Finite element	Distribution	(a)(b)	Yes	Yes	Yes	Yes	Same as above
Matrix	Distribution	(a)(b)	Yes	Yes	Yes	Yes	Treats rigid/plastic material
Weighted residuals	Distribution	(a)(b)	Yes	Yes	Yes	Yes	Very general approach

(a) $\tau = \mu\sigma_n$ (b) $\tau = m\bar{\sigma}/\sqrt{3}$

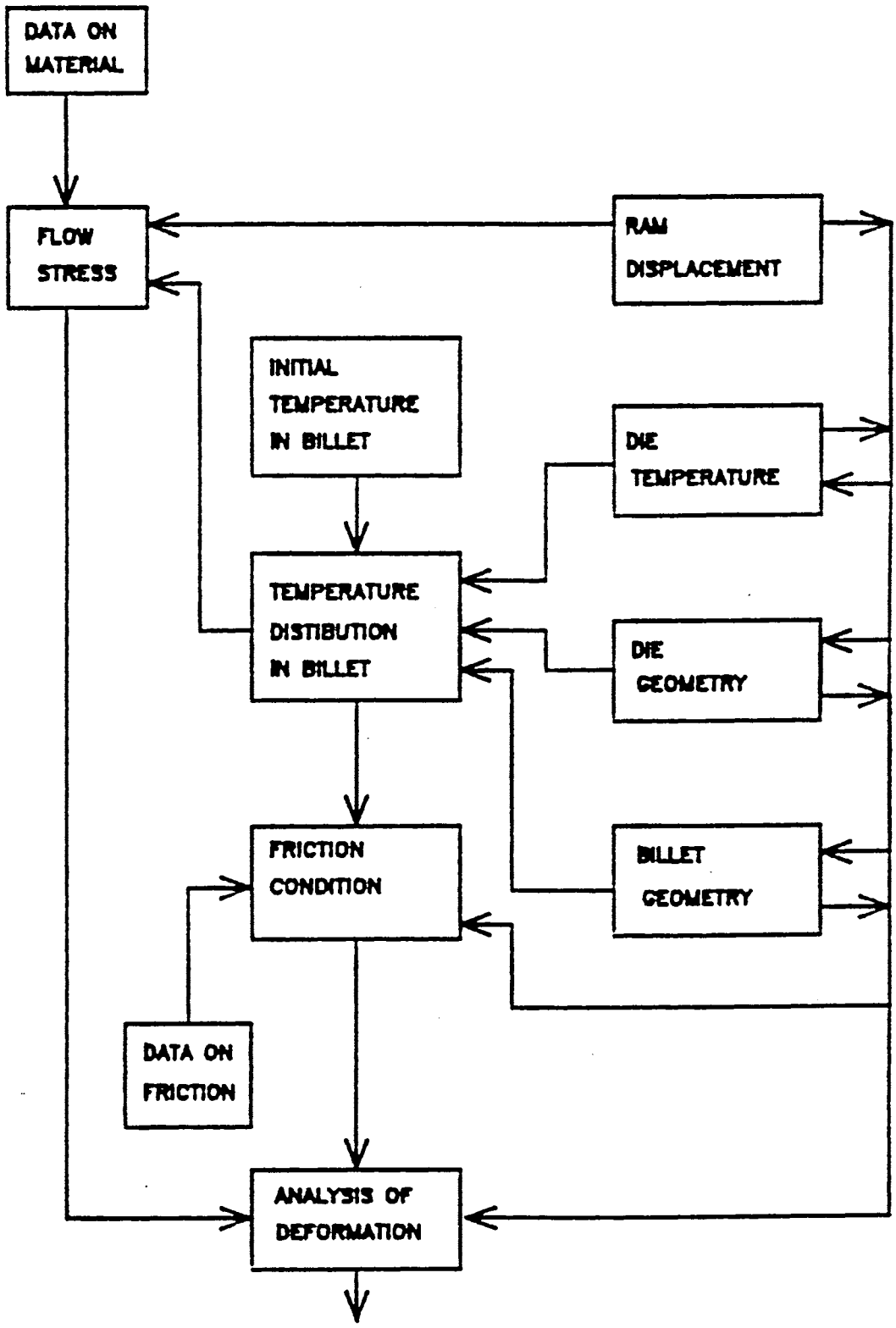

Figure 3.1 Interaction among some variables in forging

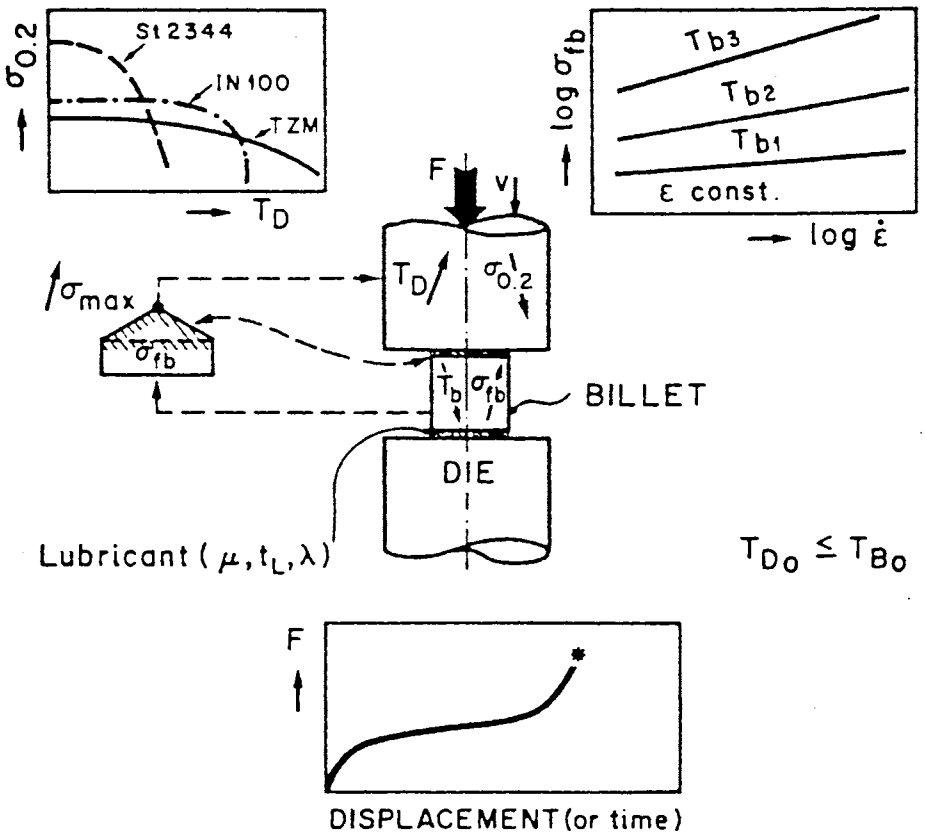

Figure 3.2 Forging system [15]

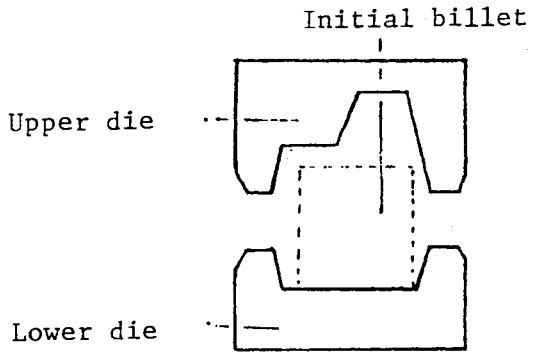

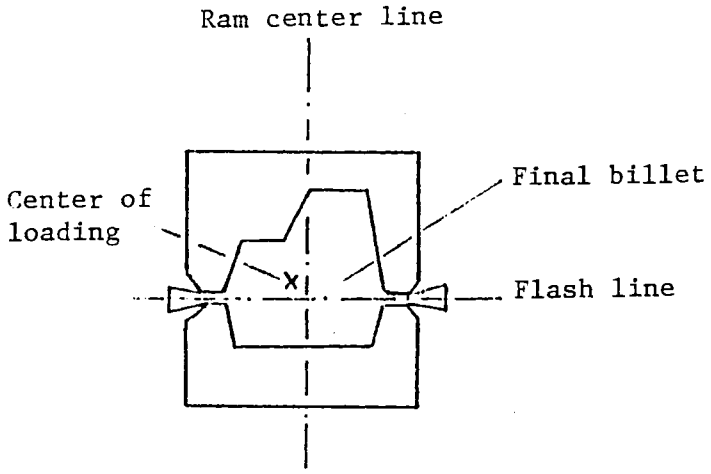

Figure 3.3 Closed die forging

CHAPTER IV

FINITE ELEMENT ANALYSIS OF ELASTIC-PLASTIC DEFORMATION

4.1 Finite Element Approach

This section introduces an elastic-plastic finite element program that has been developed for the analysis of deformation and further examination of the friction model.

Rigid Plastic and Elastic Plastic are two main approaches of finite element formulations for metal deformation problems. The Rigid Plastic approach neglects the elastic strain and cannot accurately model the early stages of a deformation when the workpiece is in the process of yielding and Elastic regions predominate. Therefore, an Elastic Plastic approach was used in the development of this program.

In the analysis of metal forming processes featuring large deformation, for the attainment of correct solutions at the end of several hundreds of incremental computation steps, possible sources of numerical errors should be carefully eliminated. The stress rate should be chosen properly in the constitutive relation and the geometric stiffness be considered adequately.

The success of the finite element method (FEM) in the solution of Elastic Plastic problems dates back to the late 1960's when the expression of the Plastic stress strain matrix (material nonlinearity) was brought out and incorporated in the standard form of FEM [24]. However, the application of this method has been largely confined to

some deformation regime where the overall strain is restricted to the order of 10^{-3} (due to the factors like neglecting the effect of rigid body rotation). Since then several attempts have been made for extending this solution to large deformations. One of the first attempts was made by Hibit, Marcal and Rice [33] who used a total Lagrangian formulation. Later, McMeeking and Rice [34] pioneered the use of an updated Lagrangian type approach which led to an improved formulation when large increments in rotation occurred.

4.1.1 Assumptions

1. Mechanical properties of the solid are time independent.
2. The stress level depends on the current degree of plastic straining (work hardening).
3. Any subsequent yield surface is parallel to the original one. In other words the work hardening model is isotropic and the Bauchinger effect is neglected.

4.1.2 Equilibrium Equations

Maybe the most general constitutive law leading to a symmetric stiffness matrix has been derived by Hill [35]. For an element of material the properties of which do not depend in any way on time:

$$\text{Stress rate} = f(\text{strain rate}) \tag{4.1}$$

where f is homogeneous and is of degree one in the components of the strain rate. If E is a homogeneous quadratic rate potential (depending on the current stress and strain history), then Equation 4.1 becomes:

$$\dot{S}_{ij} = \partial E \,/\, \partial(v_j \,/\, \partial x_i) \tag{4.2}$$

$\dot{S}_{ij}$ is the nominal stress rate and has nine independent components (non-symmetric) [28, pp. 200] and v is the velocity.

Any solution of the boundary value problem can be characterized by variational principle such that [35]:

$$\int_V \dot{S}_{ij}\, \partial(\delta v_j) / \partial x_i \, dv = \int_S \dot{F}_j \, \partial v_j \, ds + \int_V \dot{g}_j \, \partial v_j \, dv \qquad (4.3)$$

where F and g are the surface and body forces and all integration extents are in the reference configuration. By neglecting the body forces, the general form of the equilibrium equation becomes:

$$\int_V \dot{S}_{ij}\, \partial(\delta v_j) / \partial x_i dv = \int_V \dot{F}_j \, \delta v_j ds \qquad (4.4)$$

Due to the rigid body rotation the stress tensor (non-symmetric) cannot be used to represent the stress rate in constitutive equations. For clarification consider a bar under uniform tensile stress as shown in Figure 4.1.

When the bar and loads acting on it undergo a rigid body rotation with respect to the fixed coordinate system, the stress components with respect to the system change, because

$$\dot{S}_{jk} = V_i \, \partial S_{ik} / \partial X_i + \partial S_{jk} / \partial t \qquad (4.5)$$

This equation represents the material rate of change of the stress components with respect to a fixed coordinate system. The first term on the right side gives the convective part of this rate of change and the second term gives the local part. However, from the point of view of the moving body, the state of stress remains a constant. Stress rate tensor that can be used in the constitutive equation in this situation

must contain an additional term (rotary) to compensate for the local and the convective term and becomes zero. This difficulty can be avoided by choosing a reference stage that is momentarily coincident with the current state [34, 35]. In this solution it can be written [34, 35, 36] as:

$$\$ = T^{\Delta}ij - \sigma_{kj}\,\dot{\varepsilon}_{ki} - \sigma_{ik}\,\dot{\varepsilon}_{kj} + \sigma_{ik}\,v_{j,k} \tag{4.6}$$

where:

$\$$ = Nominal stress rate (non-symmetric)

$T^{\Delta}ij$ = Jaumann or corotational rate of Kirchoff stress (symmetric). This is a meaningful definition of the stress rate of which the stress components are referred to a coordinate system that participates in the instantaneous rotation of the material [36]

σ_{ij} = Cauchy or Euler stress

$\dot{\varepsilon}_{ij}$ = $1/2\ (v_{i,j} + v_{j,i})$ or Euler strain rate

In the present study no discrimination is made between the Kirchhoff and the Cauchy stress. (They differ only by terms of the order of the volume change.)

The nominal stress change in Equation 4.6 is due to the pure deformation ($T^{\Delta}ij$) and/or the change of the geometry and the orientation which act on the original state of stress.

Under this condition (new definition of stress in the current configuration) Equation 4.4 becomes [34, 35]:

$$\int_V [T^{\Delta}\partial\varepsilon_{ij} - (1/2)\sigma_{ij}\delta(2\dot{\varepsilon}_{ik}\dot{\varepsilon}_{kj} - v_{k,i}\,V_{k,j})]dv = \int_V \bar{f}\delta v_i ds \tag{4.7}$$

where all integration extents are in the current configuration.

4.1.3 Stiffness Equations

Equation 4.7 has two stiffness terms.

a. Deformation stiffness:

This stiffness arises from $\int_V T^{\Delta}\delta\varepsilon_{ij}\, dv$ and can be shown in the standard form of finite elements as

$$[K_D] = \int_V [B]^T [D] [B]\, dv \tag{4.8}$$

where

$$\{v\} = [N]\{\psi\}$$

$$\{\varepsilon\} = [B]\{\psi\}$$

$$[[B_{ij}] = (1/2)[N_i],j + (1/2)\ [N_j],i$$

ψ is defined as the rate of the nodal degree of freedom.

b. Stress correction stiffness matrix [Appendix A]:

This stiffness arises from:

$$\int_V [(-1/2)\sigma_{ij}\delta(2\dot{\varepsilon}_{ik}\dot{\varepsilon}_{kj} - v_{k,i}v_{k,j})]$$

and as was explained before is due to the changes of the geometry and can be written as

$$[K_C] = \int_V ([N_k]^T,i\ \sigma_{ij}[N_k],j - 2[B_{ki}]^T\sigma_{ij}[B_{kj}]dv \tag{4.9}$$

4.1.4 Elastic Plastic Stress Strain Matrix

In Equation 4.8, [D] is the constitutive matrix which appears as

$$\{T^{\Delta}\} = [D]\{\dot{\varepsilon}\} \tag{4.10}$$

[D] is the Elastic Plastic matrix and it is dependent on the state of the stresses and the slope of the equivalent stress versus equivalent

Plastic strain curve at each moment [24]. According to the Prandtl Reuss and in conjunction with the Von Mises criterion [Appendix B]:

$$D_{ijkl} = E/(1+\nu)[\delta_{ik}\delta_{il} + \delta_{ik}\delta_{kl}(\nu/(1-2\nu) - 3\sigma'_{ij}\,\sigma'_{kl} / (2\sigma(1+2(1+\nu)\,H' / (3E))] \qquad (4.11)$$

where:

E = Young's modulus

ν = Poisson ratio

σ'_{ij} = The deviatoric Cauchy stress

H' = Slope of the equivalent stress versus Plastic strain curve at the current value of the plastic curve

σ = The generalized or equivalent stress

δ_{ik}(Kronecker delta) = 0 IF $i \neq K$

= 1 IF $i = K$

4.1.5 Program ELPL

Based upon the preceding discussion, an interactive Elastic Plastic Program (ELPL) has been developed for the plane strain condition [Appendix D] and can be developed to plane stress and axisymmetric conditions. The input data are read interactively and echoed to the program. This program contains a main part and several subroutines. The flow chart and the description of the subroutines are included in [Appendix C].

4.1.5.1 Procedure of Computation. At the beginning of loading every part of the body is Elastic. Depending on the geometry and the boundary conditions, an increase in load causes some portions of the

material to yield while the rest are still Elastic. Departure of the stress state from Elastic to Plastic is very important and increments of displacements should be chosen somehow to make every element yield exactly at the yield point. In Plastic region the stiffness ($[K_D]$ + $[K_C]$) of the material is dependent on the state of the stress and the slope of the equivalent stress versus equivalent strain H'. It was found that our computation is very sensitive to H' at each increment and any malestimation may create instability. In some materials where H' varies by deformation, appropriate numerical techniques should be used to avoid any deviations from the original path. Figure 4.2 shows the accumulation of the errors if the slope at the beginning of each increment is used to compute $[K_D]$. In Figure 4.3, the value of H' is predicted at the end of each increment (H'_{pr}) and the average of H'_{pr} and H' is used instead of H' alone to compute $[K_D]$. H'_{pr} can be computed according to the Euler predictor method [37, pp. 331] or by other similar methods. In the present program the stress strain curve has been simplified to a form where H' is constant. This simplification reduces the computer time considerably (Figure 4.4).

4.1.5.2 The Sequence of Computations.

1. The part is divided into a number of triangular elements under plane strain conditions.

2. Elastic calculation is done by giving an incremental compression first. Nodal displacements, strains, stresses and equivalent stress of each are obtained.

3. The element with $\dot{s}_{max}$ is found and the scaling factor R is calculated by use of the following equation in plane strain conditions.

$$R = \frac{(-P + \sqrt{P^2 - 4\,O\,Q})}{2} \tag{4.12}$$

where

$P = (2AB + 2DC + 2EF + 12\sigma_{xy}\,\Delta\sigma_{xy}$

$O = (A^2 + C^2 + E^2 + \Delta\sigma^2_{xy})$

$Q = (B^2 + D^2 + F^2 + \delta^2\sigma_{xy})$

$A = \Delta\sigma x - \Delta\sigma y$

$B = \sigma x - \sigma y$

$C = \Delta\sigma y - \Delta\sigma z$

$D = \sigma y - \sigma z$

$E = \Delta\sigma z - \Delta\sigma x$

$F = \sigma z - \sigma x$

Y_o = Yield stress

4. The increments of displacements, stresses and strains are multiplied by R and σ in each element is calculated. At this stage the element with σ_{max} yielded but the rest of the elements remained in the elastic region.

5. The nodal coordinates are updated.

6. After another incremental compression the increments of nodal displacements, stresses and strains are calculated (plastic stiffness is used for the previous yielded element).

7. σ_{max} among those elements in the Elastic region in the previous stage is found and R is calculated exactly as in step 3. (σ_{max} is the maximum equivalent stress.)

8. The increments of stresses and strains are multiplied by R and added to the accumulative values of displacements, stresses and strains.

9. The nodal coordinates are updated again.

10. These loops of calculation (steps 6-9) are repeated until all the elements yielded.

11. Computation is advanced by giving proper increments of compression in the Plastic condition.

4.2 Modelling of Friction in the Present Work

In Chapter II it was illustrated that finite element modelling of friction is difficult when the geometry is non-symmetric. Indeed, the main question is how to start the analysis when direction of material flow and friction is unknown.

In this study, determination of the flow direction is based upon the concept of friction. Friction is the resistance to the relative movement between two surfaces in contact. The sources of this resistance are:

1. Asperity interlocking (Figure 2.2) which indicates sliding cannot occur until the interface shear stress reaches a critical value sufficient to cut or deform the asperities.

2. Ploughing (Figure 2.3) which indicates sliding cannot occur until the shear stress reaches a critical value sufficient to cut or deform the softer material.

3. Adhesion (Figure 2.4) which indicates sliding cannot take place until the interface shear stress reaches a critical value sufficient to rupture the adhered junctions.

These causes of friction indicate that at the beginning of deformation, the relative movement of two surfaces in contact is zero. Therefore, the analysis can be started by prescribing the tangential displacement to be zero (sticking). Sticking condition is maintained until the nodal

shear stress reaches that critical value mentioned before, the limit of static interface shear strength. Any friction model discussed in Chapter II can be examined for this critical value. Figure 4.5 illustrates the friction stress capacity (boundary between sticking and sliding) in various models.

After the commencement of sliding, the tangential force or shear stress can be applied to the free node. The direction of this force or stress is the same as that of the tangential force or stress in the previous iteration in sticking condition. Another option for determination of the friction direction is to apply a small increment of displacement after starting of sliding to find the direction of the material flow. The direction of friction is determined to be opposite to the direction of material flow.

Due to the equilibrium of the external loads, in this process, there is always one node at the boundary where shear stress is zero (or very small) and it remains in sticking condition. This node represents the neutral point. The location of the neutral point remains fixed with respect to the die. This may be permissible when deformation is small. In large deformation, due to the variation of the die/workpiece boundary, the mode of material flow changes and as well as the neutral point. Therefore, for large deformation the friction model must have enough flexibility to allow the neutral point to change its location. At each node, the conditions of sliding and sticking must be interchangeable. This type of modelling is similar to the stick-slip phenomena [6, pp 78]. According to this phenomena, a steady friction should not be expected in a sliding situation. During the sliding some asperities adhere and local shear stress increases. Shear stress

increases up to a point where the junction cannot resist and ruptures. At this point, sliding condition occurs and friction drops. The stick-slip movement continues throughout the tangential displacement. The rate of friction fluctuation depends on the properties of the metals under load (Figure 4.6) and the limits of static and kinetic friction. In finite element modelling, the limit of static friction (upper limit) can be used for initiation of sliding and kinetic friction (lower limit) for commencement of sticking.

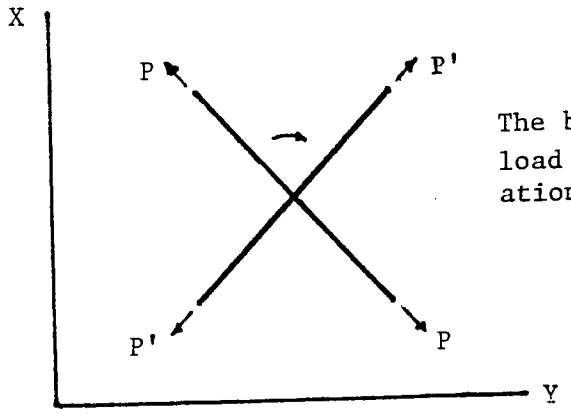

Figure 4.1 Rigid body rotation

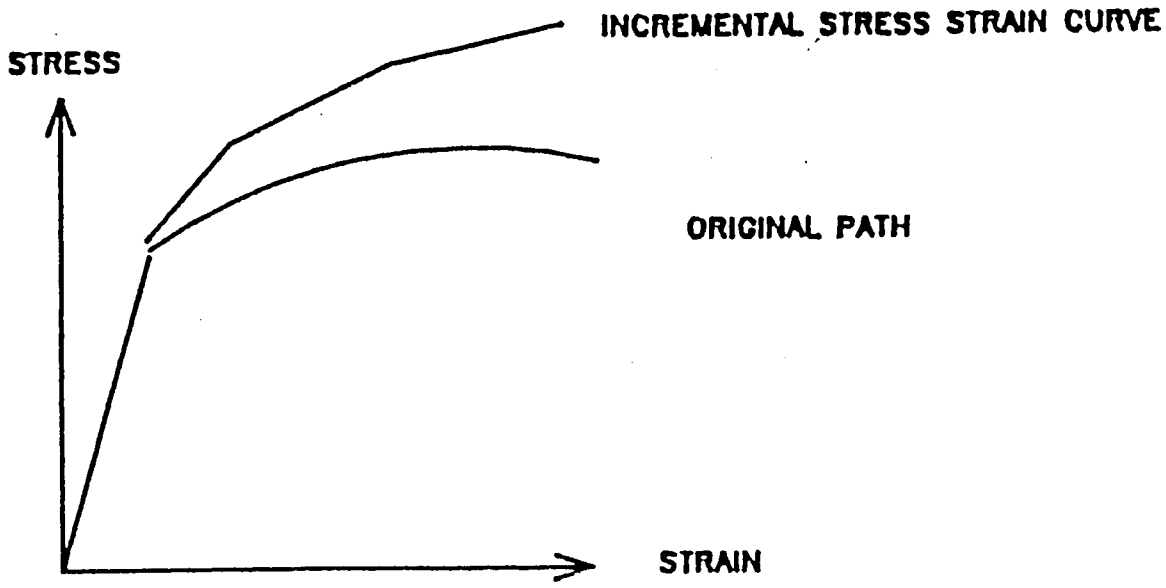

Figure 4.2 The incremental stress strain curve when the slope at the beginning of each increment is used

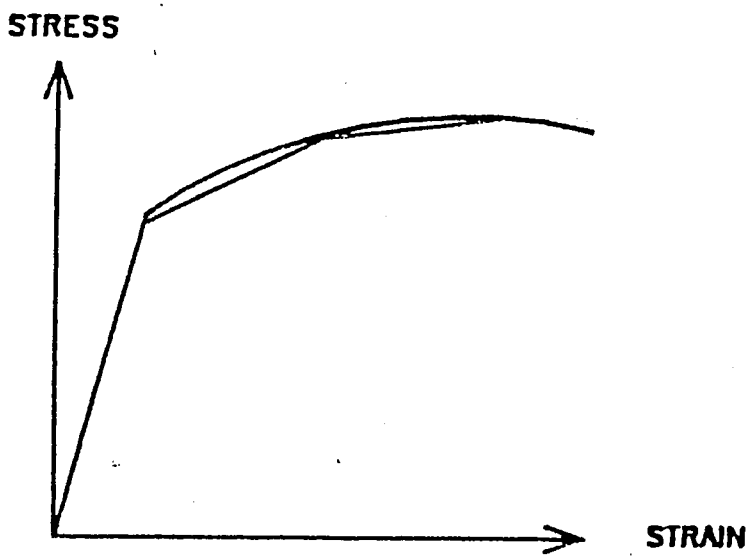

Figure 4.3 The incremental stress strain curve when the average slope is used

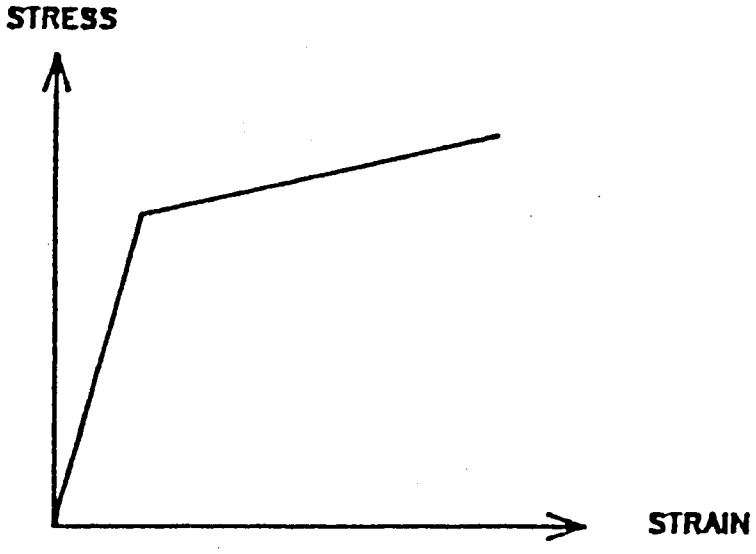

Figure 4.4 The stress strain curve in the present work

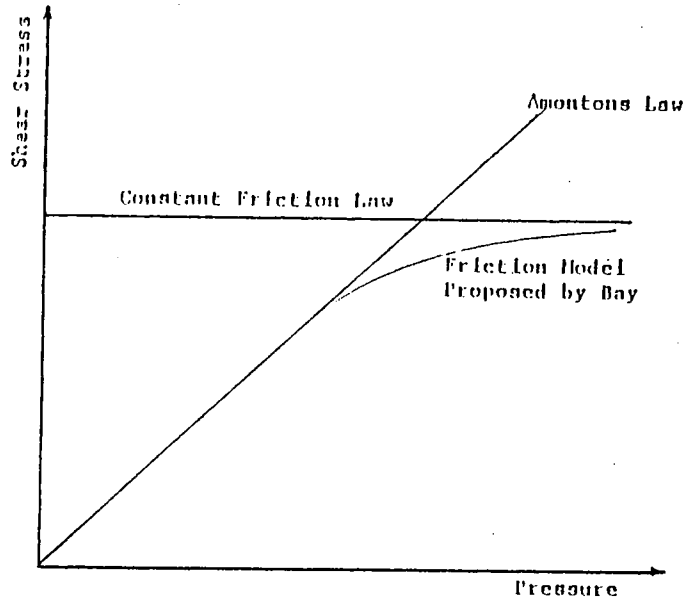

Figure 4.5 Different friction models studied in chapter 2

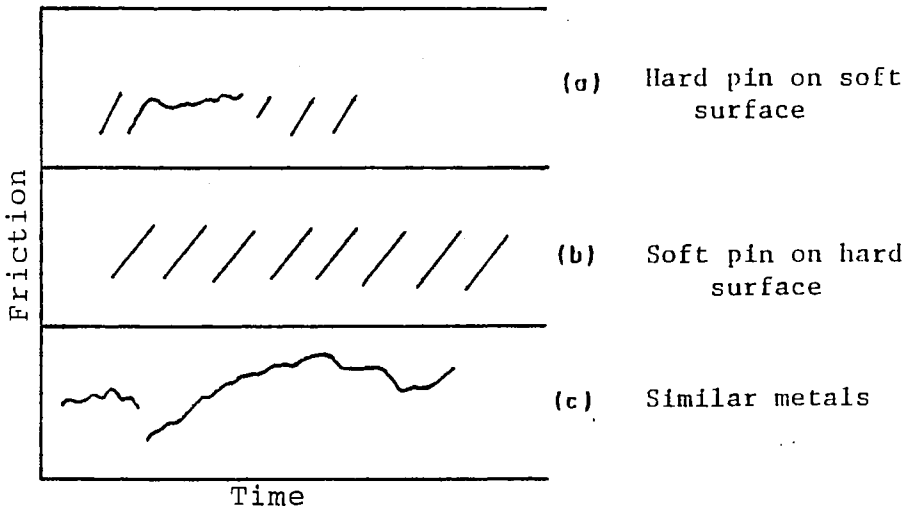

Figure 4.6 Stick slip of three metal combinations [8]

CHAPTER V

FORGING OF SYMMETRIC AND NON-SYMMETRIC PARTS

To demonstrate the numerical stability of program ELPL, analysis of compression of a rectangular block was performed. To evaluate the capability of the method of friction modelling discussed in Chapter IV, the solution to the compression of wedge-shaped specimen with frictional boundary condition was obtained. This chapter reveals the results of these analyses.

5.1 Upsetting of Rectangular Block

The solution to the upsetting of a rectangular block (2" x 2") with unit thickness under plane strain conditions was obtained. The material properties were assumed to be:

σ_o = 10,000 psi

H' = 10,000 psi

ν = 0.33

E = 10^7 psi

Due to the symmetry of the problem, a quarter section of the block was analyzed and the finite element fixed point (also the neutral point) was located at the centerline. As was mentioned before, the major objective in this analysis was to test the validity of the main program. Therefore, no friction modelling was incorporated in the computation and two simple boundary conditions were considered:

a. Sliding - 32 triangular elements and 220 increments of displacements were used to analyze the problem for 10 percent compression. This analysis was performed on the microcomputer.

b. Sticking - 162 triangular elements and 232 increments of displacements were used to analyze the problem for 10 percent compression. This analysis was performed on the VAX 780.

Figure 5.1 shows the finite element prediction of how the plastically-deforming region of the rectangular block developed in sticking condition. At 0.14 percent reduction in height, the billet had yielded fully. The finite element model first started to yield along the diagonal line from the outer corner and from the center. Subsequent deformation increased the thickness of the region. The growth of the plastic zone and the existence of the dead zone match with other works [18, pp. 328].

Figures 5.2 and 5.3 illustrate the shape of the workpiece after 10 percent compression under sticking and sliding conditions. The geometries predicted by finite element in both conditions are reasonable. In sticking condition, bulging occurred. In sliding condition the geometry remained rectangular.

Figure 5.4 illustrates the upsetting load as a function of reduction in height of the block. Load computations were based on the stresses in the elements adjacent to the interface. The maximum load in sliding condition, when loading is uniaxial, is a suitable factor to evaluate the accuracy of the finite element program. Maximum load after 10 percent compression in sliding condition by FEM was found to be 13,080 pounds. Also, this load can be found analytically as the following:

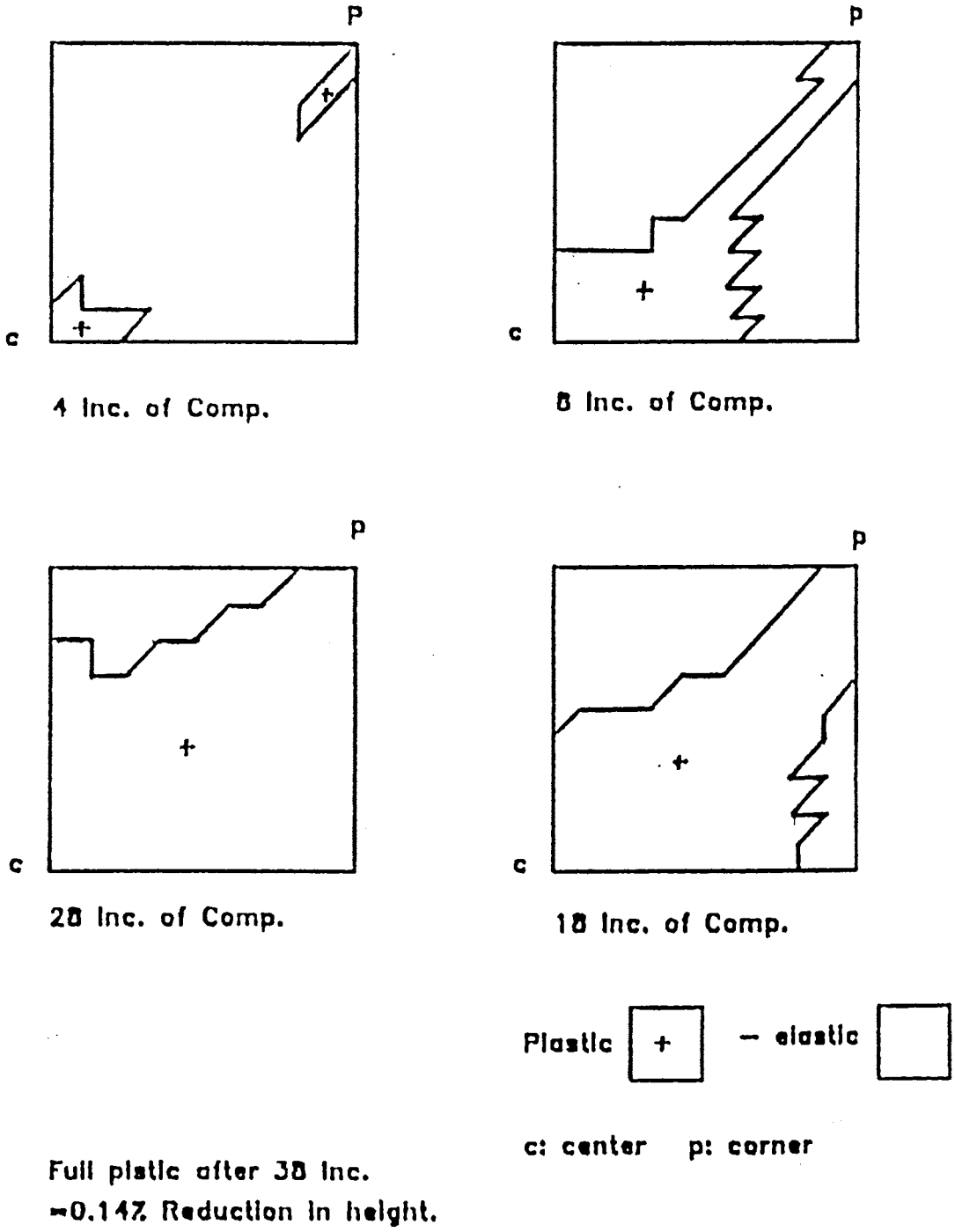

Figure 5.1 Growth of the plastic zone

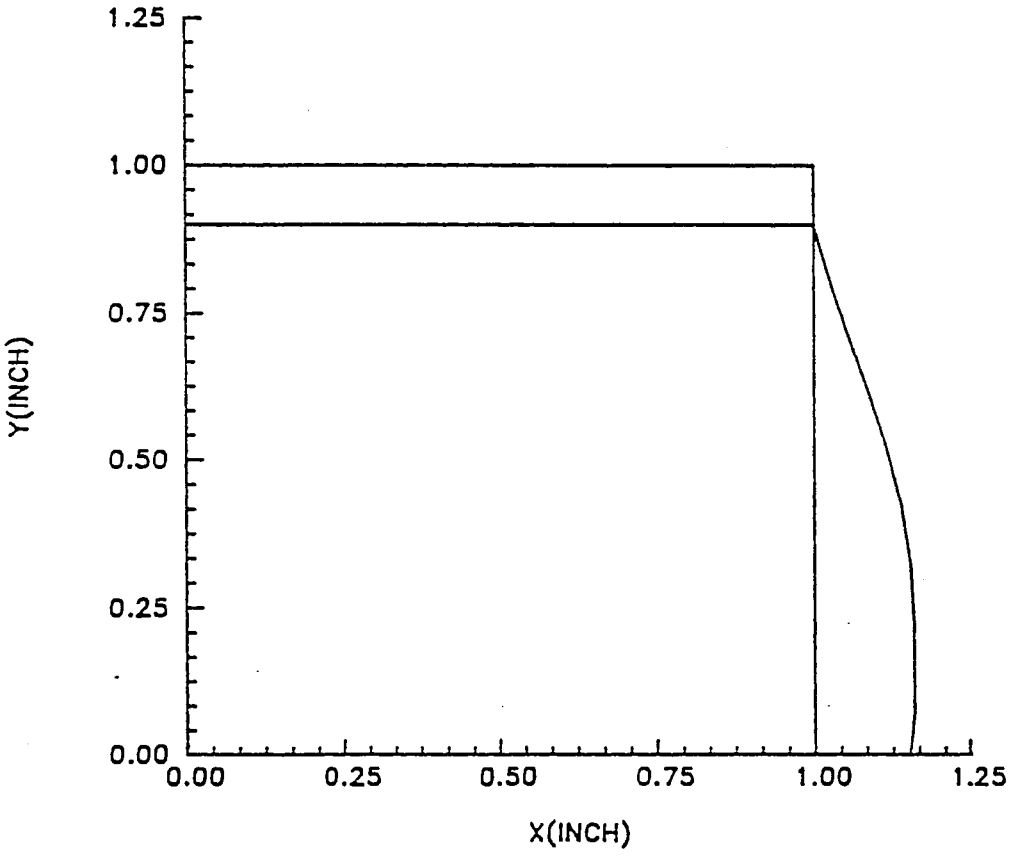

Figure 5.2 10% compression in sticking condition

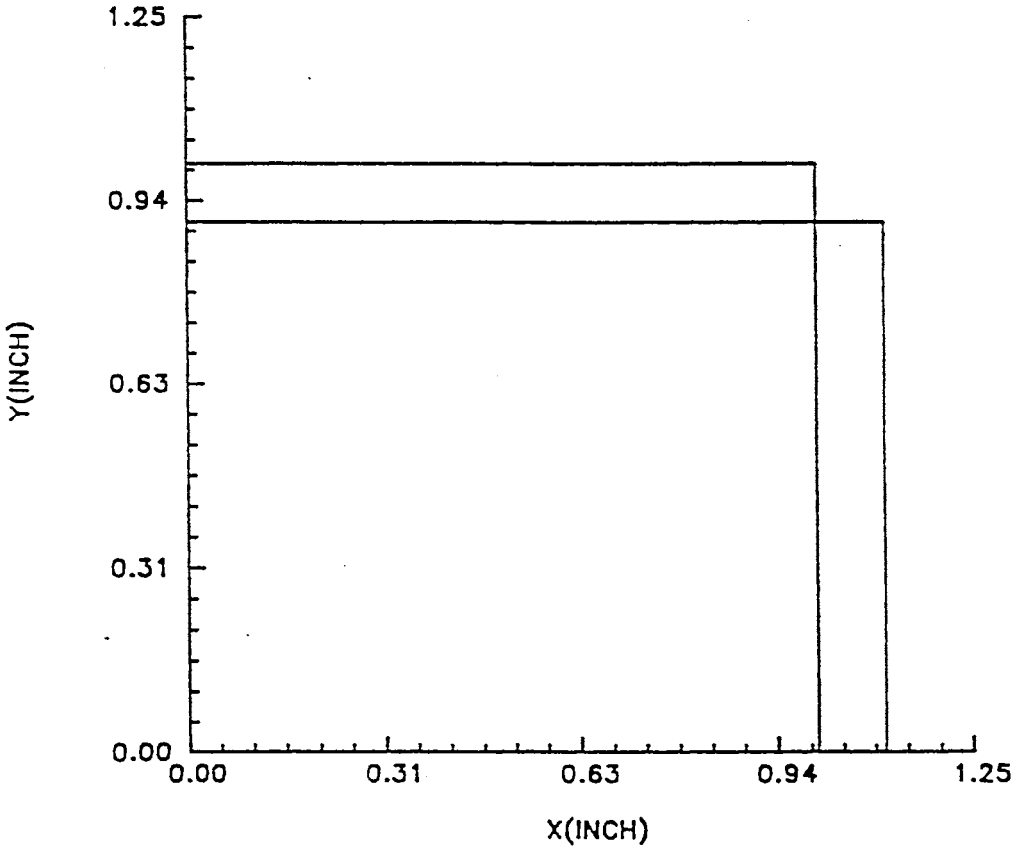

Figure 5.3 10% compression in sliding condition

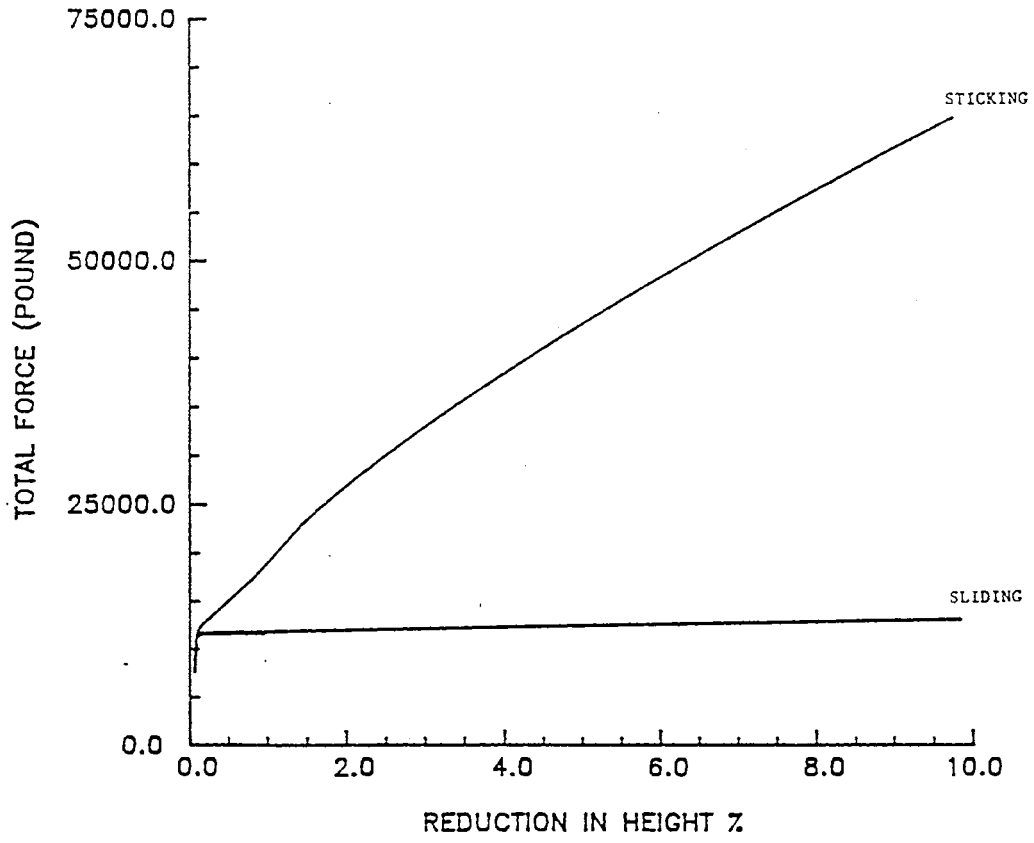

Figure 5.4 Average load in sticking and sliding conditions

For elastic, linearly strain hardening material the stress is:

$$\sigma = 10{,}000 + 10{,}000\ \varepsilon \tag{5.1}$$

After 10 percent reduction in height the true strain is:

$$|\varepsilon| = \ln \frac{1}{0.9} = 0.1043 \tag{5.2}$$

Therefore, the strength level that the material exhibits at this strain is:

$$\sigma = 10{,}000 + 10{,}000\ (0.1043) = 11043\ \text{psi} \tag{5.3}$$

The surface area A, after 10 percent reduction in height (for unit thickness), when the volume remains constant is:

$$1 \cdot 1 = A \cdot 0.9 \tag{5.4}$$

$$A = 1.11\ \text{in}^2 \tag{5.5}$$

According to the Maximum Shear Stress criterion [40, pp. 72], the force required is:

$$F = \sigma A = (11{,}043)(1.1111) = 12{,}270\ \text{lbs} \tag{5.6}$$

According to the Von Mises Criterion [40, pp. 74] the force required is:

$$F = (1.15)(11{,}043)(1.1111) = 14{,}110\ \text{lbs} \tag{5.7}$$

The predicted load by FEM (13,080 lbs) is acceptable because it is between the loads obtained by two valid theories. The percentage of error with respect to the Maximum Shear Stress Criterion is +6.7. The percentage of error with respect to the Von Mises Criterion is -7.2. These are the errors when only 32 triangular elements are considered in

the analysis. It is obvious that the accuracy of the analysis changes when the number of elements changes.

5.2 Plane Strain Compression of Wedge-Shaped Specimen With Frictional Boundary Conditions

The solution to the upsetting of a wedge-shaped specimen (Figure 5.5) under plane strain conditions was obtained. The material was AL 6061-O. One reason for choosing such geometry was the convenience in the manufacturing of the specimen. Also, compression of the wedge-shaped specimen is used in practice for workability and microstructural studies in forging [44, pp. 281]. Compared to the symmetric geometries, the boundary conditions in this analysis are more complex. In other words, the location of the neutral point and the friction direction are unknown prior to the computations. In Chapter IV a general methodology was proposed for handling the problem of the neutral point and the frictional boundary conditions in non-symmetric geometries. The main purpose of this analysis is to check the capability of the cited methodology in handling of such complex boundary conditions. Appendix E contains some experimental and numerical results regarding the materials discussed in this section.

5.2.1 Boundary Conditions

Figure 5.6 illustrates the boundary nodes. Friction exists at the nodes common between the die and the workpiece. During the deformation, some of the free nodes come in touch with the dies. Also, it is possible that some of the common nodes disengage. The condition of friction at the nodes in touch with the die and control of the boundary

nodes regarding their positions with respect to the die (engaged or disengaged) are the important parts of the boundary conditions in this analysis.

5.2.1.1 Friction. During the deformation, the effect of friction was incorporated to the die/workpiece boundary as follows:

a. Condition of friction at the beginning of deformation is sticking (boundary nodes are fixed to the die).

b. When the nodal shear stress reaches the maximum static frictional resistance, that particular node is free to move tangentially. The Amontons/Coulumb Law $\tau = \mu P$, the Constant Friction Law $\tau = fk$, and the Equations 2.23 and 2.24 were examined as the maximum limit of sticking condition.

c. After commencement of sliding and until the end of computation, the nodal frictional force is computed and applied to the corresponding node. Friction force is computed according to the same model which is used to determine the limit of sticking condition. The friction force direction is opposite to the flow direction. Always, due to the equilibrium of the external loads, there is one node at each common boundary where the shear stress is very small. This particular node remains in sticking condition and acts as the neutral point.

5.2.1.2 Control of the Boundary Nodes. During the compression process, the boundary nodes were controlled as follows:

a. At the die/workpiece boundary, the normal relative displacement at each node is zero. In other words, the boundary nodes are not allowed to move into the die.

b. At each increment of compression, the coordinate of each free

node is checked and if any node comes in contact with the die surface, it is considered to stick to the die.

c. At each increment of compression, the normal stresses of the boundary nodes are checked. If the nodal normal stress is positive, the corresponding node is allowed to separate from the die and friction force is zero.

5.2.2 Finite Element Approach

The boundary conditions cited in sections 5.2.1.1 and 5.2.1.2 were incorporated to Program ELPL. One hundred and four nodes and 171 triangular elements were used in this analysis. The mesh system was according to Figure 5.7.

5.2.3 Experimental Procedures

Some experiments were performed to obtain the required data regarding the material properties and frictional boundary conditions. Also, compression of the wedge-shaped specimen under plane strain condition was performed for evaluation of the results obtained by FEM.

5.2.3.1 Mechanical Properties of the Material. Material was initially AL 6061-T651. Following a general annealing procedure [39], it was transformed to AL 6061-O. To determine the stress-strain relation in compression, three compression tests were performed on cylindrical specimens with a 3/4 inch diameter and 3/4 inch height (Figure 5.8). The results of these tests are included in Appendix E. For each specimen, compression was carried out between two flat and

polished steel platens. To eliminate the effect of the material strain rate sensitivity, the compression was carried out very slowly. PTFE sheets were used as the lubricant between the platens and the specimens to eliminate the influence of barreling. The stress-strain relation in tension for AL 6061-0 is [40, pp. 35]:

$$\sigma = 30{,}000\ \varepsilon^{0.2} \tag{5.8}$$

From the combination of the compression tests and Equation 5.8, the simplified form of the stress-strain relation was determined as in Figure 5.9. This figure was utilized as a part of the input data to the finite element program.

To evaluate the effect of the material nonhomogeneity, two identical parts were cut from a block of aluminum (AL 6061-T651). After annealing, the parts were compressed under two different directions (Figure 5.10). No significant difference was found in the magnitude of barreling between the two specimens (less than one percent). The difference between the compression loads was around four percent. As in this analysis the normal nodal displacements are prescribed at the boundary rather than the loads, it can be said that the effect of the material nonhomogeneity is negligible on the final geometry (compared to the friction effect).

5.2.3.2 Data on Friction. In order to determine the frictional behavior at the boundary, the ring compression test was performed (Figure 5.11). This method, which has gained wide acceptance in metal forming, was proposed by Male and Cockcroft [38]. By compressing the rings of 3/4" outer diameter; 3/8" inner diameter and 1/4" height, the coefficient of friction in dry condition was found to be $\mu = 0.21$. This

value was obtained from the percent reduction in height and the percent reduction in the internal diameter (Figure 5.12). Three rings were compressed; the coefficient of friction $\mu = 0.21$ is the average of the three results. The rings were compressed very slowly between two flat and parallel steel platens. Each platen was ground by the surface grinder in two cross directions. The rings were cut by the milling machine. The parallelness of the ring faces were checked by the vernier caliper. Before performing each compression test, all the marks on the machined surfaces of the rings and the platens were removed with very fine sandpaper. Also, the surfaces were degreased using acetone. The rings were initially AL 6061-T651, but after all the machining processes, they were transformed to AL 6061-O.

The other data required for the determination of the frictional behavior at the boundary is the friction factor "f". The conventional method for the estimation of "f" is the Equation 2.20 which has been illustrated as the dashed line in Figure 2.22. According to this method, for $\mu = 0.21$, the friction factor is found to be $f = 0.75$. The other methods for determination of "f" are the solid lines in Figure 2.22 which were proposed by Bay. According to these lines two other values are estimated for "f".

$f = 0.8$ when the asperity angle is zero degrees

$f = 0.7$ when the asperity angle is fifteen degrees

Based upon these results (μ and f), four different models were found as the limit of the sticking condition cited in section 5.2.1.1. These models have been illustrated in Figure 5.13 and can be explained as follows:

a - Amontons Law: this limit has been found simply by the

substitution of $\mu = 0.21$ into $\tau = \mu P$.

b - Constant Friction Law: this limit has been found by the substitution of f and k into to the equation $\tau = fk$. Value of f in this equation is 0.75 which was found by the traditional method cited above. k is the shear strength of the material and it can be shown as

$$k = \frac{1}{\sqrt{3}} \sigma_o$$

According to the Distortion Energy Criterion (Von Mises), the yield stress σ_o under the plane strain condition is

$$\sigma_o = 1.15\ \sigma' = (1.15)(12{,}000) = 138{,}000$$

where $\sigma' = 1{,}200$ is the uniaxial yield stress and its value was found in section 5.2.3.1. Therefore, according to the Constant Friction Law, the limit of sticking condition can be written as:

$$\tau = (0.75)(\frac{1}{\sqrt{3}})(13{,}800) = 5{,}976 \text{ psi} \qquad (5.9)$$

c - Theory of friction by Bay. Based upon the discussion in section 2.1.5.2, friction changes linearly with pressure up to the limit of proportionality (P'/σ_o). The limit of proportionality for the asperity angle zero degree is 1.5 and for the asperity angle fifteen degrees is 0.8. Up to the limit of proportionality, friction variation can be found according to the equation $\tau = 0.21P$ or equation 2.23. Beyond the limit of proportionality equation 2.24 must be used:

$$\frac{\tau}{k} = \frac{\tau'}{k} + (f - \frac{\tau'}{k})\left(1 - \exp\left[\frac{(\frac{P'}{\sigma_o} - \frac{P}{\sigma_o})\frac{\tau'}{k}}{(f - \frac{\tau'}{k})\frac{P'}{\sigma_o}}\right]\right)$$

For asperity angle equal to zero, the elements of this equation were specified as the following:

σ_o = 13,800 psi (effective yield stress)

P'/σ_o = 1.5

P' = (1.5)(13,800) = 20,700 psi (pressure at the limit of proportionality

τ' = (0.21)(20,700) = 4,347 psi (friction at the limit of proportionality

f = 0.8

k = $(1/\sqrt{3})(13,800)$ = 7,967 psi

substituting these values into the equation (2.24)

$$\tau = 4,347 + 2,026\left(1 - \exp\left[\frac{(1.5 - \frac{P}{13,800})}{0.7}\right]\right) \qquad (5.10)$$

For asperity angle equal to fifteen degrees, the elements of equation 2.24 can be found as the following:

σ_o = 13,800 psi

P'/σ_o = 0.8

P' = (0.8)(13,800) = 11,040 psi

τ' = (0.21)(11,040) - 2,318 psi

f = 0.7

k = 7,967

substituting these values into the equation (2.24) it can be written:

$$\tau = 2,318 + 3,259\left(1 - \exp\left[\frac{(0.8 - \frac{P}{13,800})}{1.125}\right]\right) \qquad (5.11)$$

According to these analyses, the friction models proposed by Bay can be

shown as the following:

For asperity angle = 0°

$$\tau = 0.21\ P \quad (P \leq 20{,}700)$$

$$\tau = 4{,}347 + 2{,}026\ \left(1 - \exp\left[\frac{(1.5 - \frac{P}{13{,}800})}{0.7}\right]\right) \tag{5.12}$$

For asperity angle = 15°

$$\tau = 0.21\ P \quad (P \leq 11{,}040\ \text{psi})$$

$$2{,}318 + 3{,}259\ \left(1 - \exp\left[\frac{(0.8 - \frac{P}{13{,}800})}{1.125}\right]\right) \tag{5.13}$$

5.2.3.3 Plane Strain Compression Test. Using CNC machine, a steel die was made for plane-strain compression of the wedge-shaped specimens (Figure 5.14). The specimen was confined by two side walls, each 1-1/4 inches thick. PTFE sheets were used to eliminate the friction between the side walls and the specimen faces. The die/specimen surfaces in contact were polished with fine sandpaper and degreased with acetone prior to each test (the same as the ring compression tests). The compression was carried out very slowly up to ten percent the height of the specimen. The compression testing machine was MTS with 55 KPS

load capacity. The specimen dimensions were according to Figure 5.5. A total of 8 specimens were compressed. Among them, three of the best (the most accurate in reduction in height) were chosen for the final results. At different steps of compression, the load and the displacement were written down. After ten percent reduction in height (0.05 inches) in each test, the amount of the compression was measured by the vernier caliper and compared to the amount of the compression shown by LVDT on MTS at the end of the test. From this comparison, a correction factor was found and all the displacements shown by LVDT at the intermediate steps were multiplied by this factor and corrected. The results of these tests have been included in Appendix E. Figure 5.15 shows one of the deformed specimens inside the die. To demonstrate the mode of deformation in the specimen, some lines were drawn on the specimen before the compression. In Figure 5.15, the lines on the bottom die indicate the initial positions of the lines on the specimen. By comparing the position of each line to its initial position the amount of slip between the die and workpiece can be determined at each point. The slip between the bottom die and the specimen at lines 3 and 4 from the left is almost zero. Therefore, the neutral point must be located in this area.

5.2.4 Results of the Analysis

The friction models found in section 5.2.3.2 were examined as the boundary between the sticking and the sliding conditions (cited in section 5.2.1.1). In these examinations, the Coloumb/Amontons Law failed and could not provide any result. The cause of this failure was the high hydrostatic pressure in the forging process. Figure 5.16 helps

to describe this problem. According to the model $\tau = \mu P$, at some portions where P is very high (a multiple of the yield stress), τ becomes very big. In other words, the limit of the sticking condition becomes very high. As the maximum limit of the shear stress is the bulk shear strength of the material ($\tau = 1/\sqrt{3}\sigma_o$), sliding never occurs at these zones. The permanent condition of sticking at some regions assists to increase the pressure P in the other regions previously slid. The friction force applied in the sliding condition is computed according to $\tau = \mu P$. Therefore, by increasing the pressure the friction stress increases and it sometimes reaches a value beyond the shear strength of the material ($\tau = 1/\sqrt{3}\sigma_o$), thus causing failure.

Figure 5.17 reveals some numerical results regarding the rest of the friction models examined in this methodology. The amount of the normalized barreling w/L resulting from the Law of Constant Friction is higher than the experimental result. Also, the forging load is much higher than the real value when $\tau = fk$ is applied.

Generally it can be said that the Constant Friction Law revealed some over-strength at the interface. This had been predicted prior to the analysis. According to the model $\tau = fk$, friction reaches a high degree even when the pressure is zero. Therefore, sliding occurs late which, in turn, makes the barreling and the load very high. To demonstrate the sensitivity of the present analysis to the limit of sticking, variation of the shear stress at node number 2 are illustrated in Figures 5.18 and 5.19. In Figure 5.18 (Constant Friction Law), sliding commences when the shear stress reaches 6,000 psi. In Figure 5.19 (Bay, $\gamma = 0°$) sliding takes place when the shear stress reaches 3,500 psi. The high value of sticking limit in Figure 5.18 causes

higher barreling and forging load. The predicted load and w/L (Figure 5.17) are close to the real values when the friction model proposed by Bay ($\gamma = 0°$) is applied. The predicted results obtained by using the friction model proposed by Bay for $\gamma = 15°$ is much less than the real values. One may guess that friction must increase when the asperity angle increases and the results obtained in these analyses are not logical. Conditions exemplified in Figures 2.20 and 2.21 may result in such erroneous conclusions. According to Figure 2.20, when the asperity angle γ increases, the junction area BE increases. Therefore, friction must increase. Also, Figure 2.21 reveals that for a certain friction factor f the friction stress is higher when the asperity angle is bigger. But in Bay's friction analysis, the asperity angle and the friction factor are not independent. Figure 2.22 reveals that for the higher asperity angle the friction factor is less. Also, when the asperity angle is high, the limit of proportionality P'/σ_0 (page 24) is less. When the asperity angle is bigger, the lower friction factor and limit of proportionality cause the friction curve to bend off earlier and to approach a smaller value (Figure 5.13).

Figure 5.20 reveals the variation of the forging load up to 10 percent reduction in height of the specimen. The predicted force obtained by using $\tau = fk$ is much higher than the experimental result of the entire compression. The force obtained by Bay's friction model, when $\gamma = 0°$, is high at the beginning of deformation and gets closer to the experimental result at higher deformation. This variation is reversed when the asperity angle is 15°. However, the loads obtained by FEM, regardless of the friction model applied, must be high at the beginning of compression. This is due to the simplified stress-strain

relation (Figure 5.9) utilized in FEM. According to Figure 5.9 the yield stress is 12,000 psi. The yield stress in AL 6061-O is 8,000 psi [440, pp. 154]. However, the simplified stress-strain curve and the stress-strain model $\sigma = 30{,}000\ \varepsilon^{0.2}$ (or the experimental results in Appendix E) get close by increasing the compression. Therefore, the influence of the friction modeling on the predicted load becomes more significant when deformation increases.

Figures 5.21 and 5.22 show the grid distortion for two frictional boundary conditions, $\tau = fk$ and that proposed by Bay ($\gamma = 0°$). Compared to Figure 5.15, some important results can be obtained regarding the appropriate sticking limit in the analysis. Figure 5.15 reveals some separation between the specimen and the bottom die on the right side. This separation can be observed in Figure 5.22 as well, but not in Figure 5.21. Separation of the specimen from the die in Figure 5.22 is the result of the tensile stress explained in section 5.2.1.2c. This agreement between the experiment and the analysis (Figure 5.22) confirms the Bay's friction model ($\gamma = 0°$) to be the limit of sticking. The little arrows in Figures 5.21 and 5.22 indicate the finite element fixed nodes. The shear stresses in these nodes were under the limit of sticking and never reached a magnitude sufficient to achieve a sliding condition. These nodes also represent the neutral points where the material flow changes its direction and where the amount of slip is zero (or minimum). Compared to Figure 5.15, the location of the neutral point at the bottom edge in Figure 5.22 (node 96) is very reasonable. The predicted neutral point in Figure 5.21 (node 98) does not match with Figure 5.15. The bases of this comparison are the minimum slip and the straightness of the line passing through the neutral point.

Prediction of the neutral point in non-symmetric geometries was the major goal in this work and it can be seen that this prediction is possible when the procedure cited in section 4.2 is used.

Figure 5.23 compares the geometrical changes for two friction conditions after 10 percent compression. The degree of barreling and separation of the specimen from the bottom die were previously discussed. The mode of the material flow is an important factor which can be used to judge the correctness of the limit of sticking condition. Figure 5.15 illustrates that the specimen has more tendency to shift towards the right. In Figure 5.23 this can be observed in the predicted geometry using the friction model proposed by Bay, et al (γ = 0°). For Constant Friction Law as the limit of sticking, material incorrectly moves more towards the left. The importance of the material flow becomes more significant when the die is closed. Assume that the die is closed and there is a wall on the right side of the specimen. When the material reaches the wall, all the states of stress and strain and filling of the die cavity change. Figure 5.24 illustrates the computed effective strain at some points for two different frictional boundary conditions. Generally the effective strain at the central part is higher when τ = fk is used as the frictional boundary condition. Since the effective strain is the state variable of the material undergoing deformation, it represents the mechanical property behavior during and after deformation. Therefore, Figures 5.23 and 5.24 illustrate the manner in which friction affects the mechanical properties.

Analysis of compression of the wedge-shaped specimen indicates that the general methodology, cited in section 4.2, is the suitable procedure

for the treatment of friction in non-symmetric geometries. This method is very successful when the friction formulations proposed by Bay (γ = 0°) are applied as the limit of sticking condition. Using this method, the location of the neutral point is quite predictable.

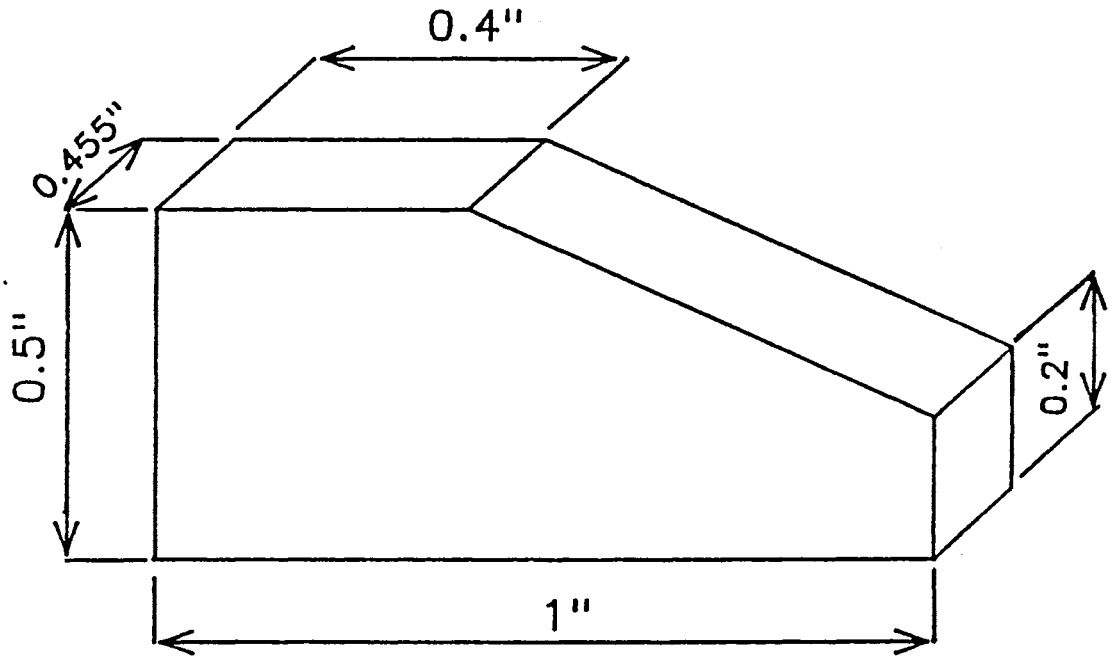

Figure 5.5 The wedge-shaped specimen

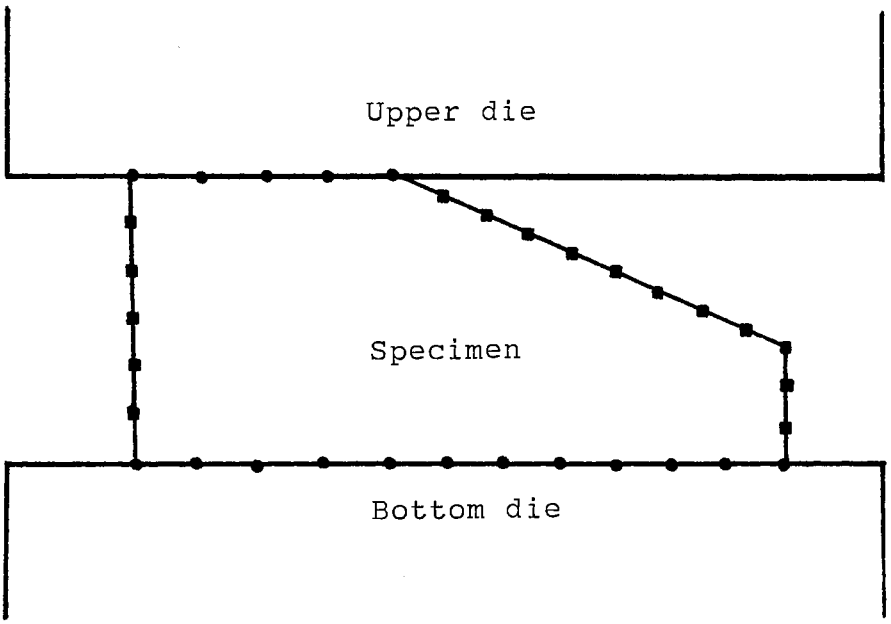

Figure 5.6 The boundary nodes.
- Common nodes
- Free nodes

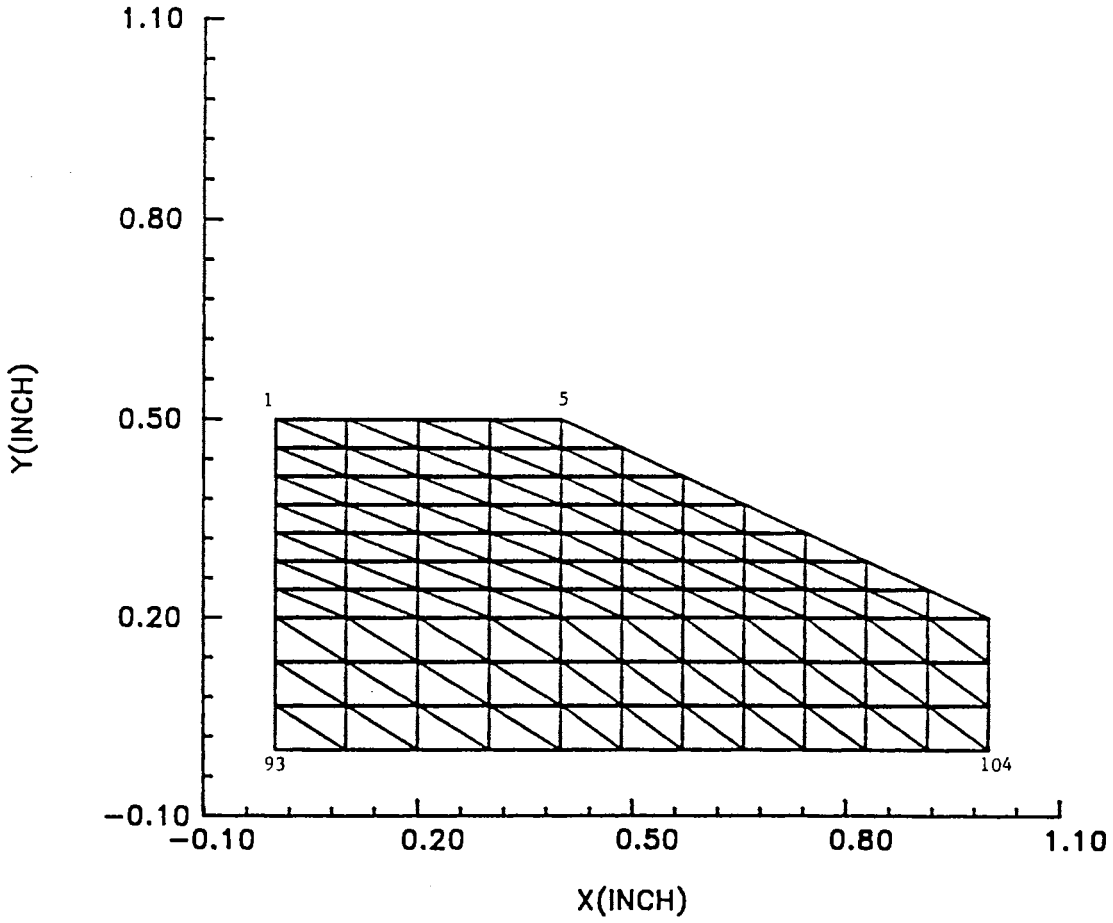

Figure 5.7 The mesh system for wedge-shaped specimen

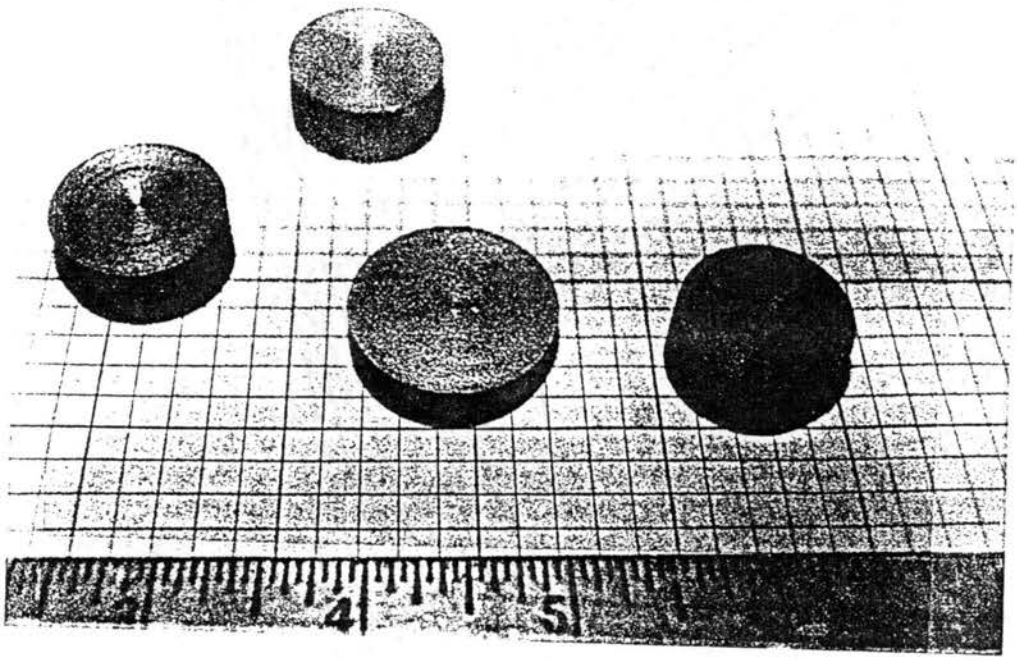

Figure 5.8 Some specimens used in compression test to determine the stress-strain curve

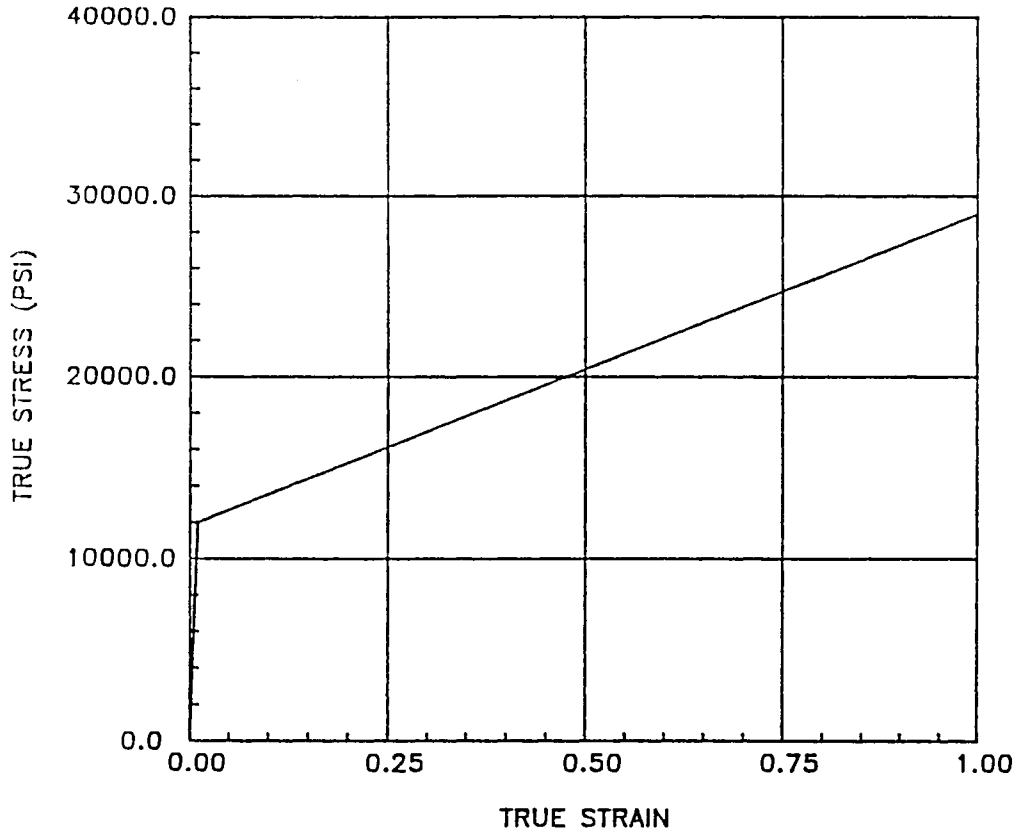

Figure 5.9 True stress-true strain in A16061-O

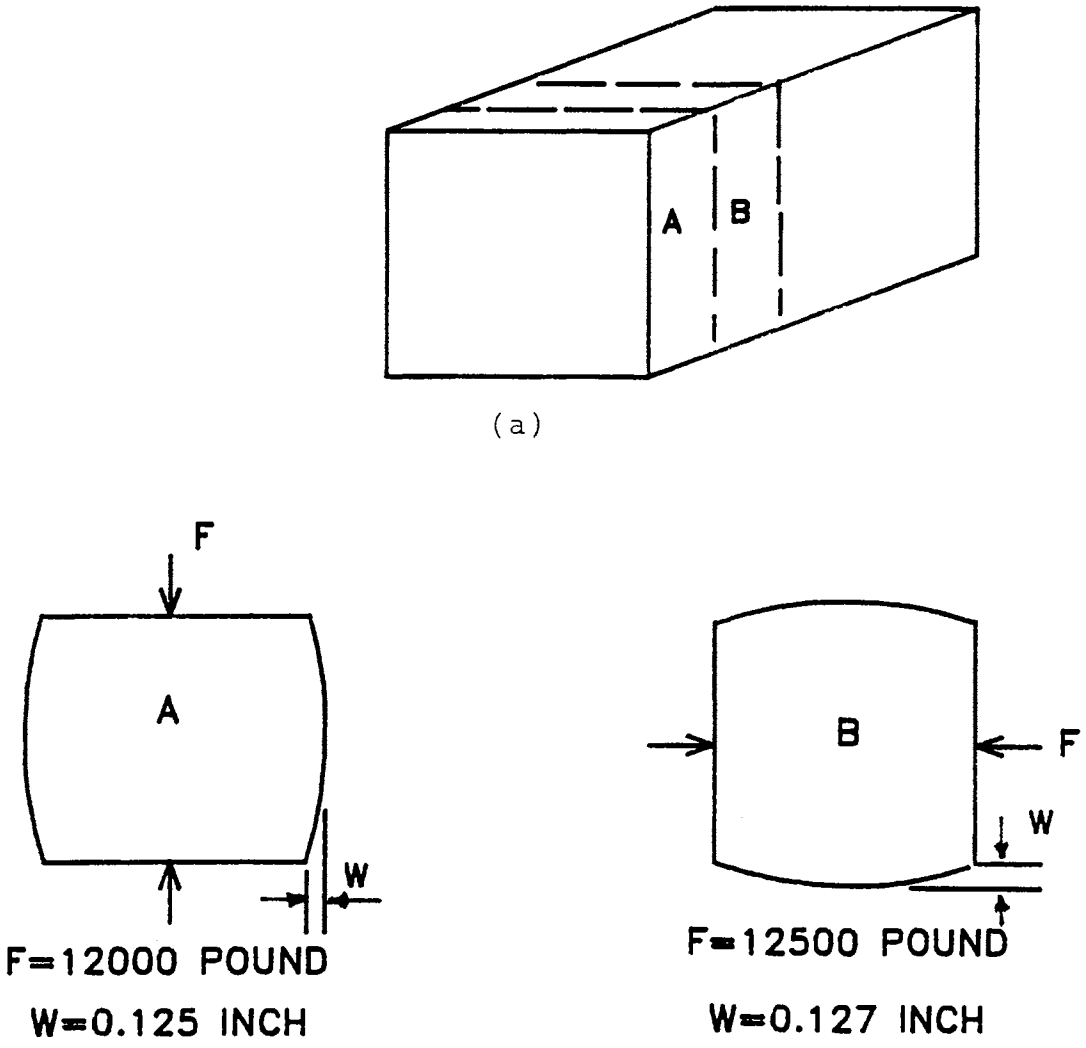

Figure 5.10 The effect of material nonhomogenity on the degree of barreling and the upsetting load. a) Two identical specimens are cut from a block of aluminum. b) The specimens are compressed under two different direction.

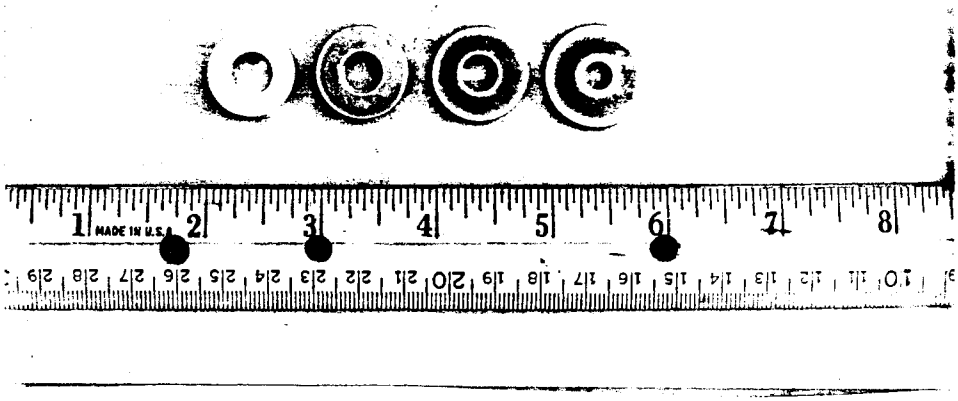

Figure 5.11 Some compressed rings for dtermination of coefficient of friction

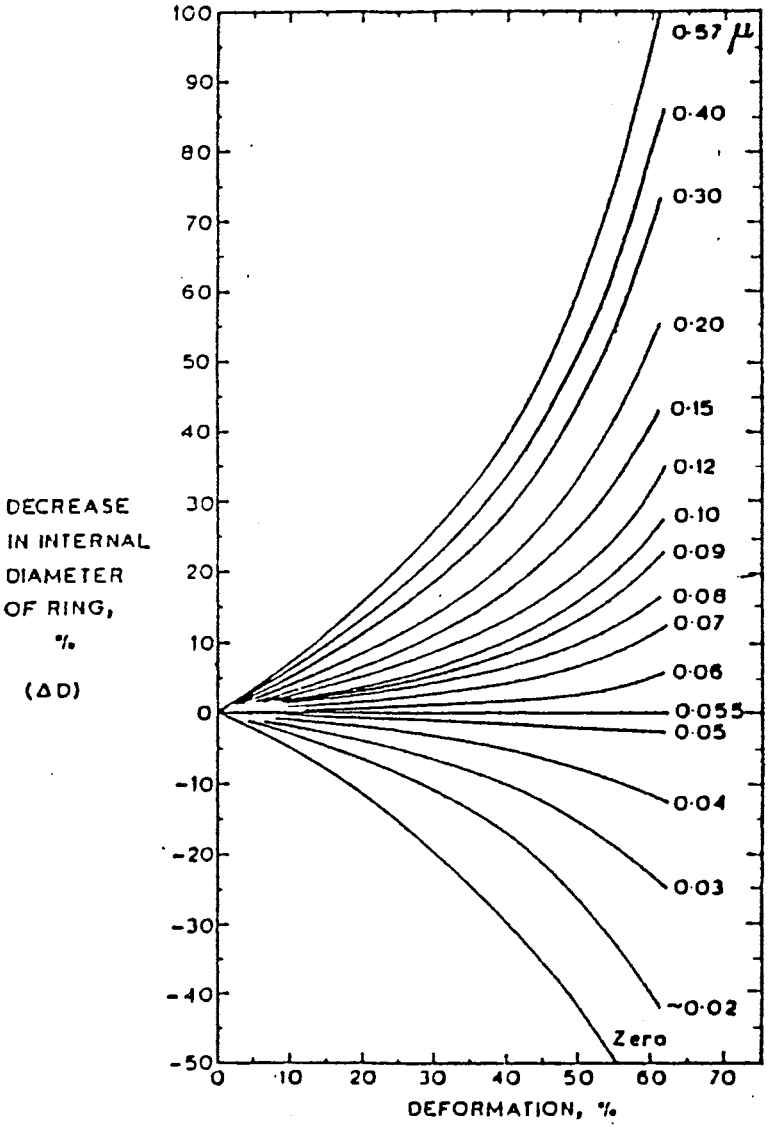

Figure 5.12 Diagrams for determination of coefficient of friction
[38]

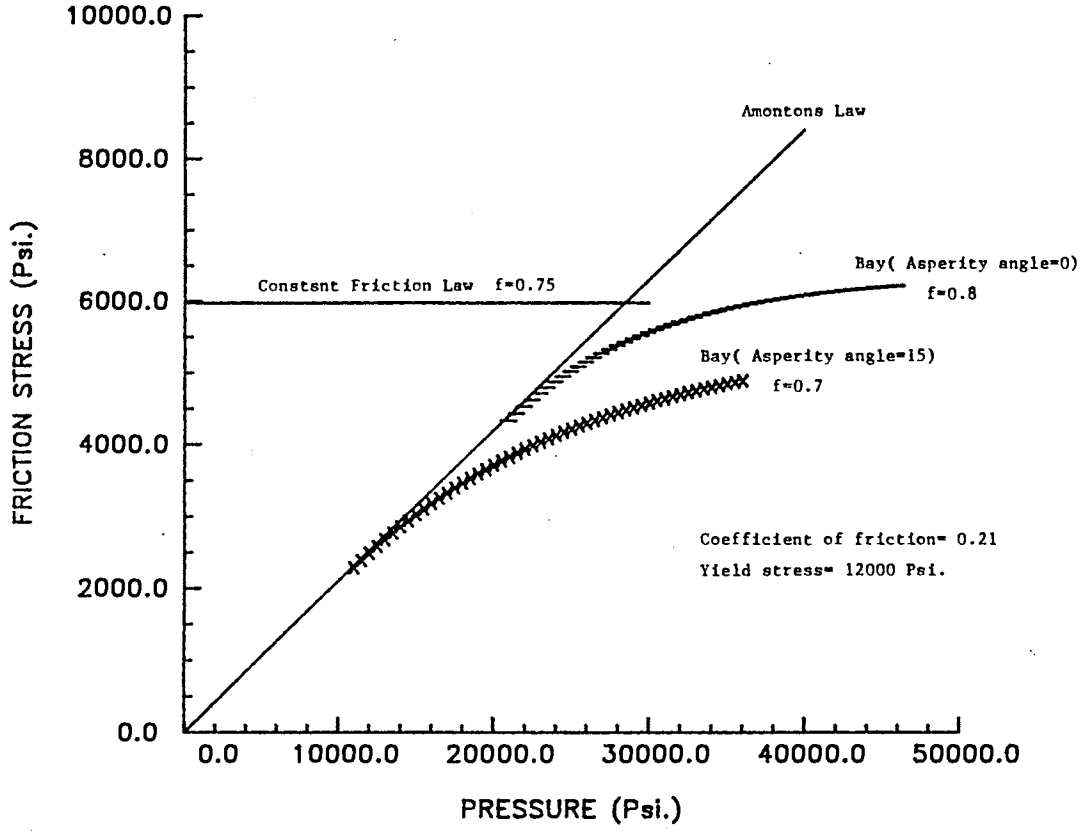

Figure 5.13 Different friction models used in this analysis

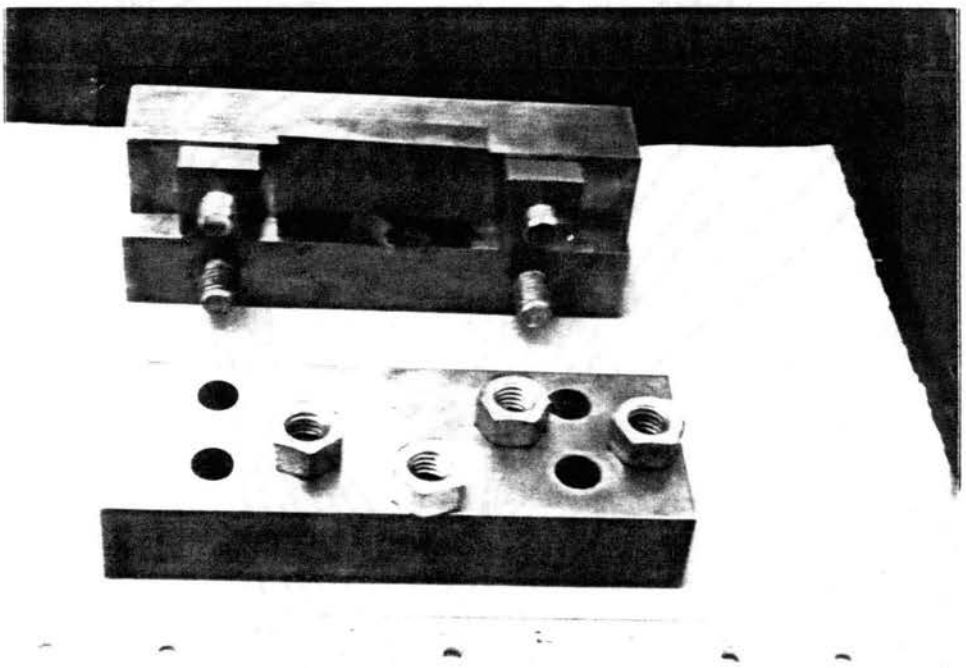

Figure 5.14 The die used for plane strain compression of the wedge-shaped specimen

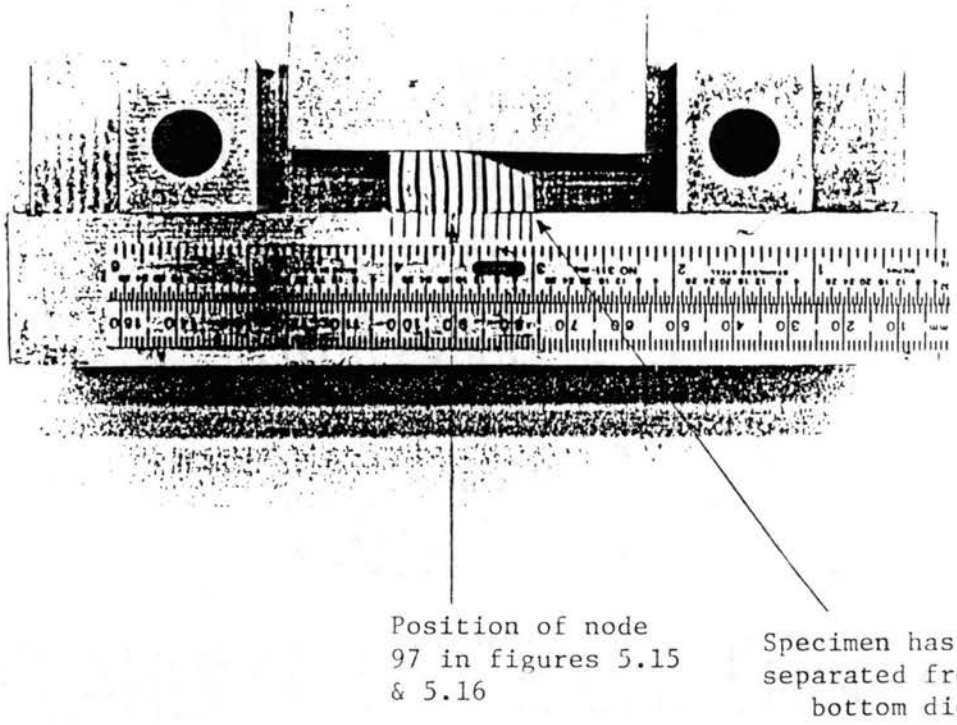

Figure 5.15 The specimen after 10% compression inside the die

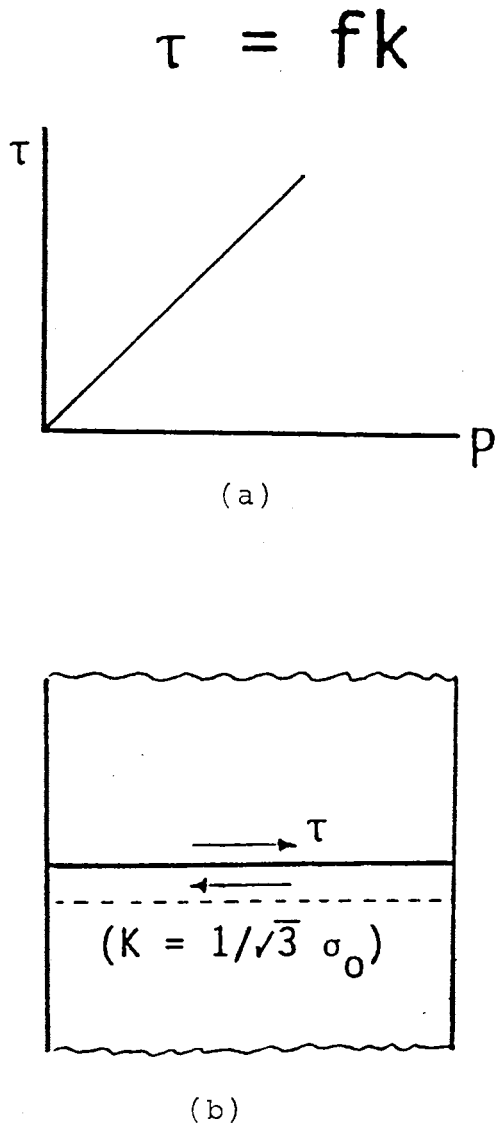

Figure 5.16 The cause of the Amontons Law failure.
a) According to this model, when the hydrostatic pressure increases to a high value, the friction stress becomes too high.
b) When the friction stress is beyond the shear strength of material, the state of equilibrium cannot be achieved and the finite - element analysis cannot provide any results.

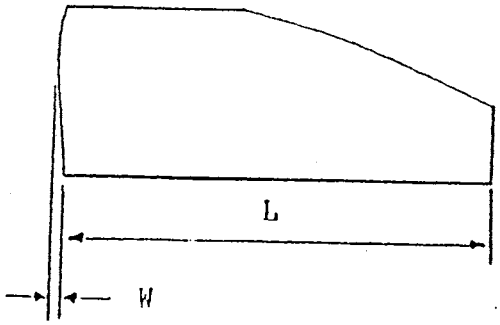

	L (Inch)	W (Inch)	W/L	Maximum Force (Pound)
Experiment	1.056	.014	.013	5900
r=fk	1.047	.022	.021	6950
Bay (γ=15°)	1.072	.009	.008	5100
Bay (γ=0°)	1.065	.012	.011	5900

Figure 5.17 Some numerical and experimental results after 10% reduction in height

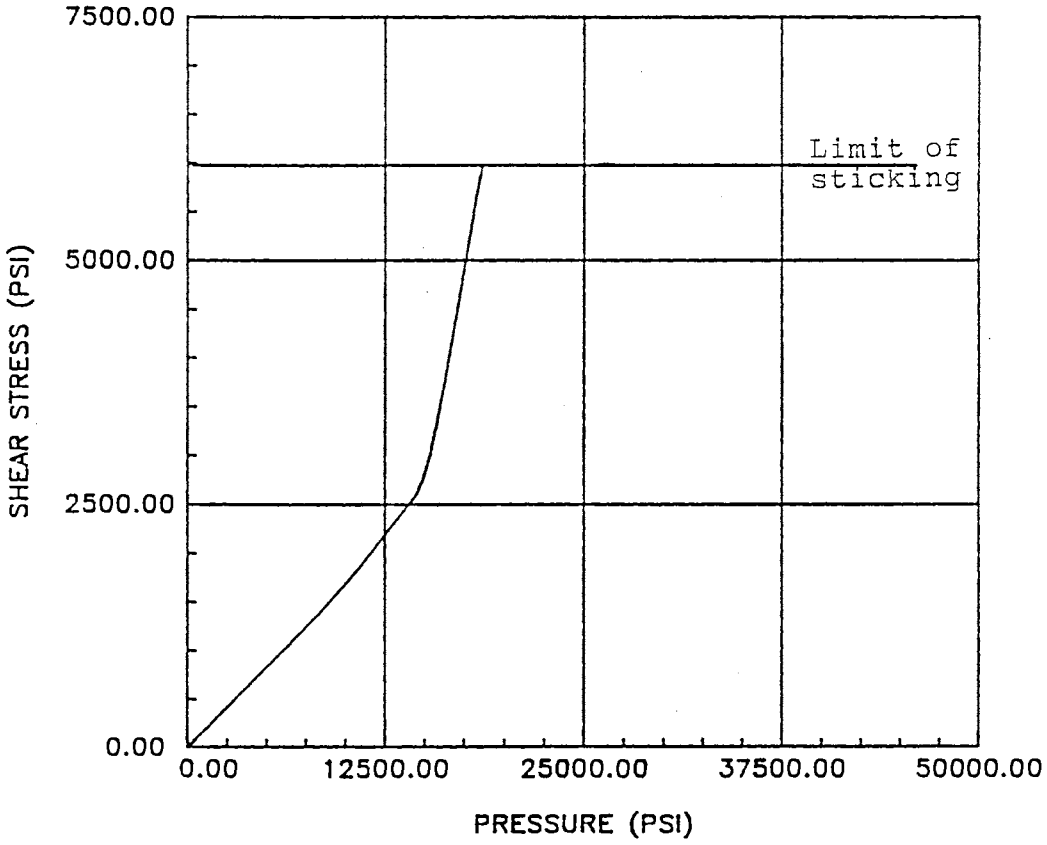

Figure 5.18 Variation of shear stress at node number 2 up to the limit of sticking(constant Fr.)

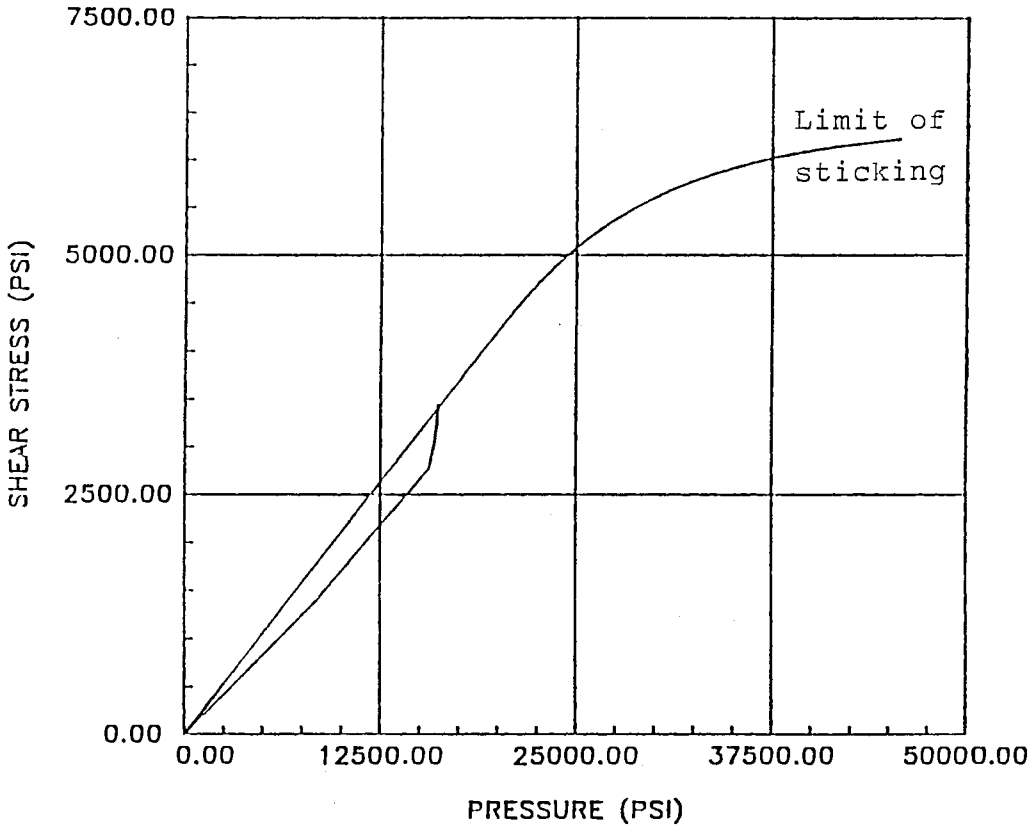

Figure 5.19 Variation of shear stress at node number 2 up to the limit of sticking(Bay)

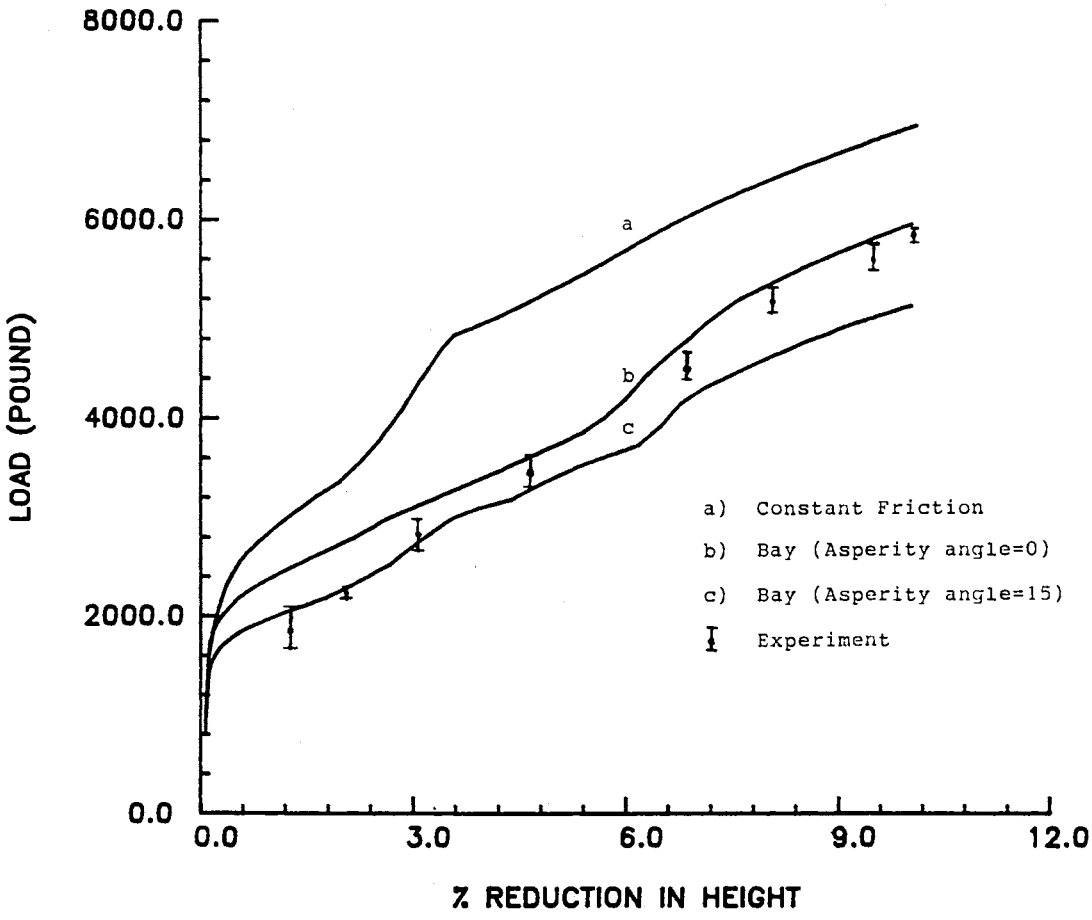

Figure 5.20 Variation Of the forging load with different sticking limit.

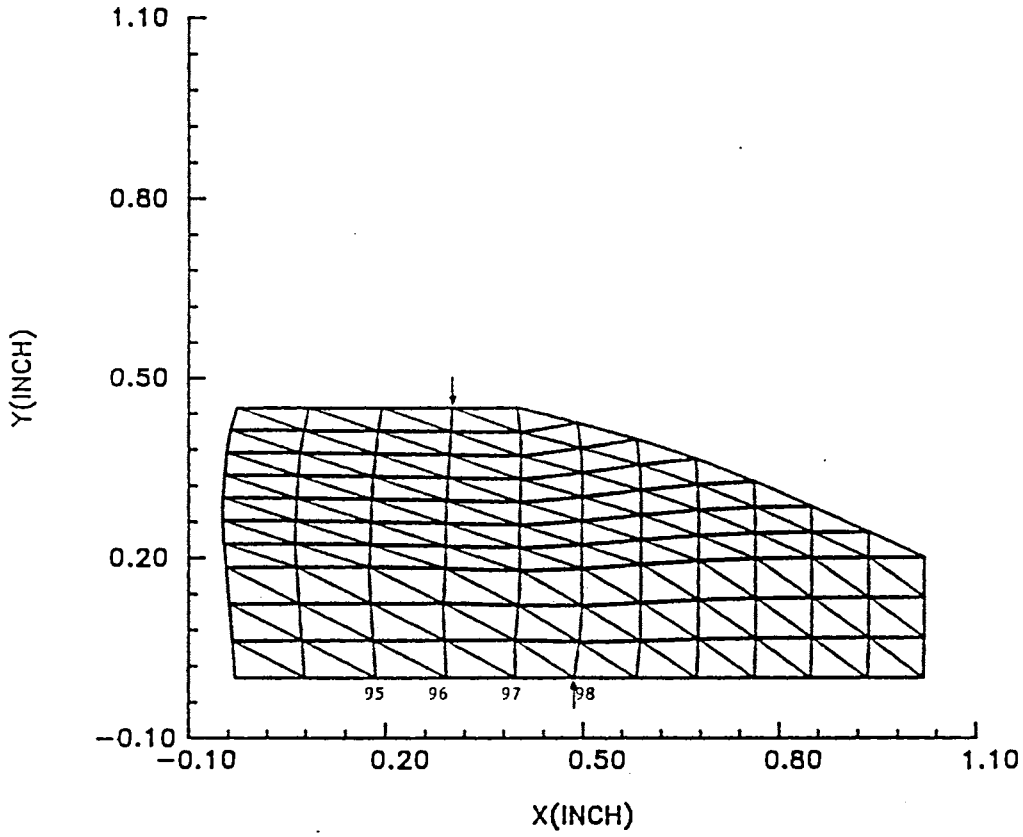

Figure 5.21 10% compression with the Constant Friction Law as the limit of sticking

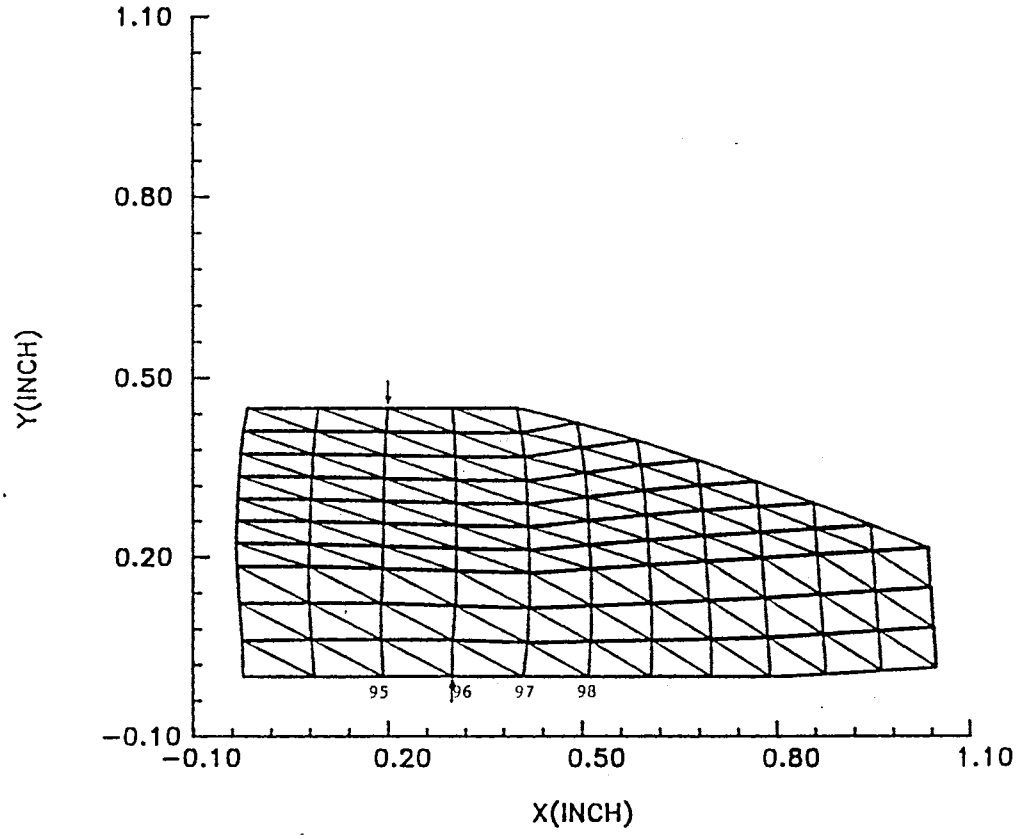

Figure 5.22 10% compression with the friction model by Bay as the limit of sticking

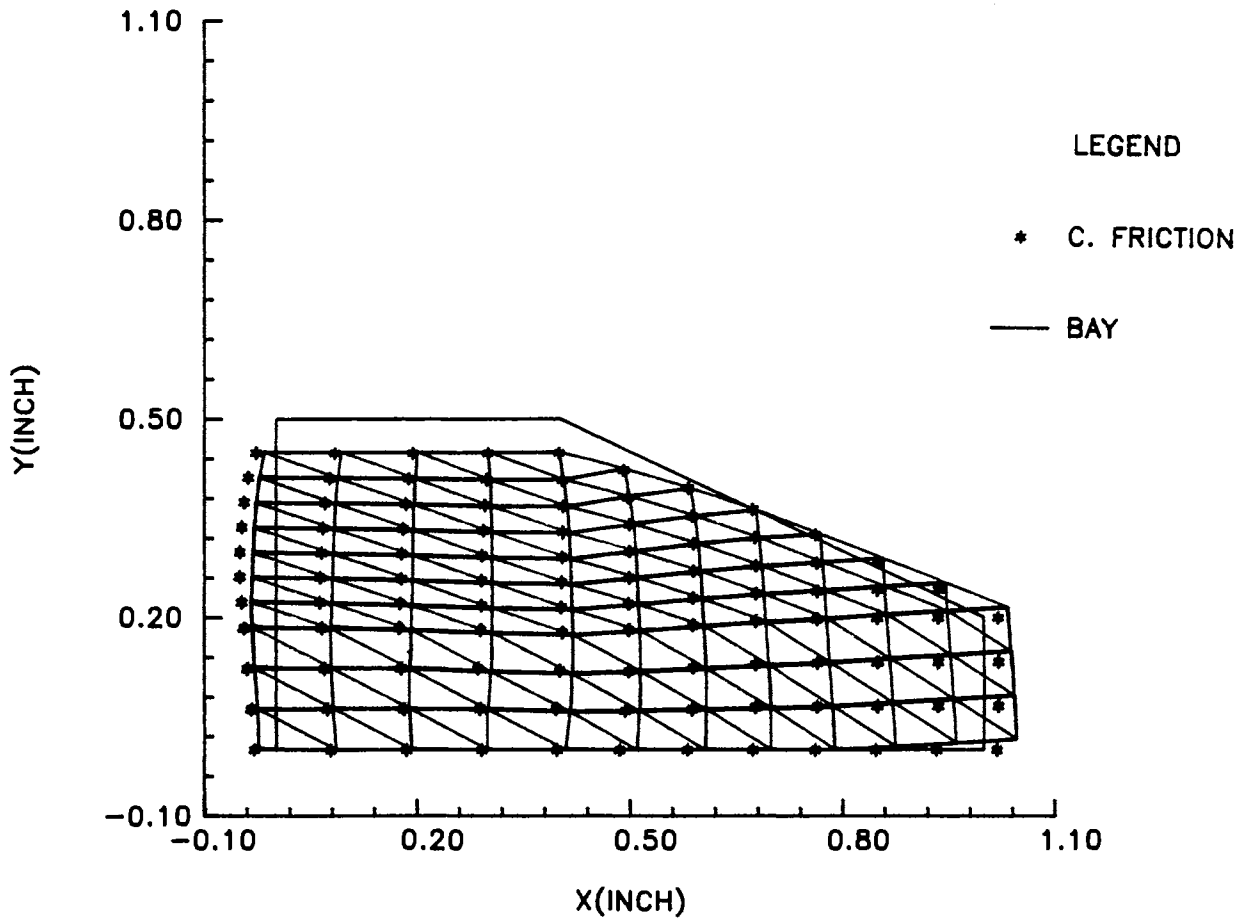

Figure 5.23 The effect of friction on final geometry.

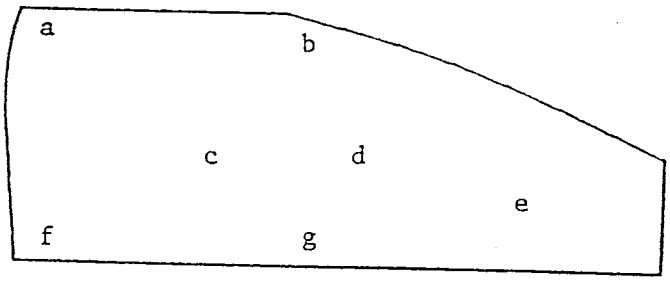

	a	b	c	d	e	f	g
$\tau = f k$	o.15	o.o3	0.14	0.06	0.00	0.10	0.14
Bay ($\gamma = 0^\circ$)	0.14	0.03	0.13	0.03	0.00	0.11	0.15

Figure 5.24 The computed effective strain at some points inside the specimen

CHAPTER VI

DISCUSSION

In the friction part of this work, two factors of significance can be observed:

a. A general methodology regarding the incorporation of the frictional boundary conditions suitable for any types of geometry.

b. Comparison of different friction formulations with the same finite element code and the same method of incorporation.

Also, program ELPL (Finite Element approach) served as a temporary tool for the development of the cited methodology.

6.1 Finite Element Approach

Program ELPL is based on Hill's variational principle (equation 4.3) for incremental deformations and is ideally suited to isotropically hardening Prandtl-Ruess material. In this program the effect of the strain rate sensitivity is neglected. Therefore, the plane strain compression test (section 5.2) was performed very slowly. The source of the finite element formulations (equations 4.7 or 4.9) was [34]. In these formulations the effect of rigid body rotation was considered.

In program ELPL, the Jaumann increment of Kirchoff stress was assumed to be equal to the increment of the Cauchy stress. This reduced the computation efforts but did not influence the results of the

analysis significantly (section 5.1). The load obtained by the analysis of the rectangular block, after 10 percent compression and under the sliding condition, was between the loads computed by the Von Mises and the Maximum Shear Stress Criterions. The growth of the plastic zone matched with that in [18].

The element type, used in program "ELPL", was triangular. In plasticity, the components of the stiffness matricies (Equations 4.8 and 4.9) are stress dependent. In any element except the triangular element, the stress is not constant. Therefore, an average stress must be used for the computation of the stiffness components which causes the increase of the computation effort and may create some types of error (e.g. by not sharing adequate and appropriate points in the computation of the average elemental stress). Application of the triangular element in program "ELPL", would avoid such problems. However, there are several other factors involved in the accuracy of programs regarding the types of elements. Data pertinent to these factors can be found in other studies ([42] pp. 158 or [43]). Other significant factors involved in program "ELPL" may be summarized as follows:

a. The increments of displacements are chosen somehow to make every element yield exactly at the yield point. These are done by the computation of a scaling factor explained in section 4.1.5.2.

b. The material is considered to be elastic-linearly plastic (Figure 4.4). This reduces the computational efforts and the numerical errors considerably when the slope of the plastic stress-strain relation is assumed to be constant.

c. Particular attention has been paid to the elimination of the

numerical errors by the application of DOUBLE PRECISION command and elimination of some complex equations such as that explained in step b.

Friction

Compression of the wedge-shaped specimen, validated the method of incorporating the frictional boundary condition into FEM. The location of the neutral point and the flow direction (Figures 5.22 and 5.23) are quite predictable by using this method. Compared to the other methods (section 2.2), this procedure can be adopted as a new approach in finite-element modelling of friction. No other method such as the slab method (Section 2.2.1) is necessary to determine the friction direction. Also, the die and the workpiece are directly in contact and no GAP element (interface element) [16] is required at the die/workpiece interface. The analysis of deformation is started with the sticking frictional boundary condition. This assumption is based upon the concept of friction. If friction is a resistance force, sliding cannot take place until this resistance is overcome. Therefore, the condition of sticking persists until the surface shear stress reaches a critical value or limit of the static friction. In the search for an appropriate critical value, different friction models were examined and compared. The failure of the Amontons Law, confirmed that explained in [5, pp. 15] (see section 2.1.2). According to this discussion, the coefficient of friction becomes meaningless at high pressure. This usually occurs in the forging process. Also, the unsatisfactory results obtained by the Constant Friction Law were in agreement with Devaux [1] who found that friction cannot remain constant

at the interface. The friction model proposed by Bay, when the asperity angle is considered zero, fit as the limit of sticking in the present work. Therefore, two important results were obtained by this comparison. First, the proposed methodology for the treatment of friction in metal forming is quite practical. Second, the proposed friction model by Bay is more realistic compared to the Amontons and the Constant Friction Laws.

Usually, in most conventional methods (direct methods), the friction stress/force is computed according to a model and introduced to the boundary . In the present work, up to the limit of sticking, friction is computed according to the equilibrium of the forces and it is independent of any model (Figure 5.19). The dependency of the friciotn to the introduced model starts when the sliding condition commences.

The sticking critical shear procedure (Figure 5.19) can be extended to model the stick-slip phenomena. According to this phenomena, friction changes between two upper and lower limits. Bowden and Tabor [6] explained this behavior in a very understandable way (after Rabinawicz, 1959):

Figure 6.1 illustrates two surfaces in contact The upper surface is attached to a spring with the stiffness k. When the lower surface is driven forward at a uniform velocity v, the spring force increases at a rate k.v.t (sticking condition) In Figure 6.2a, this process is represented by the straight line OA with the slope proportional to k.v (if the damping factor is negligible). At the Point A (limit of sticking), slip occurs. Slip continues until the spring force reaches the point B. At this point the upper surface in the Figure 6.1 comes to

rest in relation to the lower surface and no variation occurs in the spring force. After a while, the surfaces stick to each other (point C) and the spring force increases until again slip occurs (point D). These cycles continue and finally, a steady state is reached with stick-slip of constant size (Figure 6.2b). Figure 6.3 reveals the modeling of friction in the present work (solid lines) and its extension to the stick-slip model (dotted lines). In Figure 6.3, when nodal friction increases and reaches the limit of static friction (point A), instead of application of the nodal force according to the solid line, no load or stress is applied and that particular node is free to slide. Therefore, friction stress drops and reaches the kinetic limit (point B). Condition of sticking starts at point B and the behavior of stick-slip continues. For such a development, two extra steps must be accomplished.

a. A search must be done for an appropriate kinetic friction limit.

b. Condition of unloading must be considered in the finite element program.

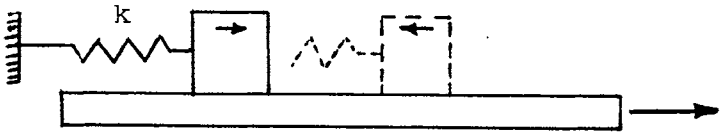

Figure 6.1 Mechanism of stick-slip

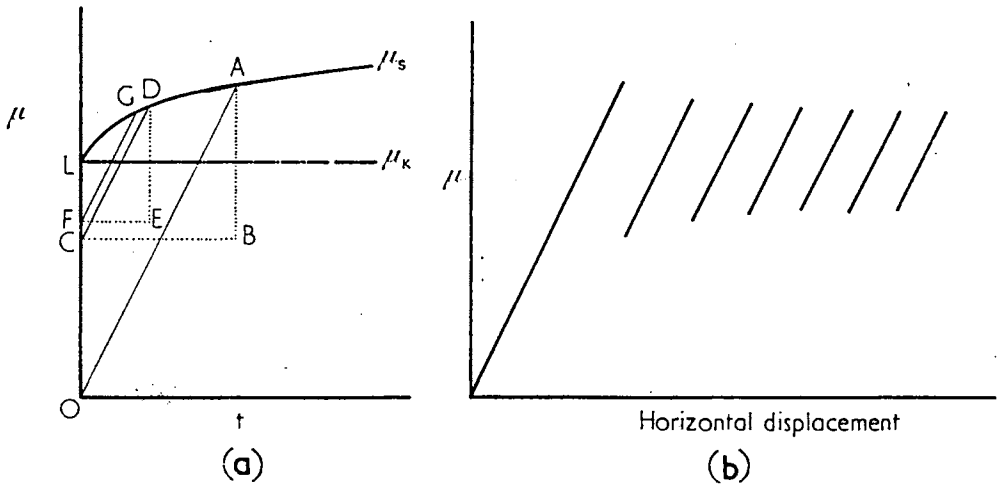

Figure 6.2 Development of intermittent motion for a system in which friction increases with time of contact t according to a typical curve [6].
a) Friction- time curve.
b) Resultant intermittent motion.

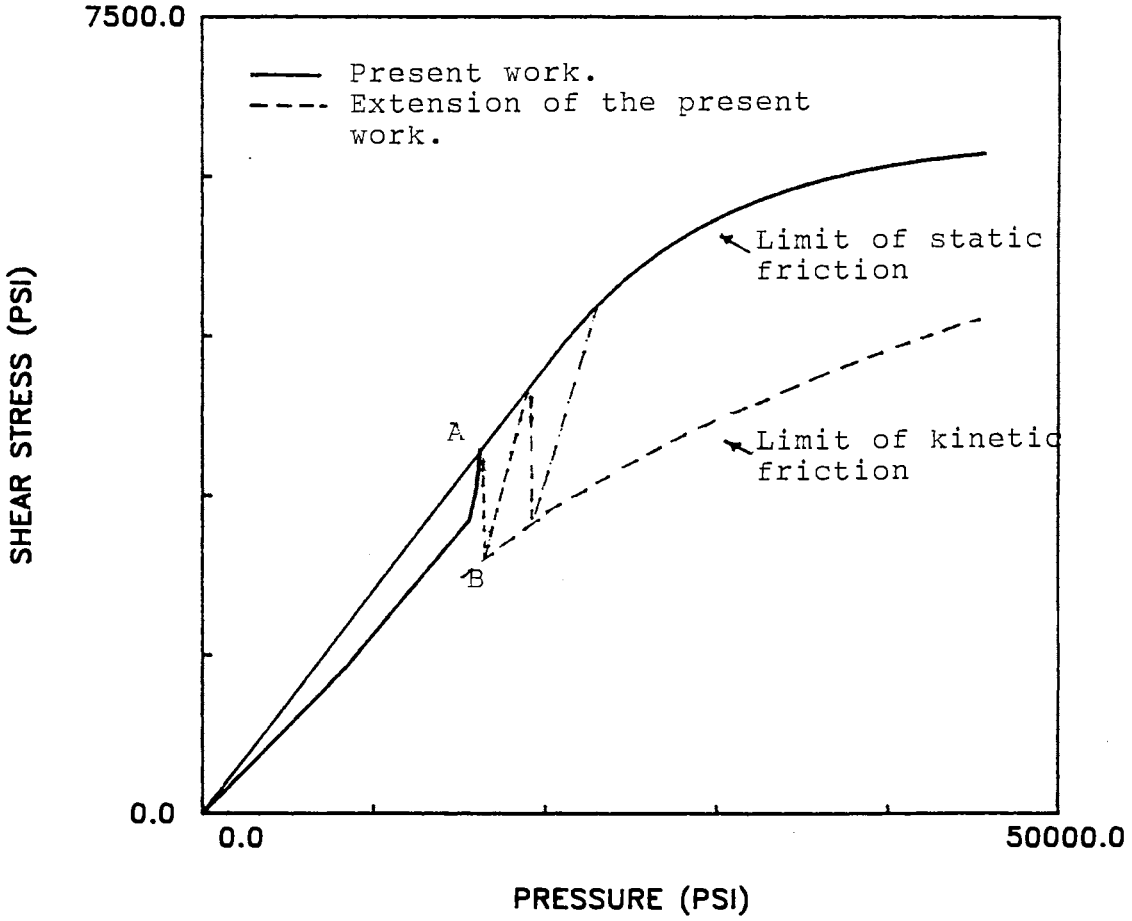

Figure 6.3 Modelling of friction in the present work and its extension.

CHAPTER VII

SUMMARY AND CONCLUSIONS AND RECOMMENDATION FOR FURTHER STUDIES

Conclusions

A General methodology for finite-element modelling of friction in non-symmetric geometries has been developed. The approach provides for the inclusion of a sticking-critical shear model for large scale deformation found in metal forming. This method does not require the use of CAP elements at the die-metal interface.

An elastic-plastic finite element computer program was developed for plane strain deformation which provided the capability of evaluating various frictional boundary condition models. The effect of rigid body rotation was considered in this development. The stability of the program was examined by obtaining the solution of upsetting of a rectangular block.

A review of the methods of incorporating friction as a boundary condition in large scale plastic deformation was conducted and the methods classified into three categories. The basic friction models were tested using the finite element code. The results of the simulations using these different methods of modelling friction were compared with experimental deformation data obtained from the deformation of wedge-shaped specimens under plane strain conditions. The recently proposed friction model by Bay [2], when incorporated into

the FEM code, provided the best correlation with the experimental results. The Bay model of sticking/friction at the die-workpiece boundary is an attempt to more accurately model the tribological/metallurgical events taking place in deformation.

The capability of the FEM elastic-plastic code, incorporating the friction model proposed by Bay, to predict the location of the neutral point in complex shapes was established by compression of a wedge-shaped specimen. It is no longer necessary to use other methods, such as the slab method, to predetermine the position of neutral points and the direction of flow at the boundary.

Recommendations

Based on the analyses and discussions presented in this work, it is recommended that the following research be undertaken:

a. To give more flexibility to the present friction modeling approach, the complete phenomena of stick-slip can be modeled. This provides an opportunity for the boundary nodes, after commencement of sliding, to stick the die again. For this purpose, it is necessary to find a suitable kinetic friction model.

b. It is suggested that the present friction work be linked to a more advanced elastic-plastic code, one with the capability of application of different element types and mesh generation. To model the phenomena of stick-slip, the condition of unloading must be considered in the computer program.

REFERENCES

1. J. Devaux, J. C. Gelin, J. Oudin, Y. Ravalard. "Theoretical Analysis and Experimental Application of Barrelling and Folding in Cylinder Upsetting Tests. Int J. Mech. Sci (1984) 555.

2. N. Bay. "Friction and Adhesion in Metal Forming and Cold Welding." Technical University of Denmark (1985).

3. "BOUNDARY LUBRICATION." An Apprisal of World Literature. ASME, New York, (1969).

4. Donald H. Buckley. "Surface Effect in Adhesion, Friction, Wear, and Lubrication. Elsvier Scientific Publishing Company, New York, (1981).

5 John A. Schey. "Tribology in Metalworking." A.S.M. Ohio (1983).

6. F. P. Bowden, D. Tabor. "The Friction and Lubrication of Solids." Pt. II. Oxford University Press (1964).

7. J. Halling. "Principles of Tribology." MacMillan Press Ltd, England (1973).

8. A. D. Sarkar. "Wear of Metals." Pergamon Press, New York (1976).

9. C. M.Edwards, J. Halling. "An Analysis of the Plastic Interaction of Surface Asperities and Its Relevance to the Value of the Coefficient of Friction." J. Mech. Eng. Sci (1968).

10. G. W. Pearsall, W. A. Backofen. "Friction Boundary Conditions in Plastic Compression." Trans. ASME, J. Engn. Ind. (1963) 68.

11. F. P. Bowden, D. Tabor. "The Theory of Metallic Friction and Role of Shearing and Ploughing." Bull. 145, Comm. of Australia, Concil Sci and Ind Res (1942).

12. N. Bay, G. Gerverd. "Tool/Workpiece Interface Stresses in Simple Upsetting." J. Mech. Work Tech (1987).

13. J. J. Park and S. Kobayashi. "Three-Dimensional Finite Element Analysis of Block Compression." Int. J. Mech. Sci (1984) 165.

14. L. J Guo, Y. J. Huang and W. Q. Chen. "Three Dimensional Finite Element Analysis of Metal Forming Processes with Special Reference to Boundary Conditions." 16th NAMRC (1984) 114.

15. C. R. Boer N. Rebelo, H. Rydsted, G. Schroder. "Process Modelling of Metal Forming and Thermomechanical Treatment." Springer-Verlog Berlin, Heidelberg (1986).

16. P. Hartley, C. E. N. Sturgess, G. W. Rowe. "Friction in Finite Element Analysis of Metal Forming Processes." Int. J. Mech. Sci (1979) 301.

17. I. Pillinger, P. Hartley, C. E. N. Sturgess, G. W. Rowe. "An Elastic Plastic Three Dimensional Finite Element Analysis of the Upsetting of Rectangular Blocks and Experimental Compression." Int. J. Mach Tool Des. Res (1985) 229.

18. A. Nagamatsu, T. Muota, T. Jimma. "On the Non Uniform Deformation of a Block in Plane Strain Compression Caused by Friction." Bull J. ASME (1972) 322.

19. W. Johnson, P. B. Mellor. "Engineering Plasticity." Halstes Press. New York (1985).

20. W. Johnson. "Estimation of Upper Bound Loads for Extrusion and Coining Operations." Proc. Inst. Mech. Engrs Londin (1959).

21. H. Kudo. "An Upper Bound Approach to Plane Strain Forging and Extrusion, parts I, II, III." J. Mech. Sci (1960) 57, 229, 366.

22. E. G. Thomsen, C. T. Yang, S. Kobayashi. "Mehcanics of Plastic Deformation in Metal Processing." Macmillan, New York (1965).

23. B. Avitzur. "Metal Forming Analysis." McGraw Hill, New York (1968).

24. Y. Yamada, N. Yoshimura, T. Sakura. "Plastic Stress Strain Matrix and Its Applications for the Solution of Elastic Plastic Problems by Finite Element Method. Int. J. Mech. Sco (1968) 343.

25. K. Iwata, K. Osakada, S. Fujino. "Analysis of Hydrostatic Extrusion by the Finite Element Mehtod." Trans. ASME, J. Engrg. for Ind (1972) 697.

26. C. H. Lee. "Numerical Analysis of Plastic Deformation Problems." Ph.D. Dissertation, University of California, Berkeley (1970).

27. C. H. Lee, S. Kobayashi. "Analysis of Axisymmetric Upsetting and Plane Strain Side Pressing of Solid Cylinders by the Finite Element Method." Trans. ASME J. of Engrg. for Ind. (1971) 445.

28. C. H. Lee, S. Kobayashi. "Elastioplastic Analysis of Plane Strain and Axisymmetric Flat Punch Indentation by the Finite Element Method. Int. J. Mech. Sci. (1970) 349.

29. C. H. Lee, S. Kobayashi. "New Solutions to Rigid Plastic Deformation Problems Using a Matrix Method. Trans. ASME J. of Engrg. for Ind. (1973) 865.

30. C. H. Lee, S. Kobayashi. "Deformation Mechanics and Workability in Upsetting Solid Circular Cylinders." Proc. North Ameri. Met. Res. Conf., Hamilton, Canada (1973) 185.

31. T. Altan, S. I. Oh, H. Gegel. "Metal Forming." Fundamentals and Applications." ASM (1983).

32. S. S. Rao. "The Finite Element Method in Engineering." Pergamon Press, New York (1982).

33. H. D. Hibit, P. V. Marcal and J. R. Rice. "A Finite Element Formulation for Problems of Large Strain and Large Displacement." Int. J. Solid Str. (1970) 1069.

34. R. M.McMeeking, J. R. Rice. "Finite Element Formulations for Problems of Large Elastic Plastic Deformations." Int. J. Solids and Structures (1975) 601.

35. R. Hill. "Some Basic Principles in the Mechanics of Solids Without a Natural Time." J. Mech. Phys. Solids (1959) 209.

36. W. Prager. "Introduction to Mechanics of Continua." Gin (1961).

37. C. F. Gerald, P. O. Weatly. "Applied Numerical Analysis." Third Ed. Addison-Wesley Menlo Park, California (1985).

38. A. T. Male, M. G. Cockcroft. "A Method for the Determination of the Coefficient of Friction of Metals Under Conditions of Bulk Deformations." J. of Inst. of Metals (1964) 38.

39. Aerospace Structural Metal Handbook. Volume 3. (1977).

40. Serope Kalpakjian. "Manufacturing Processes for Engineering Materials." Melo Park, California (1984).

41. O. C. Zienkiewicz. "The Finite Element Method in Engineering Science." McGraw Hill. London (1971).

42. "Metal forming Plasticity". IUTAM Symposium Tutzing/Germany. New York, 1978.

43. J. C. Ngtegaal, D. M. Parks and J. R. Rice. "On Numerically Accurate Finite Element Solutions in the Fully Plastic Range". Computer Methods in Applied Mechanics and Engineering. North-Holland Publishing Company, 1974.

44. S. Kobayashi, S. Oh, T. Altan. "Metal Forming and the Finite-Element Method". Oxford University Press. New York, 1989.

APPENDIX A

STRESS CORRECTION STIFFNESS

In equation (4.9) the stress correction stiffness was defined as:

$$[K_c] = \int_v [N_k]^T{}_{,i}\ \sigma_{ij}\ [NK]_{,j} - 2\ [B_{Ki}]^T\ \sigma_{ij}\ [B_{Kj}]\ dv$$

Where:

[N] = Shape function.

[B] = Strain - displacement matrix.

For a triangular element in plane strain condition equation (3.9) becomes :

$$[K_c] = \begin{vmatrix} K11 & & & \text{SYMMETRIC} & & \\ K21 & K22 & & & & \\ K31 & K32 & K33 & & & \\ K41 & K42 & K43 & K44 & & \\ K51 & K52 & K53 & K54 & K55 & \\ K61 & K62 & K63 & K64 & K65 & K66 \end{vmatrix}$$

Where:

$$K11 = A\ Y32^2 + B\ X32^2 - 2\ C\ Y32\ X32 + AA\ (Y32^2 + X34^2 / 4) + BB\ X32^2/4) - 2\ CC\ Y32\ X32$$

$$K21 = (-AA\ X32) / 4 - BB\ Y32\ X32 / 4 + CC\ Y32^2 + CC\ X32$$

$$K22 = A\ Y32^2 + B\ X32^2 - C\ Y32\ X32 - C\ X32\ Y32 + AA\ Y32^2 / 4 + BB\ Y32^2 / 4 + X32^2 - CC\ Y32\ X32 - CC\ X32\ Y32$$

$$K31 = - A\ Y31\ Y32 - B\ X31\ X32 + C\ Y31\ X32 + C\ X31\ Y32 - AA\ Y31\ Y32 - AA\ X31\ X32 / 4 - BB\ X31\ X32 / 4 + CC\ Y31\ X32 + CC\ X31\ Y32$$

```
K32= AA X31 Y32 / 4 + BB X31 Y32 / 4 + - CC X31 X32  -
     CC Y31 Y32
K33= A Y31 z + B X31 z - C Y31 X31 - C X31 Y31 + AA Y31 z + AA X31 z /4
     + BB X31 z / 4 - CC Y31 X31 - CC X31 Y31
K41= AA Y31 X32 / 4 + BB Y31 X32 / 4 - CC Y31 Y32 -CC X31 X32
K42= - A Y31 Y32 - B X31 X32 + C Y31 X32 + C X31 Y32 -
       AA Y31 Y32 / 4 - BB Y31 Y32 / 4 - BB X31 X32 +
      CC Y31 X32 + CC X31 Y32
K43= - AA X31 Y31 /4 - BB Y31 X31 / 4 + CC Y31 z + CC X31 z
K44 = A Y31 + B X31 - C Y31 X31 - C X31 Y31 + AA Y31 / 4 +
      BB Y31 / 4 + BB X31 - 2 CC X31 Y31
K51 = A Y21 Y32 + B X21 X32 - C Y21 X32 - C X21 Y32 + AA Y21 Y32
      + AA X21 X32 /4 + BB X21 X32 /4 - Y21 X32 - CC X21
K52= -AA X21 Y32 /4 - BB X21 Y32 /4 + CC Y21 Y32 + CC X21 X32
K53= - A Y21 Y31 - B X21 X31 + C Y21 X31 + C X21 Y31 -AA Y21 Y31
   - BB X21 X31 / 4 - BB X21 X31 /4 +CC Y21 X31 +C C  X21 Y31
K54 = AA X21 Y31 /4 + BB X21 Y31 /4 - CC Y21 Y31 - CC X21 X31
K55= A Y21 z + B X21 z - C Y21 X21 -C X21 Y21 + AA Y21 z + AA X21 z /  4
    + BB X21 z / 4 - 2 CC Y21 X21
K61= -AA Y21 X32 /4 -BB Y21 X32 / 4 +CC Y21 Y32 +C C  X21 X32
K62= A Y21 Y32 + B X21 X32 - C Y21 X32 - C X21 Y32 +
     AA Y21 Y32 / 4 + BB Y21 Y32 /4 + BB X21 X32
     CC Y21 X32 - CC X21 Y32
K63= AA Y21 X31 /4 + BB Y21 X31 /4 - CC Y21 Y31 - CC X21 X31
K64= -A Y21 Y31 -B X21 X31 + C Y21 X31 + C X21 Y31 -
     AA Y21 X21 /4 - BB Y21 Y31 /4 - BB X21 X31 + CC Y21 X31
```

$$+ CC\ Y21\ X31 + CC\ X21\ Y31$$

$$K65= -AA\ Y21\ X21\ /4 - BB\ Y21\ X21\ /4 + CC\ Y21^{z} + CC\ X21^{z}$$

$$K66= A\ Y21^{z} + B\ X21^{z} - C\ Y21\ X21 - C\ X21\ Y21 + AA\ Y21^{z}\ /\ 4$$
$$BB\ Y21^{z}\ /4 + BB\ X21^{z} - 2\ CC\ X21\ Y21$$

$$A= \sigma_{11} / (4\ S^{z}) \qquad B= \sigma_{22} / (4\ S^{z}) \qquad C= \sigma_{21} / (4\ S^{z})$$

$$AA= -2\ \sigma_{11} / (4\ S^{2}) \qquad BB= -2\ \sigma_{22} / (4\ S^{z}) \qquad CC= -2\ \sigma_{12} / (4\ S^{z})$$

S= Area of the triangular element

$$X_{ij} = X_j - X_i$$

$$Y_{ij} = Y_j - Y_i$$

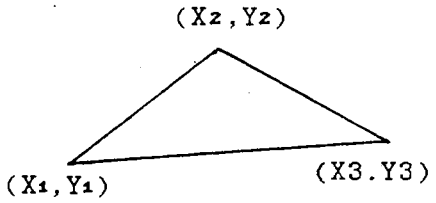

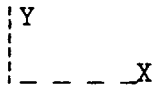

APPENDIX B

PLASTIC STRESS-STRAIN MATRIX

The Prandtl Ruess equations for the deviatoric strain increment $d\varepsilon_{ij}$ are:

$$d\varepsilon'_{ij} = \sigma'_{ij}\, d\lambda + d\sigma'_{ij} / 2G \qquad (B.1)$$

Where:

$$d\lambda = (3/2)\, d\bar{\varepsilon}^{p} / \bar{\sigma} = (3/2)\, d\bar{\sigma} / (\bar{\sigma}\, H') \qquad (B\text{-}2)$$

According to the Von Mises Yield Criterion:

$$(2/3)\, \bar{\sigma} = \sigma'_{ij}\, \sigma'_{ij} \qquad (B.3)$$

$$d\bar{\varepsilon}_{p} = (2/3)\, d\bar{\varepsilon}^{p}_{ij}\, d\bar{\varepsilon}^{p}_{ij} \qquad (B.4)$$

$H' = d\bar{\sigma} / d\bar{\varepsilon}^{p}$, correspondes to the slope of the equivalent stress ($\bar{\sigma}$) versus plastic strain ($\int d\bar{\varepsilon}^{p}$) curve.

The inverse of equation (B.1) can be writen as [18]:

$$d\sigma_{ij} = E/(1+\nu)\ \ (d\varepsilon_{ij} + \nu/(1-\nu)\, \delta_{ij}\, d\varepsilon_{ii} - \sigma'_{ij}\, \sigma'_{kl}\, d\varepsilon_{ij}/S) \qquad (B.5)$$

Where :

$$S = (2/3)\, \bar{\sigma}^{2}\, (1 + H'/3G)$$

$$\bar{\sigma} = \sqrt{(2/3\ \sigma'_{ij}\, \sigma'_{ij}}$$

Equation (B.5) can now be used to construct the stress strain matrix [D^{p}] used in equationm (3.8).

In plane strain condition :

$$[D^p]=E/(1+\nu)\begin{vmatrix} (1-\nu)/(1-2\nu)\ -\sigma_x'^2\ /S & \text{SYMMETRIC} & \\ -\sigma_x'\tau_{xy}\ /\ S & -\sigma_x'\tau_{xy}\ /\ S & \\ -\sigma_x'\tau_{xy}/\ S & -\sigma_y'\tau_{xy}/\ S & 1/2-\tau_{xy}^2/S \end{vmatrix}$$

(B.6)

APPENDIX C

SUBROUTINES AND FLOW CHART OF PROGRAM ELPL

SUBROUTINE HEA :

This subroutine is the heart of the program and all the steps explained in section 4.5.2 are carried out in this subroutine. Fig c.1 shows the flowchart of subroutine HEA.

SUBROUTINE BM :

This subroutine computes the elements of strain-displacement matrix [B] according to the infinitesimal strain theory for triangular element.

SUBROUTINE DELA :

This simple subroutine computes the elements of the elastic stress-strain matrix [De] for plane strain condition.

SUBROUTINE DPLA :

Subroutine DPLA computes the plastic stress strain matrix $[D^P]$ for plane strain condition according to the prandtl-Ruess law. Matrix $[D^P]$ relates the increments of the Jaumman stresses and strains in the plastic region. $[D^P]$ is a function of the state of stresses and the slope of the equivalent stress versus equvalent strain curve (H′) and therefore, must be computed at each increment of compression and for each element. The values of the stresses used to compute $[D^P]$ are from the results of the computations at the previous increment.

SUBROUTINE STIFF:

SUBROUTINE STIFF computes the elastic stiffness matrix of each element . The elements ofthis matrix are assembled into the banded matrix [Gs] of global coordinates.

banded matrix [Gs] of global coordinates.

SUBROUTINE PSTIFF:

The role of this subroutine is calculation of [Kd] and [Kc] according to the equations (4.8) and (4.9) and assembling the results in global coordinates to the banded matrix [Gs].

SUBROUTINE VAL:

This subroutine divides a rectangular block into a number of triangular elements according to the number of nodes in X & Y directions. The tasks of this subroutine are :

1- Numbering the degrees of freedom and elements in a way to obtain a stiffness matrix with minimum bandwith.
2- Computing the global coordinates of each node according to the coordinates of the upper right corner of the rectangle.
3- Numbering the vertices of each element (locally) and storing the correspondig global node number in the array LOC(i,j) , where i=No of element & j= No of the vertex.
4- Storing the degrees of freedom the nodes where the displacements are prescribed.
5- Storing the degrees of freedom of the fixed points under sticking or sliding conditions.

For any other geometry this subroutine must be modified.

SUBROUTINE DISL :

This subroutine computes the increment of the local nodal displacements (QL).

SUBROUTINE MATMUL :

THis simple subroutine is used for matrix multiplication.

SUBROUTINE STRESS :

Subrotine stress computes the increment of the stresse and strains.

SUBROUTINE RATIO :

This routine computes the increment of displacement for bringing an element with maximum equivalent stress to the yield point. The scalingfactor R is calculated according to the equation (4.12).

SUBROUTINE DECOMP [32]:

This subroutine decomposes the banded stiffness matrix into the upper and lower triangular matrices (METHOD OF CHOESKI) AND stores the elements of the upper triangular matrix in the original banded matrix.

SUBROUTINE SOLVE [41]:

This subroutine solves the system of equilibrium equations by using the decomposed stiffness matrix from SUBROUTINE DECOMP. Depending on the boundary conditions and the fixed points some elements of stiffness matrix shuld be modified [31,pp 457]. Subroutines Hea takes care of this modification.

SUBROUTINE FRIC :

This Subroutine checks the nodal shear stress. If the shear stress is greater than the introduced static friction stress it removes the condition of the constrained displacement from that particular node and calculate and apply the frictional force in the opposite direction of the flow.

Fig.C-1. LOGIC FLOW OF ELPL PROGRAM

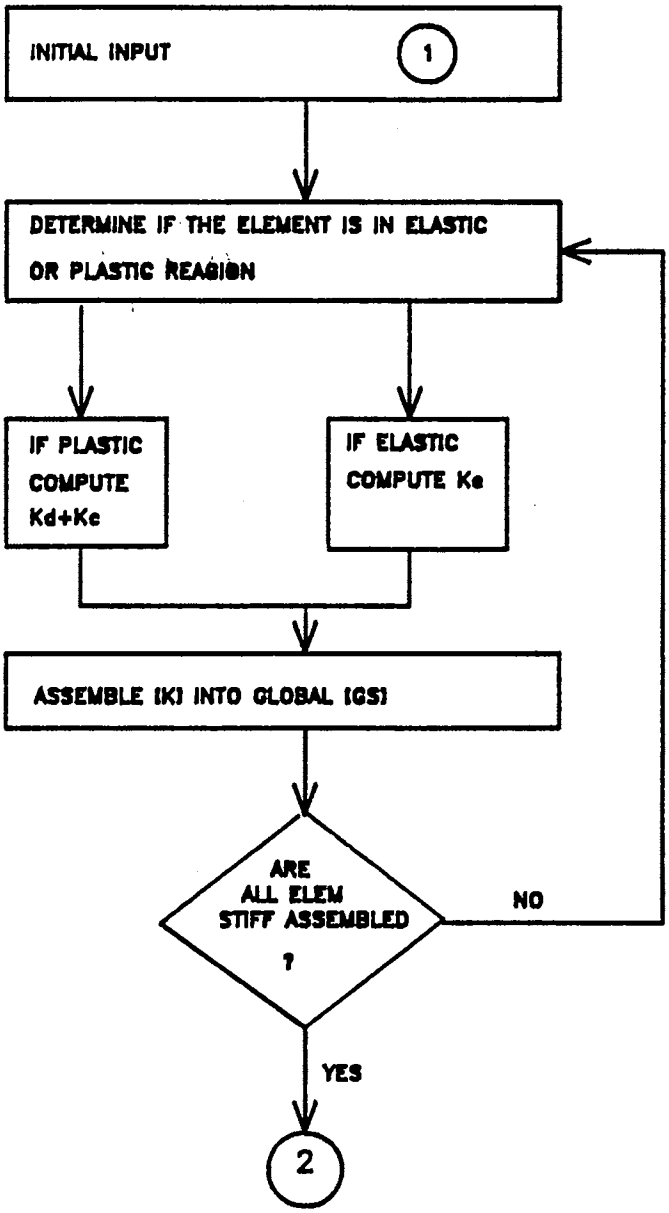

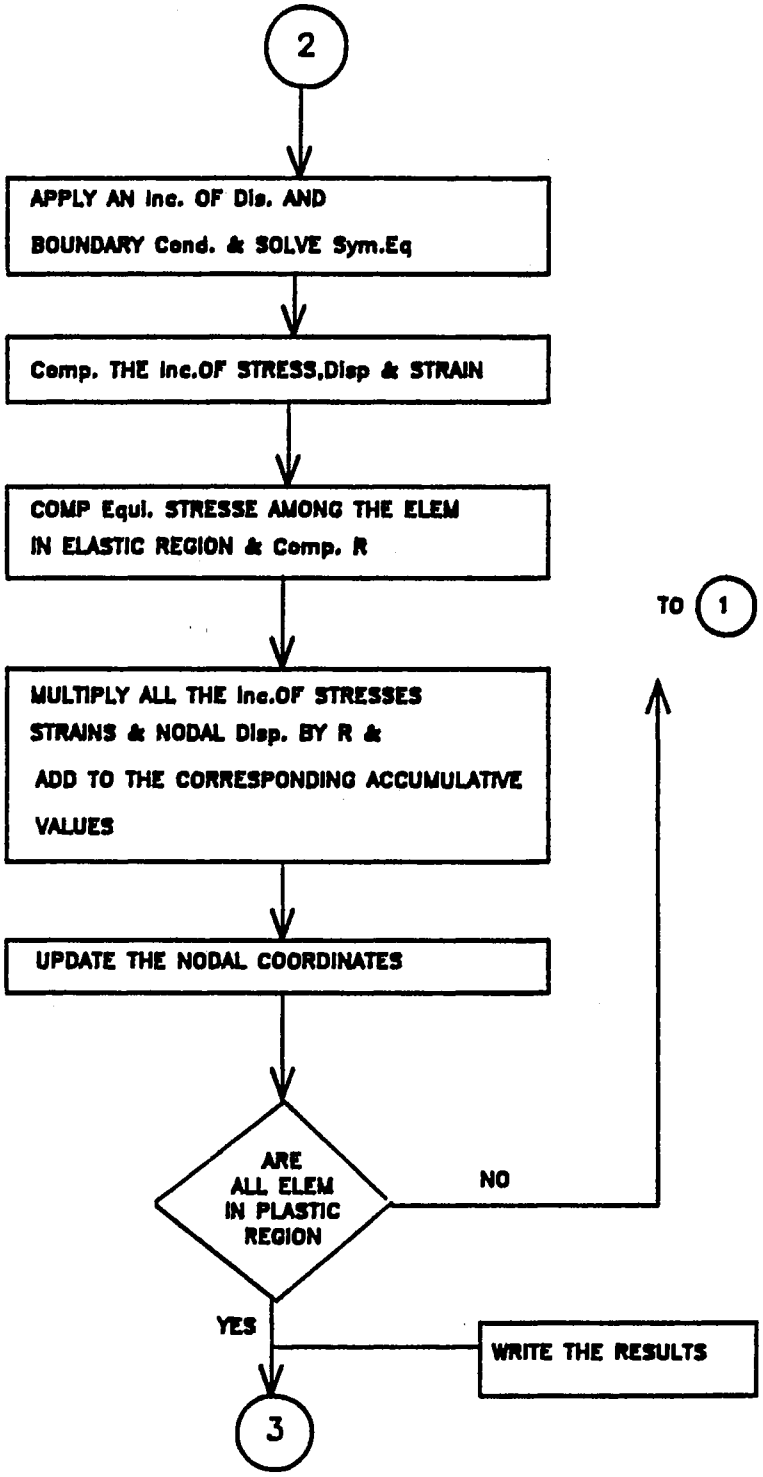
2
APPLY AN Inc. OF Dis. AND
BOUNDARY Cond. & SOLVE Sym.Eq
Comp. THE Inc.OF STRESS,Disp & STRAIN
COMP Equi. STRESSE AMONG THE ELEM
IN ELASTIC REGION & Comp. R
MULTIPLY ALL THE Inc.OF STRESSES
STRAINS & NODAL Disp. BY R &
ADD TO THE CORRESPONDING ACCUMULATIVE
VALUES
UPDATE THE NODAL COORDINATES
ARE
ALL ELEM
IN PLASTIC
REGION
NO
TO 1
YES
WRITE THE RESULTS
3

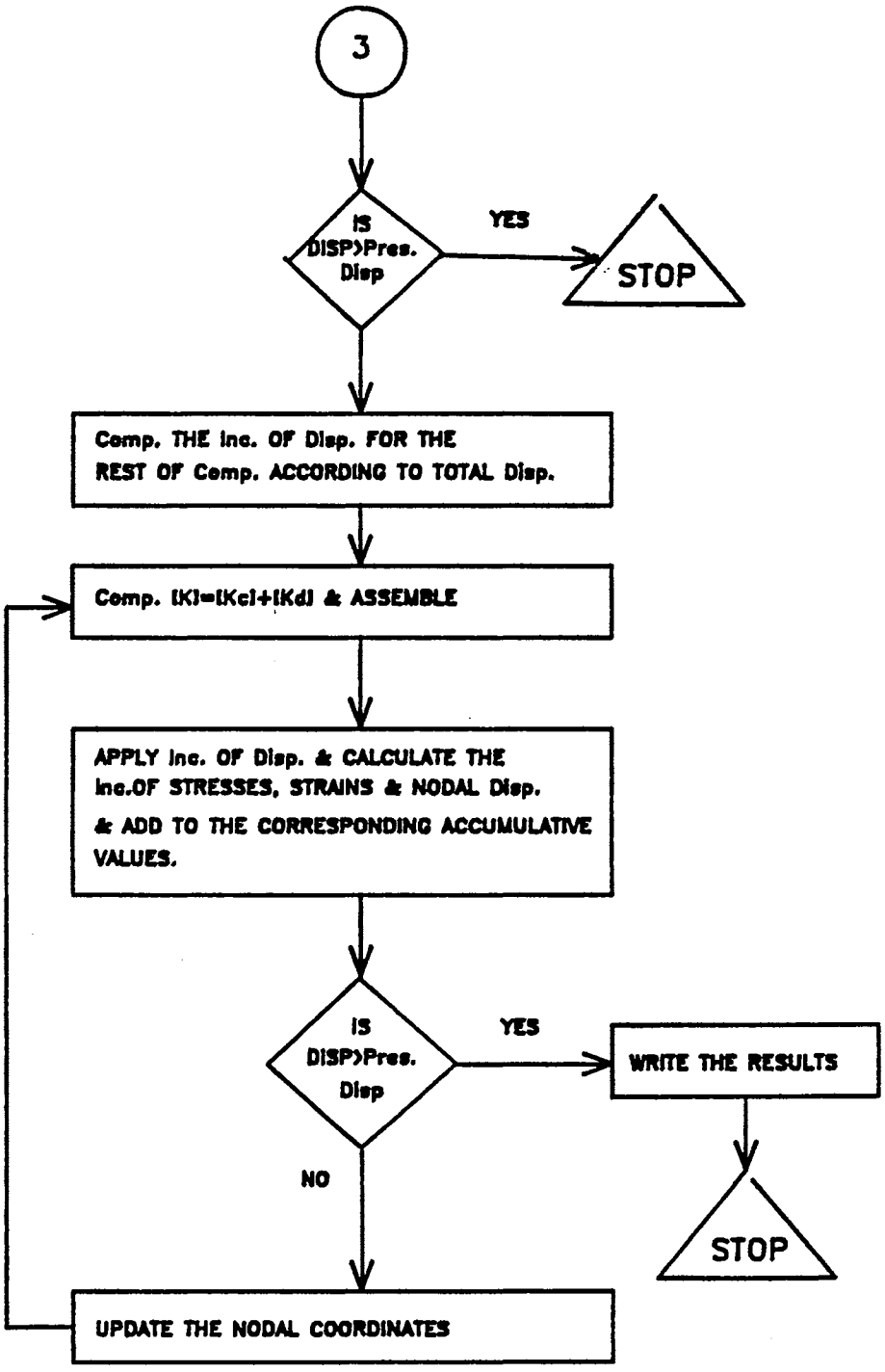
3
IS DISP>Pres. Disp
YES
STOP
Comp. THE Inc. OF Disp. FOR THE REST OF Comp. ACCORDING TO TOTAL Disp.
Comp. [K]=[Kc]+[Kd] & ASSEMBLE
APPLY Inc. OF Disp. & CALCULATE THE Inc.OF STRESSES, STRAINS & NODAL Disp. & ADD TO THE CORRESPONDING ACCUMULATIVE VALUES.
IS DISP>Pres. Disp
YES
WRITE THE RESULTS
STOP
NO
UPDATE THE NODAL COORDINATES

APPENDIX D

PROGRAM "ELPL" FOR ELASTIC-PLASTIC DEFORMATION ANALYSIS

```
      DIMENSION LOC(171,3),CX(193),CY(193),IFIX(100),P(386,1),
     2GS(386,32),STRES(335,5),IDISP(50),STRAIN(335,5),NO(335),MO(335),
     3STR(335,5),STRE(335,5),PA(386,1),IDB(50),AC(20,24),F(20),FA(20),
     4ISL(20)
      DOUBLE PRECISION DIFF(1)
         CALL VAL (N,NE,NN,ND,NB,CX,CY,LOC,IDISP,NDISP,IFIX,NFIX,IDB,
     $NDB,E,ANU,H,YO,MG,NG,MY,ISL)
 M=1
      DATA T,C,WN/1.0,26000.0,0.2/
      DO 50 I=1,ND
  50  P(I,1)=0.0
 NC=NG*2

      CALL CST(NN,NE,ND,NB,M,LOC,CX,CY,E,ANU,T,NFIX,IFIX,P,GS,DIFF,
     2STRES,NDISP,IDISP,STRAIN,YO,C,WN,NO,MO,IDIS,STRE,STR,PA,IW,H,
     3AC,F,FA,NC,MG,NG,MY,ISL)

      STOP

      END


C*************************************************************************
C THIS SUBROUTINE IS BEING USED TO BRING ALL ELEMENTS INTO ELASTIC REGION *
C*************************************************************************


      SUBROUTINE CST(NN,NE,ND,NB,M,LOC,CX,CY,E,ANU,T,NFIX,IFIX,P,GS,
     2DIFF,STRES,NDISP,IDISP,STRAIN,YO,C,WN,NO,MO,IDIS,STRE,STR,PA,
     3IW,H,AC,F,FA,NC,MG,NG,MY,ISL)


      DIMENSION LOC(NE,3),CX(NN),CY(NN),IFIX(100),P(ND,M),GS(ND,NB),
     2STRES(NE,5),AA(6,6),QL(6),DD(3,3),DP(3,3),BB(3,6),DB(3,6),
     3BBT(6,3),IDISP(100),STRAIN(NE,5),NO(NE),MO(NE),STR(NE,5),
     4STRE(NE,5),PA(ND,M),AC(NC,NB),F(NC),FA(NC),ISL(MG),SNS(40),
     5QNS(40),YNS(40),SFS(40),KF(40),NF(40),FOX(40),NEE(30),LF(40)

      DOUBLE PRECISION DIFF(1)

      OPEN(25,FILE='DISA',STATUS='NEW')
      OPEN(40,FILE='STRP',STATUS='NEW')
C     OPEN(50,FILE='SSY',STATUS='NEW')
C     OPEN(60,FILE='SSX',STATUS='NEW')
      OPEN(70,FILE='FORCE',STATUS='NEW')
C     OPEN(80,FILE='STR',STATUS='NEW')
      OPEN(90,FILE='RESULTS',STATUS='NEW')


      WRITE(*,*)'MX=',MX,'MY=',MY,'NN=',NN
      WRITE(90,402)MX,MY,NN
      WRITE(*,*)'NE=',NE,'ND=',ND,'NB=',NB
      WRITE(90,403)NE,ND,NB
      WRITE(*,*)'NFIX=',NFIX,'NDISP=',NDISP
      WRITE(90,404)NFIX,NDISP
```

```
C     DO 310 I=1,NE
C     WRITE(*,*)'LOC=',(LOC(I,J),J=1,3),'I=',I
C 310 WRITE(90,405)I,(LOC(I,J),J=1,3)
C     DO 320 I=1,NFIX
C 320 WRITE(90,406)I,IFIX(I)
C 320 WRITE(*,*)'IFIX=',IFIX(I),'I=',I
      DO 330 I=1,NDISP
 330  WRITE(90,407)I,IDISP(I)
C 330 WRITE(*,*)'IDISP=', IDISP(I)
      G=E/(2*(1+ANU))
      WRITE(*,*)'ENTER THE VALUE OF DISPLACEMENT'
      READ(*,*) UT
      WRITE(*,*)'UT(DISPLACEMENT)=',UT
      WRITE(90,408)UT
      WRITE(90,410)E,ANU,H,YO
      WRITE(*,*)'AMU AF AQP'
      READ(*,*)AMU,AF,AQP
      WRITE(90,420)AMU,AF,AQP
      WRITE(*,*)'DO YOU NEED PRINT OUT ABOUT FRIC  1  OR  NOT'
      READ(*,*)KCP
      AY=1.15*YO
      AK=AY/SQRT(3.)
      ATP=AQP*SQRT(3.)*AMU
      AFT=AF-ATP
      YP=0.995*YO
      DO 99 I=1,40
      NF(I)=0
      FOX(I)=0
      SFS(I)=0
      YNS(I)=0
      QNS(I)=0
      LF(I)=0
      99 KF(I)=0
      NMQ=2
 93   DO 11 I=1,NE
      DO 12 J=1,5
      STRES(I,J)=0.0
      STRE(I,J)=0.0
      STRAIN(I,J)=0.0
      STR(I,J)=0.0
  12  CONTINUE
      MO(I)=1
      NO(I)=1
  11  CONTINUE
      DO 13 I=1,ND
      DO 13 J=1,M
      P(I,M)=0.0
  13  PA(I,M)=0.0
      DO 15 I=1,NC
      F(I)=0.
      FA(I)=0.
      DO 14 J=1,NB
```

```
  14  AC(I,J)=0.
  15  CONTINUE
      HE=CY(1)
C**SUBROUTINE (DELA) CALCULATES D MATRIX [DD] ACCORDING TO HOOK LAW **

      CALL DELA(E,ANU,DD)
      IGH=0
  101 DT=-0.1
      WRA=0.0
      DO 10 I=1,ND
      DO 10 J=1,NB
  10  GS(I,J)=0.0
      DO 100 I=1,NE

C**SUBROUTINE (STIFF) CALCULATES THE STIFFNESS MATRIX FOR EACH********
C********ELEMENT AND STORE IT IN BANDED MATRIX [GS]********************

      IF (NO(I).EQ.1) CALL STIFF(I,LOC,DD,NN,NE,ND,NB,CX,CY,T,GS)
      IF (NO(I).EQ.2) THEN

C**SUBROUTINE (DPLA) COMPUTES D MATRIX [DP] ACCORDING TO PRANDTL REUSS*

       CALL DPLA(NE,E,YO,C,WN,STRE,STR,I,MO,DP,H)
       CALL PSTIFF(I,LOC,DP,NN,NE,ND,NB,CX,CY,T,GS,STRE)
      ENDIF
 100  CONTINUE

C*** DO 50 MULTIPLIES EVERY TERM OF [GS], CORRESPONDING TO THE FIXED **
C*** POINTS(INCLUDING THE PRISCIBED POINTS), BY A LARGE NUMBER.********
*****

      DO 50 I=1,NFIX
      IX=IFIX(I)
 50   GS(IX,1)=GS(IX,1)*1.0E6
      IF(IGH.EQ.0) GO TO 777
      DO 778 I=1,NNC
      JJJ=NF(I)+1
      III=NF(I)
      IF(KF(I).EQ.1) GS(III,1)=GS(III,1)/1.0E6
      IF(LF(I).EQ.1) GS(JJJ,1)=GS(JJJ,1)/1.0E6
 778  CONTINUE

C*********  DO 52 INTRODUCES THE PRISCRIBED DISPLACEMENTS**************

 777  DO 52 I=1,NDISP
      IZ=IDISP(I)
      P(IZ,1)=GS(IZ,1)*DT
  52  CONTINUE
      IF(IGH.EQ.0)GO TO 776
      DO 787 I=1,NNC
      IF(KF(I).EQ.1) THEN
      KHW=NF(I)
```

```
      P(KHW,1)=FOX(I)
      ENDIF
 787 CONTINUE

C** SUBROUTINE (DECOMP)  DECOMPOSES [GS] INTO LOWER AND UPPER Tr.*****
C** MATRICES AND STORES THE ELEMENTS OF THE UPPER TRIANGLE  [GS].*****
C** SUBROUTINE (SOLVE) SOLVES THE SYSTEM OF EQUATIONS [GS]{U}={P} &***
C** STORES THE RESULTS INTO {P}. NOW,{P} ARE GLOBAL NODAL  ***********
C**DISPLACEMENT INCREMENTS.   ****************************************

 776  CALL DECOMP(ND,NB,GS)
      CALL SOLVE(ND,NB,M,GS,P,DIFF)
      DO 200 I=1,NE

C**SUBROUTINE (DISL) COMPUTES THE LOCAL NODAL DISPLACEMENT  **********
C**INCREMENT{QL}.****************************************************

      CALL DISL(I,LOC,NE,ND,M,P,QL)

C**SUBROUTINE (BM) COMPUTES THE B MATRIX [BB] ACCORDING TO  **********
C**INCREMENTAL DISPLACEMENT THEORY. **********************************

      CALL BM(NE,NN,I,LOC,CX,CY,BB,AREA)

C**SUBROUTINE MATMUL MULTIPLIIES [DD] BY [BB] AND STORES IT IN [DB].**

      IF (NO(I).EQ.1) CALL MATMUL(DD,BB,DB,3,3,6)
      IF (NO(I).EQ.2) THEN
      CALL DPLA(NE,E,YO,C,WN,STRE,STR,I,MO,DP,H)
      MO(I)=MO(I)+1
      CALL MATMUL(DP,BB,DB,3,3,6)
      ENDIF

C*** SUBROUTINE (STRESS) COMPUTES THE STRESS & STRAIN INCREMENTS *****
C*** & STORE THEM IN STRES & STRAIN ARRAYS. ***************************

      CALL STRESS(NE,I,QL,BB,DB,STRES,STRAIN)

C** THE FOLLOWING 6 LINES FIND MAX EQUIVALENT STRES (STRE(I,4)) & ****
** ADDRESS OF THE CORRESPONDING ELEMENT AMONG THE ELASTIC ELEMNTS****

      IF(NO(I).EQ.1) THEN
      STRES(I,5)=ANU*(STRES(I,1)+STRES(I,2))
      SX=STRES(I,1) +STRE(I,1)
      SY=STRES(I,2) +STRE(I,2)
      SXY=STRES(I,3)+STRE(I,3)
      SZ=STRES(I,5)+STRE(I,5)
      STRE(I,4)=SQRT(0.5*((SX-SY)**2+(SY-SZ)**2+(sz-sx)**2)+3*SXY**2)
       IF (STRE(I,4).GE.WRA) THEN
        WRA=STRE(I,4)
        IN=I
       ENDIF
      ENDIF
```

```
 200  CONTINUE

C**SUBROUTINE (RATIO) COMPUTES THE SCALING FACTOR FOR BRINGING THE ***
C**ELEMENT (IN) INTO PLASTIC REGION . ********************************

      CALL RATIO(NE,IN,YO,STRES,STRE,R)
      CO=R
      PCH=P(2,M)*CO
      IF(PCH.LT.-0.0015) CO=(-.0015/P(2,M))
      IW=0
      DO 22 I=1,NE
      DO 23 J=1,3
      STRES(I,J)=STRES(I,J)*CO
C     STRE(I,J)=STRE(I,J)+STRES(I,J)
      STRAIN(I,J)=STRAIN(I,J)*CO
      STR(I,J)=STR(I,J)+STRAIN(I,J)
  23  CONTINUE
      SX=STRE(I,1)
      SXX=STRES(I,1)
      SY= STRE(I,2)
      SYY=STRES(I,2)
      SXY=STRE(I,3)
      SZ= STRE(I,5)
      IF(NO(I).EQ.2)THEN
      S1=STRAIN(I,1)
      S2=STRAIN(I,2)
      S3=STRAIN(I,3)
      SM=(SX+SY+SZ)/3.0
      SXP=SX-SM
      SYP=SY-SM
      SZP=SZ-SM
      PP=SXP*S1+SXY*S3+SYP*S2
      STRAIN(I,4)=PP/( STRE(I,4)*(1+H/(3*G)) )
      IF (STRAIN(I,4).LT.0.0)WRITE(*,*)'STRAIN(I,4)<0=',STRAIN(I,4),I
      STR(I,4)=STR(I,4)+STRAIN(I,4)
      S=(STRE(I,4)**2)*(1+H/(3*G))
      STRES(I,5)=2*G*((ANU/(1-2*ANU))*(S1+S2)-(SZP/S)*(SXP*S1+SYP*S2
     $+SXY*S3))
C     STRES(I,5)=.5*(SXX+SYY)
C     AH=(SX-.5*(SY+SZ))/(SZ-.5*(SY+SX))
C     STRES(I,5)=(ANU*AH*(SYY+SXX)+SXX-ANU*SYY-E*STRAIN(I,1))/(ANU+AH)
      ENDIF
      IF(NO(I).EQ.1) STRES(I,5)=ANU*(SXX+SYY)
      STRE(I,1)=STRE(I,1)+SXX
      STRE(I,2)=STRE(I,2)+SYY
      STRE(I,3)=STRE(I,3)+STRES(I,3)
      STRE(I,5)=STRE(I,5)+STRES(I,5)
      SX=STRE(I,1)
      SY= STRE(I,2)
      SXY=STRE(I,3)
      SZ= STRE(I,5)
      STRE(I,4)=SQRT(0.5*((SX-SY)**2+(SY-SZ)**2+(sz-sx)**2)+3*SXY**2)
      S1=STRAIN(I,1)
```

```
      S2=STRAIN(I,2)
      S3=STRAIN(I,3)
      STRAIN(I,5)=SQRT((4./9)*((S1-S2)**2+S1**2+S2**2)+(4./3)*(S3**2))
      STR(I,5)=STR(I,5)+STRAIN(I,5)
      IF(STRE(I,4).GE.YP)THEN
      NO(I)=2
      IW=IW+1
      ENDIF
   22 CONTINUE
      DO 24 I=1,ND
      P(I,M)=P(I,M)*CO
      PA(I,M)=PA(I,M)+P(I,M)
   24 CONTINUE
      DO 72 J=1,NN
      JA=2*J-1
      JB=2*J
      CX(J)=CX(J)+P(JA,1)
      CY(J)=CY(J)+P(JB,1)
   72 CONTINUE
      IF(NMQ.LE.MG) THEN
      DO 700 I=NMQ,MG
      KA=ISL(I)
      IF(CY(KA).GE.CY(1))THEN
      NMQ=NMQ+1
      KDX=2*KA-1
      KDY=2*KA
      NDISP=NDISP+1
      WRITE(*,*)' I=',I,' NMQ',NMQ,'  NDISP',NDISP
      IDISP(NDISP)=KDY
      NFIX=NFIX+2
      DO 701 J=1,NFIX
      IF(IFIX(J).GE.KDX)THEN
      JC=J
      GO TO 702
      ENDIF
   701 CONTINUE
   702 DO 703 K=JC,NFIX-2,2
      IR1=IFIX(K)
      IR2=IFIX(K+1)
      IFIX(K)=KDX
      IFIX(K+1)=KDY
      KDX=IR1
      KDY=IR2
   703 CONTINUE
      IFIX(NFIX-1)=KDX
      IFIX(NFIX)=KDY
      ENDIF
   700 CONTINUE
      ENDIF
      IGH=IGH+1
      WRITE(*,*)'  ITER=',IGH,'  DISP=',PA(2,1)
      WRITE(40,421)IGH,PA(2,1)
      CALL FRIC(NN,NE,NG,MG,STRE,SNS,QNS,YNS,NNB,NNC,
     $AQP,AY,ATP,AFT,AK,AMU,SFS,KF,NF,FOX,P,CX,ND,FORCE,CY,LF)
      PPA=100*ABS(PA(2,1))/HE
```

```
      WRITE(70,417) FORCE,PPA
      IF(KCP.NE.1)GO TO 967
      DO 113 I=1,NNC
      WRITE(40,419)I,SNS(I),YNS(I),QNS(I),SFS(I),FOX(I),CX(I),KF(I)
     $,NF(I),LF(I)
 113  CONTINUE
 967  IF(PA(2,1).LE.UT) GO TO 801
      IF(IW.LT.NE)GO TO 101
 801  WRITE(90,411)
      WRITE(*,*)' COMPRESSION:',PA(2,1)
      DO 110 I=1,NN
      J=I*2
C     WRITE(*,*)' DISPLACEMENT OF NODES',I,PA(I,1)
      WRITE(90,412)CX(I),CY(I),PA(J-1,1),PA(J,1),I
 110  CONTINUE
      DO 111 I=1,NE
C     WRITE(*,*) 'STRESS',(STRE(I,J),J=1,5)
      WRITE(90,400)I,(STRE(I,J),J=1,5)
      WRITE(90,401)I,(STR(I,J),J=1,5)
C     WRITE(*,*) 'STRAIN',(STR(I,J),J=1,5)
 111  CONTINUE
      DO 112 I=1,NE
C     WRITE (*,*)'I=',I,'NO=',NO(I),'   MO=',MO(I),'  H=',H
 112  WRITE(90,413)I,NO(I),MO(I)
      WRITE(*,*)' NFIX=',NFIX
      DO  809 I=1,NFIX
 809  WRITE(*,*)' I=',I,' IFIX=',IFIX(I)
      DO 811 I=1,NDISP
 811  WRITE(*,*)' I=',IDISP(I)
      DO 812 I=1,NN
 812  WRITE(*,*) ' I=',I,' CY',CY(I)
C*********************************************************************

      WRITE(*,*)' ENTER NO OF ITR'
      READ(*,*)ITR
      WRITE(90,409)ITR
      DT=(UT-PA(2,1))/ ITR
      IF(DT.GE.0)GO TO 800
      WRITE(*,*)'DO YOU PRINT OUT ABOUT FRIC  1=YES'
      READ(*,*)KCP
      DO 88 JR=1,ITR
      DO 31 I=1,NE
      CALL DPLA(NE,E,YO,C,WN,STRE,STR,I,MO,DP,H)
      CALL PSTIFF(I,LOC,DP,NN,NE,ND,NB,CX,CY,T,GS,STRE)
  31  CONTINUE
      DO 60 I=1,NFIX
      IX=IFIX(I)
 60   GS(IX,1)=GS(IX,1)*1.0E6
      DO 779 I=1,NNC
      III=NF(I)
      JJJ=NF(I)+1
      IF(KF(I).EQ.1) GS(III,1)=GS(III,1)/1.0E6
      IF(LF(I).EQ.1) GS(JJJ,1)=GS(JJJ,1)/1.0E6
```

```
 779  CONTINUE
      DO 62 I=1,NDISP
      IZ=IDISP(I)
      P(IZ,1)=GS(IZ,1)*DT
  62  CONTINUE
      DO 788 I=1,NNC
      IF(KF(I).EQ.1)THEN
      KHW=NF(I)
      P(KHW,1)=FOX(I)
      ENDIF
 788  CONTINUE
      CALL DECOMP(ND,NB,GS)
      CALL SOLVE(ND,NB,M,GS,P,DIFF)
      DO 210 I=1,NE
      CALL DISL(I,LOC,NE,ND,M,P,QL)
      CALL BM(NE,NN,I,LOC,CX,CY,BB,AREA)
      CALL DPLA(NE,E,YO,C,WN,STRE,STR,I,MO,DP,H)
      MO(I)=MO(I)+1
      CALL MATMUL(DP,BB,DB,3,3,6)
      CALL STRESS(NE,I,QL,BB,DB,STRES,STRAIN)
 210  CONTINUE
      DO 32 I=1,NE
      DO 33 J=1,3
      STR(I,J)=STR(I,J)+STRAIN(I,J)
  33  CONTINUE
      SX=STRE(I,1)
      SXX=STRES(I,1)
      SY= STRE(I,2)
      SYY=STRES(I,2)
      SXY=STRE(I,3)
      SZ= STRE(I,5)
      S1=STRAIN(I,1)
      S2=STRAIN(I,2)
      S3=STRAIN(I,3)
      SM=(SX+SY+SZ)/3.0
      SXP=SX-SM
      SYP=SY-SM
      SZP=SZ-SM
      PP=SXP*S1+SXY*S3+SYP*S2
      STRAIN(I,4)=PP/( STRE(I,4)*(1+H/(3*G)) )
      IF (STRAIN(I,4).LT.0.0)WRITE(*,*)'STRAIN(I,4)<0=',STRAIN(I,4),I
      STR(I,4)=STR(I,4)+STRAIN(I,4)
      S=(STRE(I,4)**2)*(1+H/(3*G))
      STRES(I,5)=2*G*((ANU/(1-2*ANU))*(S1+S2)-(SZP/S)*(SXP*S1+SYP*S2
     $+SXY*S3))
C     STRES(I,5)=.5*(SXX+SYY)
      STRE(I,1)=STRE(I,1)+SXX
      STRE(I,2)=STRE(I,2)+SYY
      STRE(I,3)=STRE(I,3)+STRES(I,3)
      STRE(I,5)=STRE(I,5)+STRES(I,5)
      SX=STRE(I,1)
      SY= STRE(I,2)
      SXY=STRE(I,3)
```

```
      SZ= STRE(I,5)
      STRE(I,4)=SQRT(0.5*((SX-SY)**2+(SY-SZ)**2+(sz-sx)**2)+3*SXY**2)
      S1=STRAIN(I,1)
      S2=STRAIN(I,2)
      S3=STRAIN(I,3)
      STRAIN(I,5)=SQRT((4./9)*((S1-S2)**2+S1**2+S2**2)+(4./3)*(S3**2))
      STR(I,5)=STR(I,5)+STRAIN(I,5)
   32 CONTINUE
      DO 34 I=1,ND
      PA(I,M)=PA(I,M)+P(I,M)
   34 CONTINUE
      DO 71 J=1,NN
      JA=2*J-1
      JB=2*J
      CX(J)=CX(J)+P(JA,1)
      CY(J)=CY(J)+P(JB,1)
   71 CONTINUE
      IF(NMQ.LE.MG) THEN
      DO 750 I=NMQ,MG
      KA=ISL(I)
      IF(CY(KA).GE.CY(1))THEN
      NMQ=NMQ+1
      KDX=2*KA-1
      KDY=2*KA
      NDISP=NDISP+1
      WRITE(*,*)'  NMQ=',NMQ,' NDISP',NDISP
      IDISP(NDISP)=KDY
      NFIX=NFIX+2
      DO 751 J=1,NFIX
      IF(IFIX(J).GE.KDX)THEN
      JC=J
      GO TO 752
      ENDIF
  751 CONTINUE
  752 DO 753 K=JC,NFIX-2,2
      IR1=IFIX(K)
      IR2=IFIX(K+1)
      IFIX(K)=KDX
      IFIX(K+1)=KDY
      KDX=IR1
      KDY=IR2
  753 CONTINUE
      IFIX(NFIX-1)=KDX
      IFIX(NFIX)=KDY
      ENDIF
  750 CONTINUE
      ENDIF
      KTC=IGH+JR
      WRITE(*,*)' **ITR=',KTC,'  DISP=',PA(2,1)
C     WRITE(40,421)KTC,PA(2,1)
      CALL FRIC(NN,NE,NG,MG,STRE,SNS,QNS,YNS,NNB,NNC,
     $AQP,AY,ATP,AFT,AK,AMU,SFS,KF,NF,FOX,P,CX,ND,FORCE,CY,LF)
      PPA=100*ABS(PA(2,1))/HE
```

```
      WRITE(70,417)FORCE,PPA
      IF(KCP.NE.1)GO TO 88
      DO 780 I=1,NNC
      WRITE(40,419)I,SNS(I),YNS(I),QNS(I),SFS(I),FOX(I),CX(I),KF(I)
     $,NF(I)
 780  CONTINUE
  88  CONTINUE
C     WRITE(*,*)'  NFIX=',NFIX,'  IFIX',IFIX
      DO 813 I=1,NFIX
 813  WRITE(*,*)' I=',I,' IFIX=',IFIX(I)
      DO 814 I=1,NDISP
 814  WRITE(*,*)' I=',I,' IDISP',IDISP(I)
C     DO 817 I=1,NN
C 817 WRITE(*,*)' I=',I,'  CY',CY(I)
      WRITE(90,414)
      WRITE(*,*)'*******TOTAL COMPRESSION [IN] :',PA(2,1),'******'
C     DO  167  I=1,NC
C     WRITE(90,415)I,FA(I),F(I)
C     WRITE(*,415)I,FA(I),F(I)
C167  CONTINUE
      DO 67 I=1,NN
      J=I*2
      WRITE(*,*) 'DISPLACEMENT OF NODES',I,PA(I,1),'  ITR=',JR
      WRITE(90,412)CX(I),CY(I),PA(J-1,1),PA(J,1),I
  67  CONTINUE
      IGH=IGH+JR
      WRITE(90,421)IGH,PA(2,1)
      WRITE(*,*)'  ITR=',IGH
      CALL FRIC(NN,NE,NG,MG,STRE,SNS,QNS,YNS,NNB,NNC,
     $AQP,AY,ATP,AFT,AK,AMU,SFS,KF,NF,FOX,P,CX,ND,FORCE,CY,LF)
      DO 913 I=1,NNC
 913  WRITE(90,419)I,SNS(I),YNS(I),QNS(I),SFS(I),FOX(I),CX(I),KF(I)
     $,NF(I),LF(I)
      DO 68 I=1,NE
      WRITE(90,400)I,(STRE(I,J),J=1,5)
      WRITE(90,401)I,(STR(I,J),J=1,5)
  68  CONTINUE
C     DO 69 I=1,NE
C 69  WRITE(90,413)I,NO(I),MO(I)
 800  DO 90 I=1,MG-1
      IF(I.EQ.1) THEN
      NEE(I)=2*(NG-1)+1
      WRITE(*,*)'  I=',I,' NE=',NEE(I)
      GO TO 90
      ENDIF
      NEE(I)=NEE(I-1)+2*(NG-1+I-1)+1
      WRITE(*,*)'  I=',I,' NE',NEE(I)
      NT=I
  90  CONTINUE
      DO  91 I=1,MY-1
      J=NT+I
      NEE(J)=NEE(J-1)+2*(MG+NG-2)
      WRITE(*,*)' J=',J,' NE=',NEE(I)
```

```
 91   CONTINUE
      NPT=1
      DO 92 K=1,MG+MY-2
      DO 96 I=NPT,NEE(K),2
      IF(K.LE.MG-1)THEN
      IF(I.EQ.NEE(K))THEN
      WRITE(25,178)CX(LOC(I,2)),CY(LOC(I,2))
      WRITE(25,178)CX(LOC(I,1)),CY(LOC(I,1))
      WRITE(25,178)CX(LOC(I,3)),CY(LOC(I,3))
      WRITE(25,178)CX(LOC(I,2)),CY(LOC(I,2))
      GO TO 96
      ENDIF
      ENDIF
      IF(K.GT.MG-1)THEN
      IF(I.GT.NPT) GO TO 95
      WRITE(25,178)CX(LOC(I,2)),CY(LOC(I,2))
      WRITE(25,178)CX(LOC(I,1)),CY(LOC(I,1))
 95   WRITE(25,178)CX(LOC(I,3)),CY(LOC(I,3))
      WRITE(25,178)CX(LOC(I,2)),CY(LOC(I,2))
      WRITE(25,178)CX(LOC(I+1,2)),CY(LOC(I+1,2))
      WRITE(25,178)CX(LOC(I,3)),CY(LOC(I,3))
      GO TO 96
      ENDIF
      WRITE(25,178)CX(LOC(I,2)),CY(LOC(I,2))
      WRITE(25,178)CX(LOC(I,1)),CY(LOC(I,1))
      WRITE(25,178)CX(LOC(I,3)),CY(LOC(I,3))
      WRITE(25,178)CX(LOC(I,2)),CY(LOC(I,2))
 96   CONTINUE
      JT=0
      DO 94 I=NPT,NEE(K),2
      JT=JT+2
      J=NEE(K)-JT+2
      WRITE(25,178)CX(LOC(J,2)),CY(LOC(J,2))
      KL=J
 94   CONTINUE
      WRITE(25,178)CX(LOC(J,1)),CY(LOC(J,1))
      NPT=NEE(K)+1
 92   CONTINUE
178   FORMAT(2F10.4)
400   FORMAT(5X,'ELEMENT:',I4,'   STRESSES:',5F10.2)
401   FORMAT(5X,'ELEMENT:',I4,'   STRAINS:',5F10.6)
402   FORMAT(5X,'MX=',I3,'   MY=',I3,'   NN=',I4)
403   FORMAT(5X,'NE=',I3,'   ND=',I3,'   NB=',I3)
404   FORMAT(5X,'NFIX=',I3,'   NDISP=',I3)
405   FORMAT(5X,'I=',I3,'  LOC=',3I3)
406   FORMAT(5X,'NFIX=',I3,'  IFIX=',I3)
407   FORMAT(5x,'NDISP=',I3,' IDISP=',I3)
408   FORMAT(5X,'TOTAL DIE DISPLACEMENT:',F10.6)
409   FORMAT(5X,'No OF ITERATION AFTER ALL ELEM IN PLASTIC',I4)
410   FORMAT(5X,'E=',F10.1,' POIS RATIO=',F4.2,'  H=',F8.2,' YO=',F10.2)
411   FORMAT(5X,'***AT THIS PONT ALL ELMENTS ARE IN PLASTIC ZONE***')
412   FORMAT(5X,4F9.5,'  DISP AT NODE:',I5)
413   FORMAT(5X,'ELEMENT No:',I4,'  NO=',I3,'   MO=',I5)
414   FORMAT(////,5X,'****** RESULTS AT THE END OF DEFORMATION******')
415   FORMAT(5X,'NODE:',I3,'  TOTAL LOAD:',F13.1,' INC LOAD:',F13.1)
```

```
417 FORMAT(5X,F13.2,5X,F13.7)
418 FORMAT(5X,F13.6,5X,F10.7)
419 FORMAT(2X,I5,6F10.3,2I5)
420 FORMAT(5X,'AMU=',F4.2,'  AF=',F4.2,'  AQP=',F4.2)
421 FORMAT(5X,'ITER:',I4,'  DISPLACEMENT:',F9.5)
     RETURN
     END


     SUBROUTINE STRESS(NE,I,QL,BB,DB,STRES,STRAIN)
     DIMENSION QL(6),BB(3,6),DB(3,6),STRES(NE,5),STRAIN(NE,5),SLOC(3),
    $ST(3)

     DO 90 II=1,3
     SLOC(II)=0.0
     ST(II)=0.0
     DO 90 JJ=1,6
     SLOC(II)=SLOC(II)+DB(II,JJ)*QL(JJ)
     ST(II)=ST(II)+BB(II,JJ)*QL(JJ)
 90  CONTINUE
     STRES(I,1)=SLOC(1)
     STRES(I,2)=SLOC(2)
     STRES(I,3)=SLOC(3)
     STRAIN(I,1)=ST(1)
     STRAIN(I,2)=ST(2)
     STRAIN(I,3)=ST(3)

     RETURN
     END


     SUBROUTINE DISL(I,LOC,NE,ND,M,P,QL)
     DIMENSION P(ND,M),QL(6),N(6),LOC(NE,3)

     J=LOC(I,1)
     K=LOC(I,2)
     L=LOC(I,3)
     N(1)=J*2-1
     N(2)=J*2
     N(3)=K*2-1
     N(4)=K*2
     N(5)=L*2-1
     N(6)=L*2
     DO 60 II=1,6
     NR=N(II)
60   QL(II)=P(NR,1)

     RETURN
     END


     SUBROUTINE STIFF(I,LOC,DD,NN,NE,ND,NB,CX,CY,T,GS)
```

```
      DIMENSION CX(NN),CY(NN),GS(ND,NB),LOC(NE,3),
     2N(6),DD(3,3),BB(3,6),DB(3,6),BBT(6,3)

      REAL KG(6,6)
      J=LOC(I,1)
      K=LOC(I,2)
      L=LOC(I,3)
      CALL BM(NE,NN,I,LOC,CX,CY,BB,AREA)
      CALL MATMUL(DD,BB,DB,3,3,6)
      DO 82 II=1,6
      DO 82 JJ=1,3
82    BBT(II,JJ)=BB(JJ,II)
      CALL MATMUL(BBT,DB,KG,6,3,6)
      TTT=T*AREA
      DO 83 II=1,6
      DO 83 JJ=1,6
83    KG(II,JJ)=TTT*KG(II,JJ)
      N(1)=J*2-1
      N(2)=J*2
      N(3)=K*2-1
      N(4)=K*2
      N(5)=L*2-1
      N(6)=L*2
      DO 40 II=1,6
      DO 40 JJ=1,6
      IK=N(II)
      JK=N(JJ)
      IN=JK-IK+1
      IF(IN.LE.0) GO TO 40
      GS(IK,IN)=GS(IK,IN)+KG(II,JJ)
40    CONTINUE

      RETURN
      END

      SUBROUTINE PSTIFF(I,LOC,DD,NN,NE,ND,NB,CX,CY,T,GS,STRE)

      DIMENSION CX(NN),CY(NN),GS(ND,NB),LOC(NE,3),STRE(NE,5),
     2N(6),DD(3,3),BB(3,6),DB(3,6),BBT(6,3),CXL(3),CYL(3)

      REAL KG(6,6),KR(6,6)
      J=LOC(I,1)
      K=LOC(I,2)
      L=LOC(I,3)
      GX=(CX(J)+CX(K)+CX(L))/3
      GY=(CY(J)+CY(K)+CY(L))/3
      CXL(1)=CX(J)-GX
      CXL(2)=CX(K)-GX
      CXL(3)=CX(L)-GX
      CYL(1)=CY(J)-GY
      CYL(2)=CY(K)-GY
      CYL(3)=CY(L)-GY
      AREA=((CXL(3)-CXL(2))*(CYL(2)-CYL(1))-(CXL(2)-CXL(1))*(CYL(3)-
```

```
     2CYL(2)))/2.0
      Y32=(CYL(3)-CYL(2))/(2.0*AREA)
      X32=(CXL(3)-CXL(2))/(2.0*AREA)
      Y31=(CYL(3)-CYL(1))/(2.0*AREA)
      X31=(CXL(3)-CXL(1))/(2.0*AREA)
      Y21=(CYL(2)-CYL(1))/(2.0*AREA)
      X21=(CXL(2)-CXL(1))/(2.0*AREA)
      DO 81 II=1,3
      DO 81 JJ=1,6
81    BB(II,JJ)=0.0
      BB(1,1)=Y32
      BB(1,3)=-Y31
      BB(1,5)=Y21
      BB(2,2)=-X32
      BB(2,4)=X31
      BB(2,6)=-X21
      BB(3,1)=-X32
      BB(3,2)= Y32
      BB(3,3)= X31
      BB(3,4)=-Y31
      BB(3,5)=-X21
      BB(3,6)= Y21
      CALL MATMUL(DD,BB,DB,3,3,6)
      DO 82 II=1,6
      DO 82 JJ=1,3
82    BBT(II,JJ)=BB(JJ,II)
      CALL MATMUL(BBT,DB,KG,6,3,6)
      AR=1
      A1=STRE(I,1)/AR
      B1=STRE(I,2)/AR
      C1=STRE(I,3)/AR
      A2=-2*STRE(I,1)/AR
      B2=-2*STRE(I,2)/AR
      C2=-2*STRE(I,3)/AR
      KR(1,1)=A1*Y32*Y32+B1*X32*X32-2*C1*Y32*X32+A2*(Y32*Y32+X32*X32/4)
     $+B2*X32*X32/4-2*C2*(Y32*X32)
      KR(1,2)=-A2*X32*Y32/4-B2*X32*Y32/4+C2*(Y32*Y32+X32*X32)
      KR(2,1)=KR(1,2)
      KR(1,3)=-A1*Y32*Y31-B1*X32*X31+C1*Y32*X31+C1*X32*Y31-A2*Y32*Y31
     $-A2*X32*X31/4-B2*X32*X31/4+C2*Y32*X31+C2*X32*Y31
      KR(3,1)=KR(1,3)
      KR(1,4)=A2*X32*Y31/4+B2*X32*Y31/4-C2*Y32*Y31-C2*X32*X31
      KR(1,5)=A1*Y32*Y21+B1*X32*X21-C1*Y32*X21-C1*X32*Y21+A2*Y32*Y21
     $+A2*X32*X21/4+B2*X32*X21/4-C2*Y32*X21-C2*X32*Y21
      KR(5,1)=KR(1,5)
      KR(1,6)=-A2*X32*Y21/4-B2*X32*Y21/4+C2*Y32*Y21+C2*X32*X21
      KR(6,1)=KR(1,6)
      KR(2,2)=A1*Y32*Y32+B1*X32*X32-C1*Y32*X32-C1*X32*Y32+A2*Y32*Y32/4
     $+B2*Y32*Y32/4+X32*X32-C2*Y32*X32-C2*X32*Y32
      KR(2,3)=A2*Y32*X31/4+B2*Y32*X31/4-C2*Y32*Y31-C2*X32*X31
      KR(3,2)=KR(2,3)
      KR(2,4)=-A1*Y32*Y31-B1*X32*X31+C1*Y32*X31+C1*X32*Y31-A2*Y32*Y31/4
     $-B2*Y32*Y31/4-B2*X32*X31+C2*Y32*X31+C2*X32*Y31
```

```
      KR(4,2)=KR(2,4)
      KR(2,5)=-A2*Y32*X21/4-B2*Y32*X21/4+C2*Y32*Y21+C2*X32*X21
      KR(5,2)=KR(2,5)
      KR(2,6)=A1*Y32*Y21+B1*X32*X21-C1*X32*Y21-C1*Y32*X21+A2*Y32*Y21/4
     $+B2*Y32*Y21/4+B2*X32*X21-C2*Y32*X21-C2*X32*Y21
      KR(6,2)=KR(2,6)
      KR(3,3)=A1*Y31*Y31+B1*X31*X31-C1*Y31*X31-C1*X31*Y31+A2*Y31*Y31+
     $A2*X31*X31/4+B2*X31*X31/4-C2*Y31*X31-C2*X31*Y31
      KR(3,4)=-A2*X31*Y31/4-B2*X31*Y31/4+C2*Y31*Y31+C2*X31*X31
      KR(4,3)=KR(3,4)
      KR(3,5)=-A1*Y31*Y21-B1*X31*X21+C1*X21*Y31+C1*X31*Y21-A2*Y31*Y21
     $-A2*X31*X21/4-B2*X31*X21/4+C2*Y31*X21+C2*X31*Y21
      KR(5,3)=KR(3,5)
      KR(3,6)=A2*X31*Y21/4+B2*X31*Y21/4-C2*Y31*Y21-C2*X31*X21
      KR(6,3)=KR(3,6)
      KR(4,4)=A1*Y31*Y31+B1*X31*X31-C1*Y31*X31-C1*X31*Y31+A2*Y31*Y31/4
     $+B2*Y31*Y31/4+B2*X31*X31-C2*X31*Y31-C2*Y31*X31
      KR(4,5)=A2*Y31*X21/4+B2*Y31*X21/4-C2*Y31*Y21-C2*X31*X21
      KR(5,4)=KR(4,5)
      KR(4,6)=-A1*Y31*Y21-B1*X31*X21+C1*Y31*X21+C1*X31*Y21-A2*Y31*Y21/4
     $-B2*Y31*Y21/4-B2*X31*X21+C2*Y31*X21+C2*X31*Y21
      KR(6,4)=KR(4,6)
      KR(5,5)=A1*Y21*Y21+B1*X21*X21-C1*Y21*X21-C1*X21*Y21+A2*Y21*Y21
     $+A2*X21*X21/4+B2*X21*X21/4-C2*Y21*X21-C2*X21*Y21
      KR(5,6)=-A2*X21*Y21/4-B2*X21*Y21/4+C2*Y21*Y21+C2*X21*X21
      KR(6,5)=KR(5,6)
      KR(6,6)=A1*Y21*Y21+B1*X21*X21-C1*Y21*X21-C1*X21*Y21+A2*Y21*Y21/4
     $+B2*Y21*Y21/4+B2*X21*X21-C2*X21*Y21-C2*X21*Y21
      TTT=T*AREA
      DO 83 II=1,6
      DO 83 JJ=1,6
   83 KG(II,JJ)=TTT*(KG(II,JJ)+KR(II,JJ))
      N(1)=J*2-1
      N(2)=J*2
      N(3)=K*2-1
      N(4)=K*2
      N(5)=L*2-1
      N(6)=L*2
      DO 40 II=1,6
      DO 40 JJ=1,6
      IK=N(II)
      JK=N(JJ)
      IN=JK-IK+1
      IF(IN.LE.0) GO TO 40
      GS(IK,IN)=GS(IK,IN)+KG(II,JJ)
40    CONTINUE

      RETURN
      END


      SUBROUTINE DSTRES(E,ANU,DD)
```

```
C ***********************************************************************
C                [D] MATRIX FOR PLANE STRESS                            *
C ***************************************** ************************
      DIMENSION DD(3,3)
      ENU=E/(1.0-ANU**2)
      DD(1,1)=ENU
      DD(1,2)=ANU*ENU
      DD(1,3)=0.0
      DD(2,1)=ANU*ENU
      DD(2,2)=ENU
      DD(2,3)=0.0
      DD(3,1)=0.0
      DD(3,2)=0.0
      DD(3,3)=(1-ANU)*ENU/2.0
      RETURN
      END


      SUBROUTINE DELA(E,ANU,DD)

      DIMENSION DD(3,3)
      PN=1-2*ANU
      ENU=E/(1+ANU)
      DD(1,1)=ENU*(1-ANU)/PN
      DD(1,2)=ENU*ANU/PN
      DD(1,3)=0.0
      DD(2,1)=DD(1,2)
      DD(2,2)=DD(1,1)
      DD(2,3)=0.0
      DD(3,1)=0.0
      DD(3,2)=0.0
      DD(3,3)=0.5*ENU

      RETURN
      END

      SUBROUTINE DPLA(NE,E,YO,C,WN,STRE,STR,I,MO,DP,H)

      DIMENSION DP(3,3),STRE(NE,5),STR(NE,5),MO(NE)
      ANU=.33
      SZ=STRE(I,5)
      SM=(STRE(I,1)+STRE(I,2)+SZ)/3
      SXP=STRE(I,1)-SM
      SYP=STRE(I,2)-SM
      S=(2.0/3.0)*(STRE(I,4)**2)*(1+2*H*(1+ANU)/(3*E))
      PN=1-2*ANU
      ENU=E/(1+ANU)
      DP(1,1)=ENU*((1-ANU)/PN -(SXP**2)/S)
      DP(1,2)=ENU*(ANU/PN - SXP*SYP/S)
      DP(1,3)=-ENU*SXP*(STRE(I,3))/S
      DP(2,1)=DP(1,2)
      DP(2,2)=((1-ANU)/(1-2*ANU)-(SYP**2)/S)*ENU
      DP(2,3)=-ENU*(SYP)*(STRE(I,3))/S
```

```
DP(3,1)=DP(1,3)
DP(3,2)=DP(2,3)
DP(3,3)=ENU*(0.5-(STRE(I,3)**2)/S)

RETURN
END


SUBROUTINE RATIO(NE,IN,YO,STRES,STRE,R)

DIMENSION STRES(NE,5),STRE(NE,5)
DOUBLE PRECISION R1,R2
X=STRES(IN,1)
Y=STRES(IN,2)
Z=STRES(IN,5)
XY=STRES(IN,3)
SX=STRE(IN,1)
SY=STRE(IN,2)
SZ=STRE(IN,5)
SXY=STRE(IN,3)
A=X-Y
B=SX-SY
C=Y-Z
D=SY-SZ
E=Z-X
F=SZ-SX
O=A**2+C**2+E**2+6*(XY**2)
P=2*(A*B+D*C+E*F+6*SXY*XY)
Q=B**2+D**2+F**2+6*(SXY**2)-2*(YO**2)
R1=(-P+SQRT(P**2-4*O*Q))/(2*O)
R2=(-P-SQRT(P**2-4*O*Q))/(2*O)
R=R1

RETURN
END


SUBROUTINE  BM(NE,NN,I,LOC,CX,CY,BB,AREA)

DIMENSION CX(NN),CY(NN),BB(3,6)
DIMENSION CXL(3),CYL(3),LOC(NE,3)
J=LOC(I,1)
K=LOC(I,2)
L=LOC(I,3)
GX=(CX(J)+CX(K)+CX(L))/3
GY=(CY(J)+CY(K)+CY(L))/3
CXL(1)=CX(J)-GX
CXL(2)=CX(K)-GX
CXL(3)=CX(L)-GX
CYL(1)=CY(J)-GY
CYL(2)=CY(K)-GY
CYL(3)=CY(L)-GY
AREA=((CXL(3)-CXL(2))*(CYL(2)-CYL(1))-(CXL(2)-CXL(1))*(CYL(3)-
```

```
     2CYL(2)))/2.0
      X32=(CXL(3)-CXL(2))/(2.0*AREA)
      Y31=(CYL(3)-CYL(1))/(2.0*AREA)
      X31=(CXL(3)-CXL(1))/(2.0*AREA)
      Y21=(CYL(2)-CYL(1))/(2.0*AREA)
      X21=(CXL(2)-CXL(1))/(2.0*AREA)
      DO 81 II=1,3
      DO 81 JJ=1,6
81    BB(II,JJ)=0.0
      BB(1,1)=Y32
      BB(1,3)=-Y31
      BB(1,5)=Y21
      BB(2,2)=-X32
      BB(2,4)=X31
      BB(2,6)=-X21
      BB(3,1)=-X32
      BB(3,2)= Y32
      BB(3,3)= X31
      BB(3,4)=-Y31
      BB(3,5)=-X21
      BB(3,6)= Y21

      RETURN
      END

      SUBROUTINE DECOMP(N,NB,A)
      DIMENSION A(N,NB)
      DOUBLE PRECISION DIFF
      A(1,1)=SQRT(A(1,1))
      DO 5 K=2,NB
5     A(1,K)=A(1,K)/A(1,1)
      DO 25 K=2,N
      KP1=K+1
      KM1=K-1
      DIFF=A(K,1)
      DO 10 JP=1,KM1
      ICOL=K+1-JP
      IF (ICOL .GT. NB) GO TO 10
      DIFF=DIFF-A(JP,ICOL)*A(JP,ICOL)
10    A(K,1)=DSQRT(DIFF)
      DO 20 J=2,NB
      IF(K+J-1 .GT. N) GO TO 25
      DIFF=A(K,J)
      DO 15 JP=1,KM1
      ICOL=K+1-JP
      JCOL=K+J-JP
      IF (JCOL .GT. NB) GO TO 15
      IF (ICOL .GT. NB) GO TO 15
      DIFF=DIFF-A(JP,ICOL)*A(JP,JCOL)
15    CONTINUE
20    A(K,J)=DIFF/A(K,1)
25    CONTINUE
      RETURN
      END
```

```
      SUBROUTINE SOLVE (N,NB,M,A,B,DIFF)

      DIMENSION A(N,NB),B(N,M)
      DOUBLE PRECISION DIFF(M)
      DO 5 J=1,M
5     B(1,J)=B(1,J)/A(1,1)
      DO 30 I=2,N
      DO 10 J=1,M
10    DIFF(J)=B(I,J)
      DO 20 K=2,NB
      IROW=I+1-K
      IF(IROW .LT. 1) GO TO 20
      ICOL=I+1-IROW
      IF (ICOL .GT. NB) GO TO 20
      DO 15 J=1,M
15    DIFF(J)=DIFF(J)-A(IROW,ICOL)*B(IROW,J)
20    CONTINUE
      DO 25 J=1,M
25    B(I,J)=DIFF(J)/A(I,1)
30    CONTINUE
      DO 35 J=1,M
35    B(N,J)=B(N,J)/A(N,1)
      DO 60 II=2,N
      I=N+1-II
      DO 40 J=1,M
40    DIFF(J)=B(I,J)
      DO 50 K=2,NB
      IK=I-1+K
      IF (IK.GT.N)GO TO 50
      DO 45 J=1,M
45    DIFF(J)=DIFF(J)-A(I,K)*B(IK,J)
50    CONTINUE
      DO 55 J=1,M
55    B(I,J)=DIFF(J)/A(I,1)
60    CONTINUE
      RETURN
      END


      SUBROUTINE MATMUL (A,B,C,L,M,N)
      DIMENSION A(L,M),B(M,N),C(L,N)
      DO 10 I=1,L
      DO 10 J=1,N
      C(I,J)=0.0
      DO 10 K=1,M
      C(I,J)=C(I,J)+A(I,k)*B(K,J)
10    CONTINUE

      RETURN
      END

      SUBROUTINE VAL (N,NE,NN,ND,NB,CX,CY,LOC,IDISP,NDISP,IFIX,NFIX,IDB,
     $NDB,E,ANU,H,YO,M,NG,MY,ISL)
```

```
      DIMENSION CX(193),CY(193),LOC(171,3),IDISP(20),IFIX(100),IDB(40),
     $ISL(20)
      DOUBLE PRECISION Q1X,Q1Y,Q2X,Q2Y

      WRITE(*,*)'ENTER THE VALUES OF [E - ANU - H - YO]'
      READ(*,*) E,ANU,H,YO
      WRITE(*,*) E,ANU,H,YO
C     OPEN(20,FILE='AN',STATUS='NEW')
      WRITE(*,*)'ENTER XA& YA'
      READ(*,*)XA,YA
      WRITE(*,*)'XB & YB'
      READ(*,*)XB,YB
      WRITE(*,*)' XC& YC'
      READ(*,*)XC,YC
      WRITE(*,*)'ENTER N  M   MY'
      READ(*,*)N,M,MY
      NG=N
      Q1X=(XB-XA)/(N-1)
      Q2X=(XC-XB)/(M-1)
      Q1Y=(YA-YC)/(M-1)
      Q2Y=YC/(MY-1)
      NB=(N+M+1)*2
      IT=1
      DO 12 J=1,M
      DO 10 I=1,N
      IP=IT+I-1
      CX(IP)=XA+(I-1)*Q1X
      CY(IP)=YA-(J-1)*Q1Y
   10 CONTINUE
      IT=IP
      IF(J.GT.1) THEN
      DO 11 K=N+1 , N+J-1
      IP=IT+K-N
      CX(IP)=XB+(K-N)*Q2X
      CY(IP)=YA-(J-1)*Q1Y
   11 CONTINUE
      ENDIF
      IT=IP+1
   12 CONTINUE
      DO 13 J=1,MY-1
      DO 14 I=1,N
      IP=IT+I-1
      CX(IP)=XA+(I-1)*Q1X
      CY(IP)=YC-J*Q2Y
   14 CONTINUE
      IT=IP
      DO 15 K=N+1 , N+M-1
      IP=IT+K-N
      CX(IP)=XB+(K-N)*Q2X
      CY(IP)=YC-J*Q2Y
   15 CONTINUE
      IT=IP+1
   13 CONTINUE
```

```
      NN=IT-1
C     DO 20 I=1,NN
C     WRITE(20,100)I,CX(I),CY(I)
C     20 WRITE(*,100)I,CX(I),CY(I)
C     WRITE(*,*)'  NN=',NN,'  M  N  MY',M,N,MY
C 100  FORMAT(/,5X,'I=',I4,' CX=',F6.3,'  CY=',F6.3)
      IC=1
      IR=0
      DO 30 I=1,M-1
      IQ=2*N-1+2*(I-1)+IC-1
      DO 31 J=IC,IQ,2
      IR=IR+1
      JJ=J+1
      LOC(J,1)=N+IR
      LOC(J,2)=LOC(J,1)-(N+I-1)
      LOC(J,3)=LOC(J,1)+1
      IF(J.GE.IQ) GO TO 35
      LOC(JJ,1)=LOC(J,2)
      LOC(JJ,2)=LOC(JJ,1)+1
      LOC(JJ,3)=LOC(J,3)
 35   ID=J
 31   CONTINUE
      IR=IR+1
      IC=ID+1
 30   CONTINUE
      DO 40 I=1,MY-1
      IA=2*(M+N-2)+IC-1
      DO 41 J=IC,IA,2
      IR=IR+1
      JJ=J+1
      LOC(J,1)=N+IR
      LOC(J,2)=LOC(J,1)-M-N+1
      LOC(J,3)=LOC(J,1)+1
      LOC(JJ,1)=LOC(J,2)
      LOC(JJ,2)=LOC(J,2)+1
      LOC(JJ,3)=LOC(J,3)
      ID=JJ
 41   CONTINUE
      IR=IR+1
      IC=ID+1
 40   CONTINUE
      NE=IC-1
      WRITE(*,*)'  NE=',NE
C     DO 36 I=1,NE
C     WRITE(20,150) I,(LOC(I,J),J=1,3)
C 36  WRITE(*,150) I,(LOC(I,J),J=1,3)
 150  FORMAT(3X,' I=',I3,' LOC=',3I7)
      DO 45 I=1,N
      ID=I
      IDISP(I)=2*I
 45   CONTINUE
      NDISP=N
```

```
      DO 50 I=1,2*N
      IFIX(I)=I
      IFB=I
 50   CONTINUE
      IR=0
      IFE=2*(NN-M-N+1)
      DO 51 I=IFB+1 , IFB+2*(M+N-1)
      IR=IR+1
      IFIX(I)=IR+IFE
      IFD=I
 51   CONTINUE
      NFIX=IFD
      ND=NN*2
C     DO 60 I=1,NDISP
C     WRITE(*,160)I,IDISP(I)
C 60  WRITE(20,160)I,IDISP(I)
      IG=0
      DO 110 I=1,M
      ISL(I)=I*N+IG
      WRITE(*,*)' M=',I,' ISL=',ISL(I)
 110  IG=IG+I
C     DO 65 I=1,NFIX
C     WRITE(*,170)I,IFIX(I)
C 65  WRITE(20,170)I,IFIX(I)
 160  FORMAT(/,5X,'I=',I4,'   IDISP=',I4)
 170  FORMAT(/,5X,'I=',I4,'   IFIX=',I4)

      RETURN
      END


      SUBROUTINE FRIC(NN,NE,NG,MG,STRE,SNS,QNS,YNS,NNB,NNC,
     $AQP,AY,ATP,AFT,AK,AMU,SFS,KF,NF,FOX,P,CX,ND,FORCE,CY,LF)

      DIMENSION  STRE(NE,5),SNS(40),QNS(40),YNS(40),SFS(40),
     $ KF(40),NF(40),FOX(40),P(ND,1),CX(NN),DN(40),AR(40),
     $ CY(NN),LF(40)
      Q=AY*AQP
      IE=0
      DO 10 I=1,NG
      DN(I)=SNS(I)
      NNB=I
      IE=2*(I-1)+1
      IF(I.EQ.1)THEN
      QNS(I)=(STRE(IE,4)+STRE(IE+1,4))/(2*SQRT(3.))
      SNS(I)=(STRE(IE,3)+STRE(IE+1,3))/2
      YNS(I)=(STRE(IE,2)+STRE(IE+1,2))/2
      AR(I)=ABS((CX(2)-CX(1))/2)
      GO TO 10
      ENDIF
      IF(I.EQ.NG)THEN
      SNS(I)=(STRE(IE-1,3)+STRE(IE,3))/2
      YNS(I)=(STRE(IE-1,2)+STRE(IE,2))/2
      QNS(I)=(STRE(IE-1,4)+STRE(IE,4))/(2*SQRT(3.))
```

```
      AR(I)=ABS((CX(NG)-CX(NG-1))/2)
      GO TO 10
      ENDIF
      SNS(I)=(STRE(IE-1,3)+STRE(IE,3)+STRE(IE+1,3))/3
      YNS(I)=(STRE(IE-1,2)+STRE(IE,2)+STRE(IE+1,2))/3
      QNS(I)=(STRE(IE-1,4)+STRE(IE,4)+STRE(IE+1,4))/(3*SQRT(3.))
      AR(I)=ABS((CX(I+1)-CX(I-1))/2)
10    CONTINUE
      IG=NE-(NG+MG-2)*2+1
      DO 20 I=1,NG+MG-1
      J=NNB+I
      NNC=J
      IE=2*(I-1)+IG
      DN(J)=SNS(J)
      JP=NN-(NG+MG-1)+I
      IF(I.EQ.1)THEN
      SNS(J)=STRE(IE,3)
      QNS(J)=STRE(IE,4)/(SQRT(3.))
      YNS(J)=STRE(IE,2)
      AR(J)=ABS((CX(JP+1)-CX(JP))/2)
      GO TO 20
      ENDIF
      IF(I.EQ.NG+MG-1)THEN
      SNS(J)=(STRE(NE,3)+STRE(NE-1,3))/2
      QNS(J)=(STRE(NE,4)+STRE(NE-1,4))/(2*SQRT(3.))
      YNS(J)=(STRE(NE,2)+STRE(NE-1,2))/2
      AR(J)=ABS((CX(NN)-CX(NN-1))/2)
      GO TO 20
      ENDIF
      SNS(J)=(STRE(IE,3)+STRE(IE-1,3)+STRE(IE-2,3))/3
      QNS(J)=(STRE(IE,4)+STRE(IE-1,4)+STRE(IE-2,4))/(3*SQRT(3.))
      YNS(J)=(STRE(IE,2)+STRE(IE-1,2)+STRE(IE-2,2))/3
      AR(J)=ABS((CX(JP+1)-CX(JP-1))/2)
20    CONTINUE
      NTP=NN-(NG+MG-1)
      DO 30 I=1,NNC
      IF(I.LE.NG) NF(I)=2*I-1
      IF(I.GT.NG) THEN
      J=(NTP+I-NG)*2-1
      NF(I)=J
      ENDIF
      PR=ABS(YNS(I))
      IF(PR.LT.Q) SFS(I)=PR*AMU
      IF(PR.GE.Q)THEN
      APW=((AQP-PR/AY)*ATP)/(AFT*AQP)
      SFS(I)=AK*(ATP+AFT*(1-EXP(APW)))
      ENDIF
      IF(ABS(SNS(I)).GE.SFS(I)) KF(I)=1
      NW=NF(I)
      IF(P(NW,1).GE.0) FOX(I)=-ABS(SNS(I))*AR(I)
      IF(P(NW,1).LT.0) FOX(I)=ABS(SNS(I))*AR(I)
30    CONTINUE
      DO 60 I=NG+1,NNC
      IF(YNS(I).GE.0) THEN
      LF(I)=1
```

```
      FOX(I)=0
      KF(I)=1
      ENDIF
      IF(CY(I).LT.0) LF(I)=0
   60 CONTINUE
      FORCE=0
      DO 40 I=1,NG
      PRT=AR(I)*YNS(I)
   40 FORCE=FORCE+ABS(PRT)
      FORCE=0.455*FORCE

      RETURN
      END
```

APPENDIX E

SOME NUMERICAL AND EXPERIMENTAL RESULTS

1- Compression of the Wedge-Shaped specimen:

Red. in hight %	Displacement (inch)	Load (pound) Test A	Test B	Test C	Average
1.2	0.006	1800	1670	2100	1857
2	0.010	2300	2200	2200	2233
3	0.015	3000	2450	2700	2716
4.6	0.023	3580	3325	3620	3508
6.8	0.034	4700	4450	4500	4550
8	0.044	5200	5330	5100	5210
9.4	0.047	5800	5500	5800	5633
10	0.050	5800	5930	5930	5886

2- Ring compression test:

Test	Red. in hight %	Red. in internal Diameter %	Coefficient of Friction
A	33	14	0.20
B	39	20	0.21
C	47	42	0.22
			Average=0.21

3- Compression of the cylindrical specimen:

P: = Load (pound)
D = Initial diameter
lo = Initial length (inch)
l = Instantaneous length (inch)
Δl = Displacement (inch)
Ao = Initial Surface area (in**2)
A = Instantaneous area (in**2)
ε = ln(lo/l) Natural strain
σ = P/A Stress (psi)

Test A:

D =0.755
lo=0.750

P	Δl	l	ε	A	σ
2200	0.012	0.736	0.016	0.455	4832
3850	0.020	0.730	0.027	0.460	8369
4380	0.027	0.723	0.036	0.464	9424
5100	0.034	0.716	0.046	0.469	10867
5600	0.042	0.708	0.057	0.474	11800
6220	0.043	0.707	0.059	0.475	13087
7620	0.066	0.684	0.092	0.491	15520
8600	0.086	0.664	0.128	0.508	16995
9450	0.115	0.635	0.166	0.529	17859
10350	0.139	0.611	0.205	0.550	18820
13000	0.193	0.557	0.297	0.603	21550
15500	0.252	0.498	0.409	0.675	22973
17800	0.288	0.462	0.484	0.727	24475

Test B:

lo=0.760
D =0.755

P	Δl	l	ε	A	σ
3880	0.016	0.744	0.021	0.457	8484
4460	0.020	0.740	0.027	0.460	9700
5140	0.025	0.735	0.033	0.463	11103
5550	0.030	0.730	0.040	0.466	11909
5900	0.035	0.725	0.047	0.469	12571
8710	0.094	0.666	0.132	0.511	17049
9100	0.105	0.655	0.149	0.519	17518
10170	0.134	0.626	0.194	0.544	18711
11110	0.147	0.613	0.215	0.555	20016
12110	0.180	0.580	0.270	0.587	20643
14080	0.218	0.542	0.338	0.628	22428
15950	0.267	0.493	0.433	0.690	23110
17360	0.289	0.471	0.478	0.722	24031

Test C:

l_o=0.750
D =0.750

P	Δl	l	ε	A	σ
2740	0.010	0.740	0.013	0.448	6119
3500	0.012	0.736	0.016	0.450	7774
4400	0.019	0.731	0.026	0.453	9707
5500	0.029	0.721	0.039	0.459	11982
6400	0.039	0.711	0.053	0.466	13733
7200	0.058	0.692	0.080	0.479	15037
7650	0.068	0.682	0.095	0.486	15741
8950	0.091	0.659	0.129	0.503	17800
9350	0.111	0.639	0.160	0.519	18031
10090	0.141	0.609	0.208	0.544	18545
13050	0.189	0.561	0.291	0.591	22095
15770	0.248	0.502	0.401	0.660	23892
17500	0.294	0.456	0.488	0.727	24071

3- The computed nodal coordinates in the Wedge-Shaped specimen:

a) Bay's Friction modal (asperity angle=0)
as the limit of sticking:

X	Y	ΔX	ΔY		
-0.01641	0.44980	-0.01641	-0.05020	DISP AT NODE:	1
0.09323	0.44980	-0.00677	-0.05020	DISP AT NODE:	2
0.20000	0.44980	0.00000	-0.05020	DISP AT NODE:	3
0.30068	0.44980	0.00068	-0.05020	DISP AT NODE:	4
0.40086	0.44980	0.00086	-0.05020	DISP AT NODE:	5
-0.02384	0.41142	-0.02384	-0.04572	DISP AT NODE:	6
0.08742	0.41078	-0.01258	-0.04636	DISP AT NODE:	7
0.19678	0.40978	-0.00322	-0.04736	DISP AT NODE:	8
0.30379	0.40793	0.00379	-0.04921	DISP AT NODE:	9
0.40730	0.40788	0.00730	-0.04926	DISP AT NODE:	10
0.49234	0.42471	0.00662	-0.03243	DISP AT NODE:	11
-0.02792	0.37337	-0.02792	-0.04092	DISP AT NODE:	12
0.08436	0.37234	-0.01564	-0.04195	DISP AT NODE:	13
0.19535	0.37069	-0.00465	-0.04359	DISP AT NODE:	14
0.30482	0.36811	0.00482	-0.04618	DISP AT NODE:	15
0.41254	0.36699	0.01254	-0.04729	DISP AT NODE:	16
0.49968	0.38285	0.01397	-0.03143	DISP AT NODE:	17
0.58515	0.39593	0.01372	-0.01836	DISP AT NODE:	18
-0.03040	0.33552	-0.03040	-0.03591	DISP AT NODE:	19
0.08254	0.33426	-0.01746	-0.03717	DISP AT NODE:	20
0.19463	0.33214	-0.00537	-0.03929	DISP AT NODE:	21
0.30551	0.32907	0.00551	-0.04236	DISP AT NODE:	22
0.41512	0.32738	0.01512	-0.04405	DISP AT NODE:	23
0.50547	0.34140	0.01975	-0.03003	DISP AT NODE:	24
0.59183	0.35384	0.02040	-0.01759	DISP AT NODE:	25
0.67764	0.36290	0.02050	-0.00853	DISP AT NODE:	26
-0.03220	0.29782	-0.03220	-0.03075	DISP AT NODE:	27
0.08125	0.29641	-0.01875	-0.03217	DISP AT NODE:	28
0.19408	0.29393	-0.00592	-0.03464	DISP AT NODE:	29
0.30588	0.29046	0.00588	-0.03811	DISP AT NODE:	30
0.41648	0.28833	0.01648	-0.04024	DISP AT NODE:	31
0.50835	0.30063	0.02263	-0.02794	DISP AT NODE:	32
0.59651	0.31171	0.02508	-0.01686	DISP AT NODE:	33
0.68241	0.32048	0.02527	-0.00809	DISP AT NODE:	34
0.76827	0.32668	0.02541	-0.00189	DISP AT NODE:	35
-0.03360	0.26021	-0.03360	-0.02550	DISP AT NODE:	36
0.08016	0.25875	-0.01984	-0.02696	DISP AT NODE:	37
0.19368	0.25599	-0.00632	-0.02972	DISP AT NODE:	38
0.30632	0.25214	0.00632	-0.03358	DISP AT NODE:	39
0.41766	0.24956	0.01766	-0.03615	DISP AT NODE:	40
0.51019	0.26025	0.02447	-0.02547	DISP AT NODE:	41
0.59933	0.26995	0.02790	-0.01576	DISP AT NODE:	42

0.68596	0.27792	0.02881	-0.00780	DISP AT NODE:	43
0.77157	0.28403	0.02871	-0.00168	DISP AT NODE:	44
0.85721	0.28981	0.02864	0.00410	DISP AT NODE:	45
-0.03491	0.22277	-0.03491	-0.02009	DISP AT NODE:	46
0.07935	0.22119	-0.02085	-0.02166	DISP AT NODE:	47
0.19318	0.21833	-0.00682	-0.02453	DISP AT NODE:	48
0.30676	0.21413	0.00676	-0.02873	DISP AT NODE:	49
0.41913	0.21100	0.01913	-0.03186	DISP AT NODE:	50
0.51209	0.22008	0.02637	-0.02277	DISP AT NODE:	51
0.60168	0.22848	0.03025	-0.01438	DISP AT NODE:	52
0.68888	0.23550	0.03172	-0.00736	DISP AT NODE:	53
0.77461	0.24128	0.03176	-0.00158	DISP AT NODE:	54
0.86011	0.24706	0.03154	0.00420	DISP AT NODE:	55
0.94566	0.25274	0.03138	0.00988	DISP AT NODE:	56
-0.03195	0.18374	-0.03195	-0.01626	DISP AT NODE:	57
0.07772	0.18387	-0.02228	-0.01613	DISP AT NODE:	58
0.19229	0.18083	-0.00771	-0.01917	DISP AT NODE:	59
0.30650	0.17651	0.00650	-0.02348	DISP AT NODE:	60
0.42012	0.17282	0.02012	-0.02718	DISP AT NODE:	61
0.51430	0.18007	0.02859	-0.01993	DISP AT NODE:	62
0.60411	0.18712	0.03268	-0.01288	DISP AT NODE:	63
0.69149	0.19323	0.03434	-0.00677	DISP AT NODE:	64
0.77747	0.19855	0.03461	-0.00145	DISP AT NODE:	65
0.86289	0.20429	0.03442	0.00429	DISP AT NODE:	66
0.94851	0.20997	0.03422	0.00997	DISP AT NODE:	67
1.03404	0.21563	0.03404	0.01563	DISP AT NODE:	68
-0.02853	0.12213	-0.02853	-0.01121	DISP AT NODE:	69
0.07946	0.12316	-0.02054	-0.01018	DISP AT NODE:	70
0.18892	0.12297	-0.01108	-0.01036	DISP AT NODE:	71
0.30401	0.11847	0.00401	-0.01486	DISP AT NODE:	72
0.41855	0.11432	0.01855	-0.01901	DISP AT NODE:	73
0.51486	0.11886	0.02914	-0.01447	DISP AT NODE:	74
0.60733	0.12310	0.03590	-0.01024	DISP AT NODE:	75
0.69555	0.12765	0.03840	-0.00568	DISP AT NODE:	78
0.78185	0.13212	0.03899	-0.00122	DISP AT NODE:	77
0.86741	0.13776	0.03884	0.00442	DISP AT NODE:	78
0.95293	0.14343	0.03864	0.01010	DISP AT NODE:	79
1.03845	0.14910	0.03845	0.01576	DISP AT NODE:	80
-0.02592	0.06071	-0.02592	-0.00596	DISP AT NODE:	81
0.08238	0.06150	-0.01762	-0.00516	DISP AT NODE:	82
0.19003	0.06204	-0.00997	-0.00463	DISP AT NODE:	83
0.29910	0.06118	-0.00090	-0.00548	DISP AT NODE:	84
0.41537	0.05651	0.01537	-0.01016	DISP AT NODE:	85
0.51318	0.05885	0.02747	-0.00782	DISP AT NODE:	86
0.60752	0.06095	0.03609	-0.00572	DISP AT NODE:	87
0.69899	0.06262	0.04185	-0.00405	DISP AT NODE:	88
0.78612	0.06580	0.04326	-0.00087	DISP AT NODE:	89
0.87179	0.07123	0.04322	0.00457	DISP AT NODE:	90
0.95732	0.07689	0.04304	0.01023	DISP AT NODE:	91
1.04285	0.08256	0.04285	0.01589	DISP AT NODE:	92
-0.02435	0.00000	-0.02435	0.00000	DISP AT NODE:	93
0.08523	0.00000	-0.01477	0.00000	DISP AT NODE:	94
0.19315	0.00000	-0.00685	0.00000	DISP AT NODE:	95

0.30000	0.00000	0.00000	0.00000	DISP AT NODE:	96
0.40832	0.00000	0.00832	0.00000	DISP AT NODE:	97
0.50884	0.00000	0.02312	0.00000	DISP AT NODE:	98
0.60543	0.00000	0.03400	0.00000	DISP AT NODE:	99
0.69878	0.00000	0.04164	0.00000	DISP AT NODE:	100
0.78974	0.00000	0.04689	0.00000	DISP AT NODE:	101
0.87617	0.00472	0.04760	0.00472	DISP AT NODE:	102
0.96172	0.01036	0.04743	0.01036	DISP AT NODE:	103
1.04724	0.01603	0.04724	0.01603	DISP AT NODE:	104

b) Bay's Friction model (asperity angle=15)
as the limit of sticking:

X	Y	ΔX	ΔY		
-0.01783	0.44977	-0.01783	-0.05023	DISP AT NODE:	1
0.09257	0.44977	-0.00743	-0.05023	DISP AT NODE:	2
0.20000	0.44977	0.00000	-0.05023	DISP AT NODE:	3
0.30076	0.44977	0.00076	-0.05023	DISP AT NODE:	4
0.40097	0.44977	0.00097	-0.05023	DISP AT NODE:	5
-0.02579	0.41174	-0.02579	-0.04540	DISP AT NODE:	6
0.08648	0.41106	-0.01352	-0.04608	DISP AT NODE:	7
0.19671	0.40999	-0.00329	-0.04715	DISP AT NODE:	8
0.30429	0.40795	0.00429	-0.04920	DISP AT NODE:	9
0.40799	0.40786	0.00799	-0.04928	DISP AT NODE:	10
0.49288	0.42533	0.00716	-0.03181	DISP AT NODE:	11
-0.02954	0.37380	-0.02954	-0.04048	DISP AT NODE:	12
0.08308	0.37297	-0.01692	-0.04132	DISP AT NODE:	13
0.19507	0.37122	-0.00493	-0.04307	DISP AT NODE:	14
0.30548	0.36832	0.00548	-0.04597	DISP AT NODE:	15
0.41372	0.36706	0.01372	-0.04722	DISP AT NODE:	16
0.50094	0.38366	0.01522	-0.03063	DISP AT NODE:	17
0.58669	0.39679	0.01526	-0.01749	DISP AT NODE:	18
-0.03136	0.33596	-0.03136	-0.03547	DISP AT NODE:	19
0.08160	0.33498	-0.01840	-0.03645	DISP AT NODE:	20
0.19401	0.33301	-0.00599	-0.03842	DISP AT NODE:	21
0.30589	0.32864	0.00589	-0.04179	DISP AT NODE:	22
0.41657	0.32763	0.01657	-0.04380	DISP AT NODE:	23
0.50730	0.34245	0.02158	-0.02898	DISP AT NODE:	24
0.59409	0.35500	0.02266	-0.01643	DISP AT NODE:	25
0.68049	0.36370	0.02335	-0.00773	DISP AT NODE:	26
-0.03279	0.29835	-0.03279	-0.03022	DISP AT NODE:	27
0.08091	0.29710	-0.01909	-0.03147	DISP AT NODE:	28
0.19360	0.29491	-0.00640	-0.03366	DISP AT NODE:	29
0.30578	0.29140	0.00578	-0.03717	DISP AT NODE:	30
0.41748	0.28896	0.01748	-0.03961	DISP AT NODE:	31
0.51047	0.30197	0.02476	-0.02661	DISP AT NODE:	32
0.59924	0.31317	0.02782	-0.01541	DISP AT NODE:	33
0.68571	0.32159	0.02857	-0.00698	DISP AT NODE:	34
0.77241	0.32566	0.02955	-0.00291	DISP AT NODE:	35
-0.03364	0.26080	-0.03364	-0.02492	DISP AT NODE:	36
0.08024	0.25948	-0.01976	-0.02624	DISP AT NODE:	37
0.19378	0.25687	-0.00622	-0.02885	DISP AT NODE:	38
0.30608	0.25322	0.00608	-0.03249	DISP AT NODE:	39
0.41788	0.25060	0.01788	-0.03512	DISP AT NODE:	40
0.51166	0.26204	0.02595	-0.02368	DISP AT NODE:	41
0.60201	0.27172	0.03059	-0.01399	DISP AT NODE:	42
0.68940	0.27929	0.03226	-0.00642	DISP AT NODE:	43
0.77568	0.28332	0.03283	-0.00239	DISP AT NODE:	44
0.86222	0.28500	0.03365	-0.00071	DISP AT NODE:	45
-0.03496	0.22355	-0.03496	-0.01930	DISP AT NODE:	46
0.07989	0.22193	-0.02011	-0.02093	DISP AT NODE:	47

0.19372	0.21917	-0.00628	-0.02369	DISP AT NODE:	48
0.30716	0.21500	0.00716	-0.02785	DISP AT NODE:	49
0.41876	0.21220	0.01876	-0.03066	DISP AT NODE:	50
0.51223	0.22229	0.02652	-0.02057	DISP AT NODE:	51
0.60302	0.23067	0.03159	-0.01219	DISP AT NODE:	52
0.69133	0.23714	0.03419	-0.00572	DISP AT NODE:	53
0.77781	0.24072	0.03495	-0.00214	DISP AT NODE:	54
0.86383	0.24246	0.03526	-0.00040	DISP AT NODE:	55
0.95005	0.24299	0.03576	0.00013	DISP AT NODE:	56
-0.03129	0.18448	-0.03129	-0.01552	DISP AT NODE:	57
0.07820	0.18477	-0.02180	-0.01523	DISP AT NODE:	58
0.19327	0.18162	-0.00673	-0.01838	DISP AT NODE:	59
0.30725	0.17730	0.00725	-0.02270	DISP AT NODE:	60
0.42061	0.17363	0.02061	-0.02637	DISP AT NODE:	61
0.51337	0.18239	0.02766	-0.01761	DISP AT NODE:	62
0.60358	0.18969	0.03215	-0.01031	DISP AT NODE:	63
0.69200	0.19523	0.03485	-0.00477	DISP AT NODE:	64
0.77890	0.19810	0.03604	-0.00190	DISP AT NODE:	65
0.86481	0.19968	0.03624	-0.00032	DISP AT NODE:	66
0.95062	0.20026	0.03633	0.00026	DISP AT NODE:	67
1.03649	0.20063	0.03649	0.00063	DISP AT NODE:	68
-0.02690	0.12239	-0.02690	-0.01094	DISP AT NODE:	69
0.08017	0.12392	-0.01983	-0.00941	DISP AT NODE:	70
0.18921	0.12398	-0.01079	-0.00935	DISP AT NODE:	71
0.30459	0.11907	0.00459	-0.01427	DISP AT NODE:	72
0.41863	0.11489	0.01863	-0.01844	DISP AT NODE:	73
0.51443	0.12005	0.02872	-0.01328	DISP AT NODE:	74
0.60480	0.12568	0.03337	-0.00765	DISP AT NODE:	75
0.69306	0.13011	0.03591	-0.00323	DISP AT NODE:	76
0.78009	0.13204	0.03723	-0.00129	DISP AT NODE:	77
0.86617	0.13304	0.03760	-0.00029	DISP AT NODE:	78
0.95176	0.13356	0.03748	0.00022	DISP AT NODE:	79
1.03731	0.13401	0.03731	0.00068	DISP AT NODE:	80
-0.02391	0.06078	-0.02391	-0.00589	DISP AT NODE:	81
0.08403	0.06171	-0.01597	-0.00495	DISP AT NODE:	82
0.19062	0.06270	-0.00938	-0.00397	DISP AT NODE:	83
0.29876	0.06187	-0.00124	-0.00480	DISP AT NODE:	84
0.41486	0.05672	0.01486	-0.00985	DISP AT NODE:	85
0.51191	0.05953	0.02819	-0.00714	DISP AT NODE:	86
0.60525	0.06182	0.03382	-0.00485	DISP AT NODE:	87
0.69389	0.06488	0.03674	-0.00179	DISP AT NODE:	88
0.78083	0.06605	0.03797	-0.00062	DISP AT NODE:	89
0.86697	0.06652	0.03840	-0.00015	DISP AT NODE:	90
0.95272	0.06670	0.03843	0.00003	DISP AT NODE:	91
1.03805	0.06711	0.03805	0.00044	DISP AT NODE:	92
-0.02263	0.00000	-0.02263	0.00000	DISP AT NODE:	93
0.08683	0.00000	-0.01317	0.00000	DISP AT NODE:	94
0.19435	0.00000	-0.00565	0.00000	DISP AT NODE:	95
0.30000	0.00000	0.00000	0.00000	DISP AT NODE:	96
0.40684	0.00000	0.00684	0.00000	DISP AT NODE:	97
0.50670	0.00000	0.02098	0.00000	DISP AT NODE:	98
0.60192	0.00000	0.03049	0.00000	DISP AT NODE:	99
0.69370	0.00000	0.03656	0.00000	DISP AT NODE:	100

0.78126	0.00000	0.03840	0.00000	DISP AT NODE:	101
0.86732	0.00000	0.03875	0.00000	DISP AT NODE:	102
0.95295	0.00000	0.03866	0.00000	DISP AT NODE:	103
1.03858	0.00000	0.03858	0.00000	DISP AT NODE:	104

c) Constant Friction model as the limit of sticking:

X	Y	ΔX	ΔY		
-0.02672	0.44948	-0.02672	-0.05052	DISP AT NODE:	1
0.08439	0.44948	-0.01561	-0.05052	DISP AT NODE:	2
0.19432	0.44948	-0.00568	-0.05052	DISP AT NODE:	3
0.30000	0.44948	0.00000	-0.05052	DISP AT NODE:	4
0.40043	0.44948	0.00043	-0.05052	DISP AT NODE:	5
-0.03778	0.41241	-0.03778	-0.04473	DISP AT NODE:	6
0.07690	0.41104	-0.02310	-0.04610	DISP AT NODE:	7
0.18810	0.41063	-0.01190	-0.04651	DISP AT NODE:	8
0.29806	0.40932	-0.00194	-0.04782	DISP AT NODE:	9
0.40517	0.40780	0.00517	-0.04935	DISP AT NODE:	10
0.49102	0.42382	0.00531	-0.03333	DISP AT NODE:	11
-0.04339	0.37487	-0.04339	-0.03942	DISP AT NODE:	12
0.07023	0.37375	-0.02977	-0.04054	DISP AT NODE:	13
0.18432	0.37226	-0.01568	-0.04202	DISP AT NODE:	14
0.29573	0.37061	-0.00427	-0.04368	DISP AT NODE:	15
0.40632	0.36823	0.00632	-0.04606	DISP AT NODE:	16
0.49704	0.38189	0.01133	-0.03239	DISP AT NODE:	17
0.58226	0.39665	0.01083	-0.01763	DISP AT NODE:	18
-0.04676	0.33733	-0.04676	-0.03410	DISP AT NODE:	19
0.06699	0.33612	-0.03301	-0.03531	DISP AT NODE:	20
0.18036	0.33479	-0.01964	-0.03664	DISP AT NODE:	21
0.29397	0.33235	-0.00603	-0.03908	DISP AT NODE:	22
0.40580	0.32972	0.00580	-0.04171	DISP AT NODE:	23
0.49906	0.34111	0.01334	-0.03032	DISP AT NODE:	24
0.58733	0.35428	0.01590	-0.01715	DISP AT NODE:	25
0.67272	0.36431	0.01558	-0.00712	DISP AT NODE:	26
-0.04940	0.30003	-0.04940	-0.02854	DISP AT NODE:	27
0.06510	0.29852	-0.03490	-0.03005	DISP AT NODE:	28
0.17860	0.29706	-0.02140	-0.03151	DISP AT NODE:	29
0.29169	0.29472	-0.00831	-0.03386	DISP AT NODE:	30
0.40490	0.29157	0.00490	-0.03700	DISP AT NODE:	31
0.49898	0.30098	0.01326	-0.02759	DISP AT NODE:	32
0.58903	0.31250	0.01761	-0.01607	DISP AT NODE:	33
0.67577	0.32160	0.01863	-0.00697	DISP AT NODE:	34
0.76140	0.32646	0.01855	-0.00211	DISP AT NODE:	35
-0.04991	0.26232	-0.04991	-0.02339	DISP AT NODE:	36
0.06345	0.26120	-0.03655	-0.02452	DISP AT NODE:	37
0.17785	0.25934	-0.02215	-0.02637	DISP AT NODE:	38
0.29094	0.25689	-0.00906	-0.02882	DISP AT NODE:	39
0.40377	0.25380	0.00377	-0.03191	DISP AT NODE:	40
0.49861	0.26113	0.01290	-0.02458	DISP AT NODE:	41
0.58903	0.27124	0.01782	-0.01447	DISP AT NODE:	42
0.67725	0.27916	0.02011	-0.00656	DISP AT NODE:	43
0.76313	0.28364	0.02032	-0.00207	DISP AT NODE:	44
0.84838	0.28530	0.02031	-0.00042	DISP AT NODE:	45
-0.04691	0.22240	-0.04691	-0.01946	DISP AT NODE:	46
0.06671	0.22354	-0.03709	-0.01932	DISP AT NODE:	47
0.17658	0.22467	-0.02342	-0.02092	DISP AT NODE:	48

[illegible]	[illegible]	[illegible]	-0.02384	DISP AT NODE:	49
[illegible]	[illegible]	[illegible]	-0.02699	DISP AT NODE:	50
[illegible]	[illegible]	[illegible]	-0.02135	DISP AT NODE:	51
[illegible]	0.23014	0.01752	-0.01272	DISP AT NODE:	52
[illegible]	0.23709	0.02008	-0.00577	DISP AT NODE:	53
[illegible]	0.24084	0.02104	-0.00201	DISP AT NODE:	54
[illegible]	0.24245	0.02098	-0.00041	DISP AT NODE:	55
[illegible]	0.24274	0.02098	-0.00012	DISP AT NODE:	56
-0.04548	0.18425	-0.04348	-0.01575	DISP AT NODE:	57
0.00566	0.19455	-0.03434	-0.01545	DISP AT NODE:	58
0.17512	0.18462	-0.02498	-0.01538	DISP AT NODE:	59
0.28975	0.18132	-0.01025	-0.01818	DISP AT NODE:	60
0.40472	0.17773	0.00472	-0.02227	DISP AT NODE:	61
0.49810	0.18167	0.01238	-0.01833	DISP AT NODE:	62
0.58846	0.18915	0.01703	-0.01085	DISP AT NODE:	63
0.67656	0.19509	0.01971	-0.00491	DISP AT NODE:	64
0.76302	0.19829	0.02076	-0.00171	DISP AT NODE:	65
0.84905	0.19959	0.02108	-0.00041	DISP AT NODE:	66
0.93507	0.19988	0.02108	-0.00012	DISP AT NODE:	67
1.02108	0.19997	0.02108	-0.00003	DISP AT NODE:	68
-0.03923	0.12296	-0.03923	-0.01037	DISP AT NODE:	69
0.00918	0.12346	-0.03082	-0.00988	DISP AT NODE:	70
0.17773	0.12363	-0.02227	-0.00970	DISP AT NODE:	71
0.23627	0.12405	-0.01373	-0.00929	DISP AT NODE:	72
0.40130	0.12005	0.00130	-0.01328	DISP AT NODE:	73
0.49796	0.11945	0.01224	-0.01388	DISP AT NODE:	74
0.58860	0.12517	0.01717	-0.00816	DISP AT NODE:	75
0.67693	0.12987	0.01979	-0.00346	DISP AT NODE:	76
0.76382	0.13209	0.02096	-0.00124	DISP AT NODE:	77
0.84977	0.13304	0.02119	-0.00029	DISP AT NODE:	78
0.93548	0.13323	0.02119	-0.00011	DISP AT NODE:	79
1.02118	0.13328	0.02118	-0.00005	DISP AT NODE:	80
-0.03377	0.06133	-0.03377	-0.00534	DISP AT NODE:	81
0.07395	0.06196	-0.02605	-0.00471	DISP AT NODE:	82
0.18172	0.06208	-0.01828	-0.00458	DISP AT NODE:	83
0.28915	0.06242	-0.01085	-0.00425	DISP AT NODE:	84
0.39631	0.06263	-0.00369	-0.00403	DISP AT NODE:	85
0.49355	0.05935	0.00784	-0.00732	DISP AT NODE:	86
0.58754	0.06147	0.01611	-0.00520	DISP AT NODE:	87
0.67655	0.06467	0.01940	-0.00200	DISP AT NODE:	88
0.76357	0.06599	0.02071	-0.00067	DISP AT NODE:	89
0.84908	0.06648	0.02111	-0.00018	DISP AT NODE:	90
0.93543	0.06660	0.02114	-0.00007	DISP AT NODE:	91
1.02117	0.06659	0.02117	-0.00008	DISP AT NODE:	92
-0.02924	0.00000	-0.02924	0.00000	DISP AT NODE:	93
0.07901	0.00000	-0.02099	0.00000	DISP AT NODE:	94
0.18588	0.00000	-0.01412	0.00000	DISP AT NODE:	95
0.29225	0.00000	-0.00775	0.00000	DISP AT NODE:	96
0.39773	0.00000	-0.00227	0.00000	DISP AT NODE:	97
0.46571	0.00000	0.00000	0.00000	DISP AT NODE:	98
0.58104	0.00000	0.00961	0.00000	DISP AT NODE:	99
0.67330	0.00000	0.01616	0.00000	DISP AT NODE:	100
0.76122	0.00000	0.01836	0.00000	DISP AT NODE:	101
0.84753	0.00000	0.01896	0.00000	DISP AT NODE:	102
0.93335	0.00000	0.01907	0.00000	DISP AT NODE:	103
1.01909	0.00000	0.01909	0.00000	DISP AT NODE:	104

4- The computed forging load in the Wedge-Shaped specimen:

a) Bay's Friction model as the (asperity angle=0) as the limit of sticking:

Force (pound)	Reduction in height %
923.90	0.0688498
1698.37	0.1309693
1736.98	0.1412282
1749.39	0.1456203
1772.08	0.1543050
1797.72	0.1655355
1819.19	0.1761579
1880.09	0.2120082
1918.93	0.2413612
1972.44	0.2873378
2011.83	0.3301894
2027.41	0.3508841
2139.11	0.5185214
2192.35	0.6346235
2294.96	0.8891857
2329.29	0.9831882
2388.59	1.1508088
2486.89	1.4341595
2576.09	1.6943870
2675.30	1.9858477
2708.61	2.0716910
2797.41	2.3456366
2896.87	2.6117108
2954.62	2.7263918
3051.96	3.0263920
3167.80	3.3263917
3355.61	3.6263916
3476.77	3.8198411
3496.94	3.8603208
3529.92	3.9461401
3621.58	4.2461400
3646.00	4.3165030
3746.44	4.6165032
3849.45	4.9165030
3953.05	5.2081552
4059.03	5.5081549
4074.93	5.5449519
4189.28	5.8449516
4207.89	5.8908734
4313.18	6.1908731

4432.74	6.4559660
4579.98	6.7559662
4601.74	6.7909918
4745.87	7.0909920
4854.18	7.2695627
4955.06	7.5695624
5072.90	7.8695626
5191.78	8.1695623
5227.79	8.2462034
5322.79	8.5462036
5412.42	8.8462029
5515.72	9.1462030
5619.70	9.4462032
5753.26	9.7462025
5889.48	10.0462027

b) Bay's Friction model (asperity angle=15)
as the limit of sticking:

Force (pound)	Reduction in height %
785.31	0.0688498
1443.61	0.1309693
1476.43	0.1412282
1486.98	0.1456203
1506.27	0.1543050
1528.06	0.1655355
1546.31	0.1761579
1598.07	0.2120082
1631.09	0.2413612
1676.57	0.2873378
1710.05	0.3301894
1723.34	0.3510185
1818.61	0.5196947
1864.03	0.6383848
1952.72	0.9036185
2020.39	1.1392404
2055.15	1.2701501
2132.56	1.5701500
2189.83	1.7839741
2289.68	2.0839741
2407.41	2.3839743
2526.56	2.6839743
2696.72	2.9839742
2855.22	3.2839742
3000.58	3.5839741
3083.57	3.8839738
3145.95	4.1839738
3170.21	4.3148227
3178.81	4.3898458
3300.04	4.6898460
3400.37	4.9898458
3501.18	5.2898455
3584.24	5.5898452
3656.74	5.8898454
3733.66	6.1898451
3913.23	6.4898453
4154.39	6.7898455
4295.93	7.0898452
4398.75	7.3898449
4483.75	7.6462126
4583.11	7.9462128
4671.67	8.2462120
4766.93	8.5462122
4846.58	8.8462124
4932.66	9.1462116
4950.19	9.2194080
5014.77	9.5194082
5083.17	9.8194075
5129.30	10.0398865

c) Constant Friction model as the limit of sticking:

Force (Pound)	Reduction in height %
923.90	0.0688498
1111.59	0.0828399
1200.24	0.0895286
1536.17	0.1148519
1564.95	0.1176124
1600.65	0.1220989
1619.89	0.1250570
1634.52	0.1275557
1682.69	0.1364742
1731.92	0.1475635
1735.70	0.1484974
1805.89	0.1662754
1816.99	0.1694434
1870.47	0.1849853
1935.61	0.2058427
1964.92	0.2160415
2100.45	0.2665507
2153.48	0.2907103
2162.65	0.2953303
2322.84	0.3780988
2346.02	0.3943539
2368.54	0.4109188
2434.20	0.4615031
2441.17	0.4677172
2562.87	0.5780740
2638.57	0.6662615
2667.56	0.7061642
2767.89	0.8502644
2901.57	1.0650535
3067.49	1.3650534
3221.73	1.6650535
3357.03	1.9650536
3560.15	2.2650535
3770.66	2.5239460
4061.70	2.8239460
4401.43	3.1239462
4711.96	3.4239459
4836.58	3.5843897
4924.19	3.8843896
5016.52	4.1843896
5118.15	4.4843893
5227.01	4.7843890
5242.66	4.8230171
5350.48	5.1230168
5460.12	5.4230170
5579.69	5.7230167

5702.92	6.0230165
5828.01	6.3230166
5944.78	6.6230164
6057.68	6.9230161
6160.25	7.2230163
6256.15	7.5230160
6347.31	7.8230157
6432.55	8.1230154
6516.97	8.4230156
6596.81	8.7230158
6678.24	9.0230150
6754.85	9.3230152
6819.67	9.5672522
6876.46	9.8035860
6949.34	10.1035862

VITA

Ahmad Assempoor

Candidate for the Degree of

Doctor of Philosophy

Thesis: CONSIDERATION OF FRICTIONAL BOUNDARY MODELLING IN METAL FORMING

Major Field: Mechanical Engineering

Biographical:

Personal Data: Born in Tehran, Iran, June 20, 1955, the son of Mr. and Mrs. Assempoor.

Education: Graduated from Kharazmi High School, Tehran, Iran, in June 1974; received the Bachelor of Science degree in Mechanical Engineering from Tehran Polytechnic, Tehran, Iran in September 1979; received the Master of Science, in Mechanical Engineering from Tehran Polytechnic, Tehran, Iran, in December 1985; completed requirements for the Doctor of Philosophy degree in December, 1989, at Oklahoma State University, Stillwater, Oklahoma.

Professional Experience: Design Engineer, Iranian Research Organization for Science and Technology, January 1983, to February 1984; Design Engineer, National Iranian Gas Company, February 1984, to August 1985; Graduate teaching and research assistant, School of Mechanical and Aerospace Engineering, Oklahoma State University, August, 1987 to present.